APOE4 is Associated with Differential Regional Vulnerability to Bioenergetic Deficits in Aged *APOE* Mice

Tal Nuriel[1,2,*], Delfina Larrea[1,3], David N. Guilfoyle[4], Leila Pirhaji[5], Kathleen Shannon[6], Hirra Arain[1,2], Archana Ashok[1,2], Marta Pera[1,3], Qiuying Chen[7], Allissa A. Dillman[8], Helen Y. Figueroa[1,2], Mark R. Cookson[8], Steven S. Gross[7], Ernest Fraenkel[5,9], Karen E. Duff[1,2,10, †], and Estela Area-Gomez[1,3, †]

[1]Taub Institute for Research on Alzheimer's Disease and the Aging Brain, Columbia University, 630 West 168th Street, New York, NY 10032, USA.

[2]Department of Pathology and Cell Biology, Columbia University, 630 West 168th Street, New York, NY 10032, USA.

[3]Department of Neurology, Columbia University, 630 West 168th Street, New York, NY 10032, USA.

[4]Center for Biomedical Imaging and Neuromodulation, Nathan S. Kline Institute, Orangeburg, NY 10962, USA.

[5]Department of Biological Engineering, Massachusetts Institute of Technology, 350 Brookline Street, Cambridge, MA 02139, USA.

[6]Animal Facility, Nathan S. Kline Institute, Orangeburg, NY 10962, USA.

[7]Department of Pharmacology, Weill Cornell Medical College, 1300 York Avenue, New York, NY 10065, USA.

[8]Cell Biology and Gene Expression Section, Laboratory of Neurogenetics, National Institute on Aging, National Institutes of Health, Bethesda, Maryland, 20892

[9]Broad Institute, 415 Main Street, Cambridge, MA 02142, Cambridge, Massachusetts, 02139, USA.

[10]Division of Integrative Neuroscience in the Department of Psychiatry, New York State Psychiatric Institute, 630 West 168th Street, New York, NY 10032, USA.

* Corresponding author: Tal Nuriel, email: tn2283@cumc.columbia.edu

[†]These two authors contributed equally to this work and are co-senior authors.

ABSTRACT

The ε4 allele of apolipoprotein E (*APOE*) is the dominant genetic risk factor for late-onset Alzheimer's disease (AD). However, the reason for the association between *APOE4* and AD remains unclear. While much of the research has focused on the ability of the apoE4 protein to increase the aggregation and decrease the clearance of Aβ, there is also an abundance of data showing that *APOE4* negatively impacts many additional processes in the brain, including bioenergetics. In order to gain a more comprehensive understanding of the *APOE4*'s role in AD pathogenesis, we performed a multi-omic analysis of *APOE4* vs. *APOE3* expression in the entorhinal cortex (EC) and primary visual cortex (PVC) of aged *APOE* mice. These studies revealed region-specific alterations in several bioenergetic pathways, including oxidative phosphorylation (OxPhos), the TCA-cycle and fatty acid metabolism. Follow-up analysis utilizing the Seahorse platform revealed decreased mitochondrial respiration in the hippocampus and cortex of aged *APOE4* vs. *APOE3* mice, but not in the EC of these mice. Additional studies, as well as the original multi-omic data suggest that bioernergetic pathways in the EC of aged *APOE* mice may be differentially regulated by *APOE4* expression. Given the importance of the EC as one of the first regions to be affected by AD pathology in humans, this differential bionenergetic regulation observed in the EC vs. other brain regions of aged *APOE4* mice may play an important role in the pathogenesis of AD, particularly among *APOE4* carriers.

INTRODUCTION

Possession of the ε4 allele of apolipoprotein E (*APOE*) is the major genetic risk factor for late-onset Alzheimer's disease (AD). In normal physiology, the apoE protein plays a vital role in the transport of cholesterol and other lipids through the bloodstream, as well as within the brain (*1-3*). Although the three common isoforms of apoE (E2, E3 and E4) differ from each other by only two amino acids—apoE2 (Cys112, Cys158), apoE3 (Cys112, Arg158), apoE4 (Arg112, Arg158)—this small change in amino acid

sequence has a large effect on protein structure, causing the apoE4 protein to possess a more globular structure due to increased interaction between its N- and C-terminal domains. This difference in structure, in turn, affects the type of lipids that each isoform binds, as well as the affinity of each isoform for the numerous receptors that mediate the uptake of apoE and its cargo into cells (see reviews by (*1, 4*)).

Importantly, these isoform differences also have a major impact on the pathogenesis of late-onset AD. Although the *APOE2*, *APOE3* and *APOE4* alleles are present at a relative frequency of about 8%, 77% and 15% in the normal population (*5, 6*), the *APOE4* allele is present at a relative frequency of 36-64% in AD patients (*7-10*), with individuals who possess one or two *APOE4* alleles having a 3- or 12-fold increased risk of developing AD, respectively (*11*). Although a number of mechanisms have been proposed to help explain this *APOE4*-associated susceptibility to AD, the precise cause remains a source of debate. The prominent hypothesis is that this increase in AD risk is due to the ability of apoE4 to increase the aggregation and decrease the clearance of Aβ (*12-18*). However, *APOE4* expression has also been shown to have deleterious effects on numerous Aβ-independent pathways, including lipid metabolism, tau pathology, bioenergetics, neuronal development, synaptic plasticity, the neuro-vasculature, and neuro-inflammation [see reviews by (*19*) and (*20*)], any number of which could play a pivotal role in the pathogenesis of AD among *APOE4* carriers.

In terms of *APOE4*'s effects on bioenergetics, a number of pivotal reports have demonstrated that *APOE4* expression leads to widespread dysregulation of the brain's bioenergetic capacity. For example, early reports by Eric Reiman and colleagues demonstrated that both young and old *APOE4* carriers display decreased glucose utilization, as measured by fluorodeoxyglucose positron emission tomography (FDG-PET), in similar brain regions to that seen with AD patients (*21-23*). Additional reports detail the wide-range of bioenergetic insults that *APOE4* expression can cause in the brain, including impaired insulin signaling (*24, 25*), reduced cerebral blood volume and cognitive function in response to a high fat diet (HFD) (*26, 27*), altered genetic expression of glucose-regulating enzymes and transporters (*28, 29*), and the generation of a toxic C-terminal fragment of apoE4 that can directly target electron transport chain (ETC)

complexes in the mitochondria (*30-32*).

In order to study the diverse effects that *APOE4* expression has in the brain, we performed an initial multi-omic study of differential *APOE* isoform expression in an AD-vulnerable vs. an AD-resistant brain region from aged *APOE* targeted replacement mice, which express human *APOE* in place of their mouse *Apoe* gene and do not develop overt AD pathology. The EC was chosen as our AD-vulnerable brain region because it is one of the first brain regions to develop AD-related tau pathology, in humans (*33, 34*), and also because the morphology of the EC has been shown to be specifically affected by *APOE4* gene expression. (*35, 36*). The PVC was chosen as our AD-resistant region because it is relatively spared in AD (*33, 37, 38*). As described below, these studies revealed *APOE4*-specific alterations in the levels of numerous genes and small-molecules related to energy metabolism, which were explored further using the Seahorse platform. In agreement with previous data, this analysis revealed *APOE4*-associated deficits in mitochondrial respiration in several brain regions. However, contrary to what we observed in other brain regions, the EC displayed increases in oxidative metabolism in the context of *APOE4* expression, suggesting that, under metabolic stress, brain region-specific counterbalancing mechanisms are in play in the EC of aged *APOE4* mice. Additional studies and further mining of the multi-omic data was then used to elucidate this differential bioenergetic regulation in the EC of aged *APOE4* mice, which may play a causative role in the pathogenesis of AD and may point to novel therapeutic interventions for preventing or slowing the disease.

RESULTS

Multi-omic analysis reveals differential expression of energy-related genes and metabolites in the EC of aged *APOE4* mice

In order to investigate the effects of *APOE4* expression in an untargeted manner, we performed a multi-omic analysis (transcriptomics and metabolomics) on RNA and small-molecules extracted from an AD-vulnerable brain region (the EC) vs. an AD-resistant brain region (the PVC) of 14-15 month-old *APOE*

targeted replacement mice. For the transcriptomic analysis, RNA was Trizol-extracted from the EC and PVC of aged *APOE* mice (10 *APOE3/3* and 19 *APOE3/*4 males). For the metabolomics analysis, small-molecules were extracted from the EC and PVC of aged *APOE* mice (8 *APOE3/3*, 9 *APOE3/4* and 7 *APOE4/4* males) using a methyl tert-butyl ether (MTBE)/methanol extraction protocol modified from previous reports (*39, 40*). The RNA and small-molecules were then analyzed using RNA-sequencing and untargeted metabolomics, respectively.

The data generated from these transcriptomics and metabolomics analyses (summarized in Tables 1 and 2 and Supplementary Tables S1 and S2) have recently been published as parts of larger studies on *APOE4*'s impact on endosomal-lysosomal dysregulation (*41*) and neuronal hyperactivity (*42*), respectively. However, as is often the case with omics and other systems biology approaches, the large amounts of data generated from these analyses inform us about changes in multiple biological pathways that cannot all be investigated in one study. In the case of the transcriptomics analysis, in addition to the dysregulation of endosomal-lysosomal genes that were revealed in our pathway analysis (and which we investigated further for our previously published study), another major KEGG pathway that was observed to be significantly enriched for differentially expressed genes was "Oxidative Phosphorylation" (Fig. 1A). This was driven by a large number of differentially expressed genes encoding for subunits of ETC complexes I-V, with each of these genes being upregulated in the EC of aged *APOE3/4* mice, as compared to aged *APOE3/3* mice (Fig. 1B). This increased transcription of ETC genes may also be related to the increases in energy-related metabolites that we observed in the EC of aged *APOE4/4* mice (which we reported as part of our neuronal hyperactivity study). These metabolites include several TCA cycle metabolites (malate, citrate and isocitrate), as well as fructose-6-phosphate, carnitine, and ATP, each of which had higher levels in the EC of aged *APOE4/4* vs. *APOE3/3* mice (Fig. 2A). Furthermore, the metabolomics data indicates a higher ATP:ADP ratio in the EC of aged *APOE4/4* vs. *APOE3/3* mice (Fig. 2C), which suggests an increase in the rate of oxidative metabolism in this region. Thus, in addition to the *APOE4*-associated differences in endosomal-lysosomal regulation and neuronal activity that these original studies highlighted, the data from

both the transcriptomics and metabolomics studies also pointed to specific differences in several bioenergetic pathways.

Intriguingly, our metabolomics data also revealed an *APOE4*-associated decrease in the levels of numerous free fatty acids in aged *APOE4/4* vs. aged *APOE3/3* mice (Fig. 2B), which, unlike most of the previously mentioned energy-related metabolites, were similarly differentially altered in both the EC and the PVC. Although it is disputed whether or not free fatty acids can be utilized in the brain as an alternative energy source via β-oxidation (*43-45*), there is compelling evidence to suggest that it can (*46-48*). Thus, it is tempting to speculate that the decreased fatty acid levels observed in both the EC and PVC may be a result of increased β-oxidation in both of these brain regions, which may also be related to the observation that carnitine, a metabolite that is necessary for importing fatty acids into the mitochondria for energy utilization by the carnitine-palmitoyl transferase system, was the only energy-related metabolite in Fig. 2A whose levels were shown to be higher in both the EC and the PVC of the aged *APOE4/4* mice.

Seahorse analysis reveals decreased mitochondrial respiration in the PVC, hippocampus and cortex of aged *APOE4* vs. *APOE3* mice, but not in the EC.

In order to validate and expand upon the bioenergetic differences that we observed in our multi-omic analysis, we conducted a series of Seahorse experiments on mitochondria isolated from the EC and other brain regions of aged *APOE4/4* vs. *APOE3/3* mice. Utilizing the Seahorse XF24 platform (see methods section), we first measured the oxygen consumption rate (OCR; a measure of OxPhos efficiency) of mitochondria from the EC and PVC of 15-month-old *APOE* mice (4 *APOE3/3* and 4 *APOE4/4* males; samples pooled within each genotype and region). As shown in Supplementary Fig. S1, we observed a significant reduction in both the Complex I-mediated and Complex II-mediated OCR of mitochondria from the PVC of the *APOE4/4* vs. *APOE3/3* mice, but no difference in the OCR between genotypes in the mitochondria isolated from the EC region. In order to investigate whether this decreased OCR in the PVC was unique to the PVC or whether it represented a more global decrease in mitochondrial respiration within

the aged *APOE4* brain, we performed an additional experiment measuring the OCR of mitochondria isolated from the EC, hippocampus (Hip) and cortex (Ctx) of 20-month-old *APOE* mice (2 *APOE3/3* and 2 *APOE4/4* males; samples pooled within each genotype and region). As shown in Fig. 3, we observed a significant reduction in the OCR of mitochondria from the Hip and the Ctx of *APOE4/4* vs. *APOE3/3* mice, with the most abundant differences observed in the Complex I-mediated OCR. However, in mitochondria from the EC of *APOE4/4* vs. *APOE3/3* mice, we did not observe any significant differences in Complex I-mediated basal mitochondrial respiration or in complex II-mediated OCR, and we observed significant increases in State 3 respiration in Complex I-mediated OCR in mitochondria from the EC (Fig. 3B). Furthermore, using the data generated from this Seahorse analysis, we determined the respiratory control ratio (RCR) (state3u/state4o), which is a measure of the coupling efficiency between OxPhos and ATP production (*49, 50*) (Fig. 3C). This analysis indicates that EC mitochondria from *APOE4* mice are highly coupled, resulting in increased production of ATP per unit of oxygen.

These observations suggest that, while *APOE4* expression leads to an overall reduction in mitochondrial function in the brains of aged *APOE4* mice, a result consistent with the *APOE4*-associated bioenergetic deficits observed using alternative approaches (*24-29*), mitochondria in the EC seem to undergo differential bioenergetic regulation, characterized by increased coupling efficiency. Importantly, these region-specific differences in the effects of differential *APOE* isoform expression on mitochondrial respiration did not appear to be the result of changes in mitochondrial mass, as the levels of Tom20 protein, as well as the levels of PGC1α RNA and the ratio of Mitochondrial:Nuclear DNA, were unchanged between *APOE* genotypes in the EC, Hip, and Ctx of 21-month-old *APOE* mice (Supplementary Fig. S2A, C & D). Differential *APOE* isoform expression also did not result in changes in the levels of specific ETC complex proteins in the EC, Hip or Ctx (Supplementary Fig. S2B).

Computational analysis of untargeted metabolomics data reveals differential expression of ketones in the EC of aged *APOE4* mice

In order to investigate the source of these differential bioenergetic effects in the EC, we conducted a series of additional analyses on the EC of aged *APOE4/4* vs, *APOE3/3* mice. First, we utilized the PIUMet (Prize-collecting Steiner forest algorithm for Integrative Analysis of Untargeted Metabolomics) method (*51*) to predict identities of the untargeted metabolites that we uncovered in the EC of aged *APOE4/4* vs. *APOE3/3* during our original metabolomics analysis. PIUMet uses network optimization to analyze the data in the context of a vast database of protein-protein and protein-metabolite interactions, revealing both known and uncharacterized pathways that contain the putative metabolites and other molecules. PIUMet also allows for the incorporation of additional datasets, allowing us to utilize our targeted metabolomics results in the analysis.

We used PIUMet to analyze the 304 untargeted metabolite features whose levels were differentially altered between *APOE4/4*and *APOE3/3* in the EC of aged *APOE* mice (corrected p-value < 0.05). Among these features, 124 had matches in PIUMet's underlying database of metabolites (Supplementary Table S5). PIUMet was able to infer the identity of 32 metabolite features, and revealed a network of protein-protein and protein-metabolite interactions associated with their dysregulation. The resulting network is enriched in 18 putative GO biological processes (Table 3) and 124 total metabolites (Supplementary Fig. S3). Among these, the most intriguing GO biological processes were fatty acid metabolic process, IMP metabolic process, ketone catabolic process, steroid metabolic process, and vitamin metabolic process. The most interesting putative identifications were acetone, adenylosuccinate, alpha-tocotrienol, and oleamide. Alpha-tocotrienol is a vitamin E metabolite, which bolsters the observation in the targeted metabolomics result that vitamins and vitamin-derivatives (including tocopherol, another vitamin E metabolite) were found to be increased in the EC and PVC of aged *APOE4/4* mice in our targeted metabolomics analysis (Tables 1 and 2). Similarly, the changes in the levels of adenylosuccinate support the idea that the purine nucleotide cycle is affected in *APOE4/4* EC, as this metabolite is downstream of IMP and upstream of succinoadenosine, both of which were identified in our targeted analysis (Table 1). Importantly, the identification of acetone and of the ketone catabolic process GO term may also represent a substantial finding. Ketone bodies (acetone, acetoacetone and β-hydroxybutyrate) are primarily generated in the liver

from fatty acid breakdown via β-oxidation, and are used as a supplemental energy source when glucose levels are low. These ketone bodies readily cross the blood brain barrier and can act as a potent fuel for the brain (*52-54*). Alternatively, there is evidence that astrocytes also have the ability to produce ketones (*55-57*), both through the breakdown of fatty acids, as well as through the breakdown of ketogenic amino acids, most notably leucine (*58, 59*).

Proton nuclear magnetic resonance spectroscopy analysis reveals differential expression of phosphocreatine, glutamate and GABA in the EC of anesthetized aged *APOE4* mice.

^{1}H NMR spectroscopy provides *in vivo* measurements of brain metabolites and has been used in many studies of neurodegenerative disorders in both humans and rodents. This method allows for the simultaneous acquisition of several highly abundant metabolites in the brain, including neurotransmitters such as glutamate and gamma-aminobutyric acid (GABA), as well as other biological metabolites such as creatine, glutathione, and N-acetylaspartate (NAA). It also allows for the accurate quantification of individual metabolite concentrations. Since metabolomics and ^{1}H NMR spectroscopy have been described as complimentary techniques, with advantages and disadvantages to both [see review by (*60*)], we chose to perform ^{1}H NMR spectroscopy on the EC of 18-19 month-old *APOE* mice (7 *APOE3/3* and 7 *APOE4/4* males) in order to gain additional information about the metabolic changes occurring in the EC of aged *APOE* mice. While the EC is located in a very NMR unfriendly brain area because of its close proximity to sinus spaces, we were able to achieve full width half maximums of 8 – 15 Hz using a customized second and third order shim coil. Fig. 4A shows the position of the volume of interest (VOI) that was used to measure metabolite levels in the EC of these aged *APOE* mice. A representative spectrum from this region is shown in Fig. 4B, along with the spectral position of some of the major metabolites. To our knowledge, this is the first in vivo ^{1}H NMR study of the EC in mice.

As shown in Fig. 4C and Table 4, this ^{1}H NMR study revealed significant differences in the levels of multiple metabolites in the EC of aged *APOE4/4* vs. *APOE3/3* mice, including decreased levels of creatine (Cre), glutamate (Glu), GABA, and taurine (Tau) in the EC of aged *APOE4/4* mice, as compared

to that of aged *APOE3/3* mice. Perhaps the most interesting observation, however, was the large increase in the levels of phosphocreatine (PCr) and the ratio of PCr:Cr observed in the *APOE4* EC. Creatine is mainly phosphorylated in mitochondria, where creatine kinase uses the newly synthesized ATP to produce PCr and ADP (*61*). This PCr is then shuttled to the cytosol where it acts as a rapidly mobilized reserve of phosphate groups that can be used to replenish ATP levels, whereas the increased levels of ADP in the mitochondria will stimulate oxygen uptake and oxidative metabolism, especially during enhanced neuronal activity (*62*). Thus, the observation that PCr levels are increased in aged *APOE4/4* mice supports and expands upon the bioenergetics observations from our transcriptomics, metabolomics and Seahorse analyses. In addition to these changes in PCr levels, the observation that glutamate and GABA are both decreased in the EC of *APOE4/4* mice may also be related to these bioenergetic differences between *APOE* genotypes and brain regions. Although glutamate and GABA are mostly known for their roles as neurotransmitters in excitatory and inhibitory neurons, respectively, they can also be utilized as energy metabolites (*63-66*).

Taken together, our data suggest that, contrary to other brain region such as the cortex and hippocampus, the EC of aged *APOE4/4* vs. *APOE3/3* mice exhibit an increased rate of oxidative metabolism and ATP turnover, which may play a causative role in the pathogenesis of AD.

DISCUSSION

Possession of the *APOE4* allele greatly increases an individual's risk of developing AD. Although numerous theories have been proposed, the precise cause of this association remains unknown. In order to further investigate the effects of *APOE4* gene expression in AD-relevant brain regions, we initially chose to perform a multi-omic analysis on RNA and small-molecules extracted from an AD-vulnerable brain region (the EC) vs. an AD-resistant brain region (the PVC) of aged *APOE* targeted replacement mice. In addition to our recently published reports describing *APOE4*'s impact on endosomal-lysosomal dysregulation (*41*) and neuronal hyperactivity (*42*), these studies also revealed *APOE4*-associated

alterations in the levels of numerous genes and small-molecules related to energy metabolism (Fig. 1 and 2). Follow-up experiments utilizing the Seahorse platform revealed *APOE4*-associated deficits in mitochondrial respiration in several brain regions, including the PVC, the Hip, and the Ctx as a whole, which is consistent with previous reports showing that *APOE4* expression has numerous deleterious effects on the brain's bioenergetic capabilities (*24-29*). Intriguingly, however, this *APOE4*-associated decrease in mitochondrial respiration was not observed in the EC, with Complex-1 mediated respiration actually increasing in the EC of 20-month-old *APOE4* mice. (Fig. 3). Additional studies, including proton nuclear magnetic resonance (^{1}H NMR) spectroscopy and a bioinformatics analysis of our untargeted metabolomics data provided further support and elucidation of this region-specific bioenergetic regulation by *APOE4*, including the observations of increased PCr levels and decreased glutamate and GABA levels (Fig. 4), as well as an upregulation of the ketone pathway (Table 3), in the EC of aged *APOE4* mice.

Bioenergetic regulation in the brain is a complex process involving multiple interconnected pathways and cell-types, which makes it difficult to decipher the mechanism or impact of these region-specific bioenergetic effects of *APOE4* expression. It is important to note that the decline in mitochondrial functionality that we observed in the cortex and hippocampus, while significant, is likely below the pathological threshold (*67*). Mitochondria are part of a multifaceted network of metabolic pathways that are modulated by the cell to compensate for any reductions in respiratory activity and ATP production (*68*, *69*). Moreover, mitochondria have a "reserve respiratory capacity" that allows them to increase their oxidative capacity and ATP production depending on the cell's demand (*70*). Furthermore, mitochondrial adaptability is tissue and cell-type specific, depending on the different compensatory mechanisms and the availability of substrates (*67*, *71*)

The most intriguing finding from our study, however, is that, within the brain, mitochondria appear to have *regional* differences in their response to metabolic stressors, at least in this case of *APOE4* expression in aged *APOE* mice. In both the EC and the PVC, for example, it appears that there are attempts to use alternative fuel sources to compensate for *APOE4*'s effects on mitochondrial function. This is best represented by the decreased fatty acid levels and increased carnitine levels in the metabolomics data,

perhaps due to increased efforts to supply the TCA cycle with additional acetyl-CoA molecules via β-oxidation of fatty acids. However, the data from our ^{1}H NMR spectroscopy study, as well as further mining of our transcriptomics and metabolomics data, suggest that the mitochondria in the EC of aged *APOE4* mice have additional mechanisms that allow them to counteract the *APOE4*-associated reductions in mitochondrial respiration. Specifically, we hypothesize that mitochondria in the EC of aged *APOE4* mice are distinctively able to increase their respiratory capacity by increasing the coupling efficiency between oxygen consumption and ATP production.

This hypothesis is supported by our Seahorse data, where mitochondria in the EC of aged *APOE4* mice show increased ADP-stimulated oxygen consumption and increased maximal respiration rate, without changes in proton leak (Fig. 3 and Supplemental Fig. S1) or mitochondrial mass (Supplementary Fig. S2). In addition, we also observed that the RCR is increased in the EC of aged *APOE4/4* vs. *APOE3/3* mice (Fig. 3C and Supplementary Fig. S1C), further confirming that ADP-driven mitochondrial respiration in the aged *APOE4* EC is better coupled to ATP production than in the Hip and the Ctx. Interestingly, the reductions in mitochondrial respiration observed in the Hip and Ctx of aged *APOE4/4* vs. *APOE3/3* mice by Seahorse analysis appears to be more robust in complex I-mediated respiration compared to complex II-mediated respiration, whereas in the EC, complex I-mediated respiration in aged *APOE4* begins to outpace complex I-mediated respiration in *APOE3* mice with increasing age (Fig. 3 and Supplemental Fig. S1). Since complex I-mediated mitochondrial respiration is driven by pyruvate, this suggests that the *APOE4*-associated bioenergetic deficits observed in the hippocampus and cortex of aged *APOE4* mice are primarily related to decreased aerobic respiration that occurs downstream of glycolysis, whereas in the EC we observe an amplification of this process.

While the reason for the increased efficiency in OxPhos in the EC of aged *APOE4* mice requires further investigation, we note that the expression of some mitochondrial transporter genes is specifically upregulated in mitochondria from this brain region, as detected in the transcriptomics data (Supplementary tables S1 and S2). In order to ensure a sufficient rate of solute flux into mitochondria to fuel metabolic pathways, numerous mitochondrial transporters link biochemical pathways in the cytosol and mitochondria

(*72*). Regulation of these transporters is an essential part of the overall regulation of cellular metabolism, and their expression is highly variable depending on the tissues and the metabolic conditions. Intriguingly, the expression of the adenine nucleotide translocase (ANT) genes, ANT1 (*Slc24a4*) and ANT2 (*Slc24a5*), were significantly increased in the EC of aged *APOE3/4* vs. *APOE3/3* mice. ANT participates in ATP-for-ADP exchange through the inner mitochondrial membrane, which supplies the cytoplasm with newly synthesized ATP from OxPhos. Interestingly, ANT can also interact with creatine kinase (CK), gaining preferential access to ATP, which is needed to synthesize PCr in cells with high energetic needs (*73*). Similarly, the expression of the genes for the voltage dependent-anion channel (VDAC1; Vdac1), one of the main gatekeepers for the regulation of the crosstalk between mitochondria and cytosol (*72*), is also increased in the EC of aged *APOE3/4* mice, as is the gene for the mitochondrial phosphate transport protein (PTP; *Slc25a3*), which transports inorganic phosphate (P_i) to the mitochondrial matrix in order to supply the P_i required for ADP phosphorylation into ATP (*72*).

Another important mitochondrial transporter that ensures the balanced cooperation between OxPhos and glycolysis (and to a lesser extent the pentose phosphate pathway) in order to maintain ATP levels is the malate-aspartate shuttle. Briefly, in order for the two NADH molecules generated during glycolysis to be translocated into mitochondria, malate must be produced in the cytosol via conversion of oxaloacetate (OAA) by malate dehydrogenase (MDH1), for which NADH is a necessary cofactor, and then malate is converted back to OAA by MDH1 inside mitochondria (converting NAD+ back to NADH in the process). Since this newly formed OAA cannot be transported back to the cytosol, OAA must first be converted to aspartate by glutamate oxaloacetate transaminase 1 (GOT1; *Slc25a22*). But this requires the donation of an amino radical from glutamate. Thus, glutamate is an essential component for maximizing the number of ATPs produced in glycolysis per molecule of glucose metabolized. Interestingly, our transcriptomic data reveals that the expression of both Slc25a22 (GOT1) and *Mdh1* are upregulated in the EC of aged *APOE3/4* vs. *APOE3/3*, suggesting that activity of the malate-aspartate shuttle is increased in the EC of these mice.

A summary of all these bioenergetics-related changes that we observe in the EC of aged *APOE4* mice is depicted in Fig. 5. Taken together, the observed differences on mitochondrial functionality among the brain regions studied suggests that the EC possesses a different subset of compensatory mechanisms in order to improve OxPhos efficiency under metabolic stress. While this apparent compensation of EC mitochondria may be regarded as a positive attribute, it is plausible that it may have negative consequences in the long run. For example, it has been shown that, over time, elevated mitochondrial respiratory activity and increased coupling efficiency can result in an excess of free radical production and resulting oxidative damage within cells (*74*).

More work will be necessary in order to further elucidate this phenomenon, including an understanding of the specific contributions of different cell-types such as neurons, astrocytes and microglia. It will also be important to investigate whether the other phenotypes that we have observed in the EC of these aged *APOE4* mice, such as endosomal-lysosomal dysregulation and neuronal hyperactivity, are related to the bioenergetic observations described here. For example, Zhao et al. recently reported that *APOE4* expression causes insulin receptors to be inefficiently recycled via the endosomal-lysosomal system, potentially causing the insulin resistance that the authors observed in the brains of aged *APOE4* mice (*25*). As the endosomal-lysosomal dysregulation that we observed in the brains of aged *APOE4* mice was not restricted to the EC (*41*), this may play a role in the *APOE4*-associated bioenergetic deficits that we observed throughout the brains of these mice. On the other hand, the neuronal hyperactivity that we observed did appear to be primarily localized to the EC within the hippocampal formation (*42*). Intriguingly, neuronal activity and glucose utilization have previously been shown to exist in a near stoichiometric relationship (*75*), suggesting that the bioenergetic counterbalancing that we are observing in the EC of aged *APOE4* mice may be directly correlated to the observed neuronal hyperactivity in these mice (*42*).

Finally, it will be important to determine whether these bioenergetic differences in the EC are involved in the increased risk of AD among *APOE4* carriers. The EC is a unique brain region in many ways. It is vital for learning and memory (especially spatial memory), acting as a bridge between the hippocampus and the neocortex (*76*, *77*). As such, it is known to have higher energy demands and to be more

metabolically active that many other brain regions (*78*). In AD, the EC is one of the first regions to develop tauopathy, which eventually spreads into the hippocampus and other cortical regions as the disease progresses (*33*). It is possible, therefore, that due to its unique bioenergetic needs, the EC may possess additional mechanisms for increasing its bioenergetic capacity under conditions of metabolic stress such as *APOE4* expression. However, perhaps in the process of inducing these mechanisms, other negative consequences may result, such as increased ROS production or increased tau hyperphosphorylation or increased neuronal hyperactivity, such that it results in an earlier onset of AD.

METHODS

Mice

Human APOE targeted replacement mice were first developed by Sullivan et al. (*79, 80*) and were acquired from Taconic Biosciences. All mice used in this study were treated in accordance with the National Institutes of Health Guide for the Care and Use of Laboratory Animals and approved by the Columbia University Medical Center and SUNY Medical Center Institutional Animal Care and Use Committee (IACUC).

RNA-Sequencing

Male mice expressing human *APOE3/3* (10 mice) or *APOE3/4* (19 mice) were aged to 14-15 months, at which point they were sacrificed by cervical dislocation, and brain tissues containing the EC and PVC were dissected and snap frozen on dry-ice. Brain tissues were stored in RNase-free eppendorf tubes at -80°C prior to extraction. Total RNA was extracted from frozen tissues by homogenizing each tissue sample using a battery-operated pestle mixer (Argos Technologies, Vernon Hills, IL) in 1 ml of TRIzol reagent according to the manufacturer's protocol (Life Technologies, Carlsbad, CA). RNA concentration was measured using a nanodrop 1000 (Thermo Fisher Scientific, Waltham, MA), and RNA integrity (RIN) was assessed using an Agilent 2100 Bioanalyzer (Agilent Technologies, Santa Clara, CA). All RNA samples possessed a RIN

of 8 or higher. RNA was stored at -80˚C prior to use. Starting with 2 µg of total RNA per sample, Poly(A)+ mRNA was purified, fragmented and then converted into cDNA using the TruSeq RNA Sample Prep Kit v2 (Illumina cat# RS-122-2001) as per the manufacturer's protocol (Illumina, San Diego, CA). For RNA-Sequencing of the cDNA, we hybridized 5 pM of each library to a flow cell, with a single lane for each sample, and we used an Illumina cluster station for cluster generation. We then generated 149bp single end sequences using an Illumina HiSeq 2000 sequencer. For analysis, we used the standard Illumina pipeline with default options to analyze the images and extract base calls in order to generate fastq files. We then aligned the fastq files to the mm9 mouse reference genome using Tophat (v2.0.6) and Bowtie (v2.0.2.0). In order to annotate and quantify the reads to specific genes, we used the Python module HT-SEQ with a modified NCBIM37.61 (containing only protein coding genes) gtf to provide reference boundaries. We used the R/Bioconductor package DESeq2 (v1.10.1) for comparison of aligned reads across the samples. We conducted a variance stabilizing transformation on the aligned and aggregated counts, and then the Poisson distributions of normalized counts for each transcript were compared across *APOE3/4* vs. *APOE3/3* groups using a negative binomial test. We corrected for multiple testing using the Benjamini-Hochberg procedure and selected all genes that possessed a corrected p-value of less than 0.05. Finally, a heat map based on sample distance and a volcano plot based on fold change and adjusted p-values were generated using the R/Bioconductor package ggplot2 (v2.0.0). For pathway analysis, enriched KEGG pathways were identified using the ClueGo application (version 2.1.7) in Cytoscape (version 3.2.1). Briefly, all differentially expressed EC genes from the RNA-Seq analysis were entered into the application and searched for significantly enriched KEGG pathways possessing a Benjamini-Hochberg adjusted p-value of less than 0.05.

Metabolomic Analysis

Male mice expressing human *APOE3/3* (8 mice), *APOE3/4* (9 mice), or *APOE4/4* (7 mice) were aged to 14-15 months, at which point they were sacrificed by cervical dislocation to maintain the brain environment, and individual brain regions were immediately removed and snap-frozen on dry ice. Tissues were stored at

-80°C for prior to extraction. Metabolite extraction was performed using a methyl tert-butyl ether (MTBE)/methanol extraction protocol modified from previous reports (*39, 40*). Briefly, individual EC or PVC tissues were homogenized in 400 µl of ice-cold methanol using a bead mill homogenizer (TissueLyser II, Qiagen) at 25 beats/sec, 2x for 45 sec each. Following homogenization, samples were incubated in 1200 µl of MTBE for 1 hr at room temperature to separate organic-soluble lipids from aqueous-soluble lipids and other small-molecules. Finally, 360 µl of ultrapure water was added (for a final ratio of 3:1:0.9 MTBE:methanol:water) to resolve the two liquid phases, and each samples were centrifuged at 10,000 x g for 10 min. The lower aqueous phase and the upper organic phase was collected from each sample and stored in separate tubes, and the remaining protein pellets were resuspended in 25 mM ammonium bicarbonate, pH 8, with 2.5% SDS. A BCA protein assay was performed on each protein fraction, and both the aqueous phase and organic phase were normalized to their protein concentration equivalent with 50% and 100% methanol respectively. All samples were then stored at -80°C prior to analysis. Metabolite profiling was performed using an Agilent Model 1200 liquid chromatography (LC) system coupled to an Agilent Model 6230 time-of-flight (TOF) mass analyzer as described previously (*81*). Metabolite separation was accomplished using aqueous neutral phase (ANP) gradient chromatography on a Diamond Hydride column (Microsolv), with mobile phase buffer A consisting of 50% isopropanol and 0.025% acetic acid, and mobile phase buffer B consisting of 90% acetonitrile and 5 mM ammonium acetate. Each aqueous phase sample was analyzed in both positive and negative ion detection mode for comprehensive coverage of metabolites with a mass of 50-1000 Da. Prior to analysis, it was observed that one APOE3/4 PVC sample possessed a chromatographic error and was removed from all future analysis.

Following MS analysis, the raw data was analyzed using Agilent Profinder (version B.06.00) and Mass Profiler Professional (version 12.0) software. Briefly, Profinder performs batch recursive feature extraction, which consists of a first-pass identification of features (ions) that possess a common elution profile (e.g. identical mass-to-charge [m/z] ratios and retention times), followed by a recursive analysis to re-mine each sample for the presence of features that were identified in at least one sample. Feature

extraction was limited to the top 2000 metabolites per ion detection mode, with each metabolite possessing a minimum abundance of 600 ion counts. Each feature was also manually validated following extraction (with investigators blinded to genotype assignments during validation), and re-integration was performed when necessary. In addition to this untargeted feature extraction, we also used ProFinder to perform a targeted feature extraction, matching features against a proprietary database of 626 biologically-relevant metabolites whose mass and retention times were previously determined using pure chemical standards. For this analysis, we allowed for a maximum mass deviation of 10 mDa and a retention time deviation of 1 min, and identified features were manually validated following extraction. For both untargeted and targeted feature extraction, Profinder analysis was followed up by multivariate and differential expression analysis using Mass Profiler Professional. Following differential expression analysis, metabolites identified as differentially expressed were further validated for chromatographic and biological accuracy, and non-validated metabolites were removed.

Seahorse Analysis

In order to investigate the effect of differential apoE isoform expression on electron transport chain activity, mitochondria were isolated from tissues collected from 12-17 month old apoE3/3 or E4/4 mice (10 mice per group, separated into three experiments), and the oxygen consumption rates (OCR) were measured in a complex I or complex II-mediated fashion, as previously described (*49*). Briefly, each mouse was sacrificed by cervical dislocation, and the different brain areas from each brain hemisphere were immediately removed and placed into ice-cold PBS containing protease inhibitors. For each experiment, tissues were pooled from 3-4 mice per apoE group. Following tissue collection, samples were homogenized in ~10 volumes of isolation buffer (70 mM sucrose, 210 mM mannitol, 5 mM HEPES, 1 mM EGTA and 0.5% fatty acid-free BSA, pH 7.2) and rinsed 3 times. Tissues were then homogenized using a Teflon glass homogenizer with 2-3 strokes. Homogenized samples were then centrifuged at 800 x g for 10 min at 4°C. Following centrifugation, fat/lipid was aspirated off, and the remaining supernatant was decanted through 2 layers of cheesecloth into a separate tube and centrifuged at 8000 x g for 10 min at 4°C. After removal of

the supernatant, the pellet was resuspended in mitochondrial isolation buffer, and the centrifugation was repeated. The resulting pellet was resuspended in mitochondrial isolation buffer, and total protein concentrations were determined using Bradford Assay reagent (Bio-Rad).

For complex I experiments, 8 μg of protein was added to each well and for complex II analysis 6 μg per well.

To prepare samples for OCR measurements, samples were prepared in mitochondrial assay buffer (70 mM sucrose, 220 mM mannitol, 10 mM KH2PO4, 5 mM MgCl2, 2 mM HEPES, 1 mM EGTA and 0.2% fatty acid-free BSA, pH 7.2) plus substrate (pyruvate and malate for complex I-mediated ETC activity assay, or succinate and rotenone for complex II-mediated ETC activity assay).

Respirometry was performed using the XF24e Extracellular Flux Analyzer (Seahorse Bioscience). Oxygen consumption was measured in basal conditions (Seahorse media with 25 mM glucose and 2 mM pyruvate) and after the sequential addition of 1 μM oligomycin (Complex V inhibitor), 0.75 μM FCCP (uncoupler) and 1 μM rotenone/1 μM antimycin A (Complex I and Complex III inhibitors respectively). All results are averages of five or more biological replicates. Every biological replicate consisted of three technical replicates.

OCR data was generated by the Seahorse XF24 1.5.0.69 software package and displayed in point-to-point mode. Final calculations of total OCR were performed by normalizing apoE4/4 values to apoE3/3 for each of the three experiments and then combining the data in Prism.

PIUMet Analysis

We used the previously published PIUMet algorithm (*51*) to analyze the untargeted metabolomics data from APOE4/4and APOE3/3 in the EC of aged APOE mice. PIUMet discovers dysregulated molecular pathways and components associated with changes in untargeted metabolomic data by analyzing a network built from curated protein-protein and protein-metabolite interactions (PPMI). PIUMet represents each metabolite peak as a node in this network and connects it to metabolites with masses that correspond to the m/z values of the peak. Using the prize-collecting Steiner tree algorithm, it searches the PPMI interactome to find an optimum subnetwork that connects the input metabolite peaks via their putative identities and other metabolites and proteins that were not detected in the experiments. The Gene Ontology (GO) analysis

of the resulting network further reveals associated molecular pathways with the *APOE4* phenotype. We selected peaks 304 untargeted metabolite peaks or features that were significantly altered between APOE4/4and APOE3/3 models (corrected p-value <0.05). We then assigned a prize to each input data point to show the significance of their alterations, as –log (P values) of the significance of changes between two phenotypic conditions. PIUMet accepts several parameters that regulate the size of the resulting networks, including w and beta. While w tunes the number of trees in the resulting network, beta tunes the number of input nodes that are included in the output. Another parameter, mu, controls the bias toward high degree nodes. Higher values of mu results in a lower number of high degree nodes in the resulting networks, and thus less bias to highly studied molecules or ubiquitous interactions such as those with ions. We determined the optimum parameters (w=6.0, beta=0.5, and mu=0.0005) based on their effects on the size of the resulting networks. We further generated 100 networks by adding random noise to the underlying database, and calculated robustness scores for each node. Nodes with robustness scores less than 60% were removed from the results. Additionally, for each node we calculated a specificity score, based on the number of their presence in the 100 random networks obtained from a set of mock metabolite peaks randomly selected from the input feature list that mimic real input. A score of 100 indicates that the node did not show in any of the randomly generated networks, while a zero score shows the node appears in all the randomly generated networks. 79% of the resulting nodes have specificity score of over 60%.

^{1}H NMR Spectroscopy

All animal procedures for in vivo proton MR spectroscopy were performed following the National Institutes of Health guidelines with approval from the Institutional Animal Care and Use Committee at the Nathan S. Kline Institute for Psychiatric Research. All animals were anesthetized using an isoflurane vaporizer set at the following percentages: 3% for induction, 2% during pilot scanning and 1.5% during data acquisition. An animal monitoring unit (model 1025, SA Instruments, Stony Brook, NY, USA) was used to record respiration and rectal temperature. Respiration was measured with a pressure transducer placed under the abdomen just below the ribcage. Body temperature was maintained using forced warm air, controlled by a

feedback circuit between the heater and thermistor. After induction, the animals were placed on a holder and restrained using a bite bar and ear bars placed half way into the auditory canal. Oxygen was used as the carrier gas delivered to a cone positioned before the bite bar, where gases mixed with air and passed over the rodent's nose. All animals were maintained at 37.0 ± 0.2 °C. All data were obtained on a 7.0 T Agilent (Santa Clara, CA, USA) 40 cm bore system. The gradient coil insert had an internal diameter of 12 cm with a maximum gradient strength of 600 mT/m and minimum rise time of 200 µs, with customized second and third order shim coils. A Rapid (Rimpar, Germany) volume transmit coil (72mm ID) and a two-channel receive-only surface coil was used for RF transmission and reception, respectively.

The shim settings for the selected volume of interest (VOI) were automatically adjusted using FASTMAP[1] (Fast, Automatic Shimming Technique by Mapping Along Projections), a high order shim method, which samples the magnetic field along a group of radial columns which focus on the center of a localized voxel. It is a method for optimizing the field homogeneity in a cubical local region.

The water signal was suppressed using variable power RF pulses with optimized relaxation delays (VAPOR)[2]. The spectral acquisition consisted of a short echo time Point Resolved Spectroscopy (PRESS)[3] sequence with the following parameters: repetition time = 4s, echo time = 7.5 ms, number of averages = 512 acquired in blocks of 128, number of points = 2048 and bandwidth of acquisition = 5 kHz, total acquisition time = 34 minutes. Outer volume suppression was also used to minimize signal contamination by extra cranial muscle and lipids. The VOI size was 3.3 µl (2.0x1.3x1.3 mm^3) placed in the entorhinal cortex (EC). The target VOI is depicted in Fig. 4 overlaid on a schematic of the coronal brain slice at approximately – 2.92 mm relative to Bregma. An anatomical T_2 weighted pilot scan was used to position the VOI (coronal). These scans were acquired with a fast spin echo sequence with the following parameters: field of view = 20 mm with 256x256 matrix size, slice thickness = 0.5 mm, number of slices = 11, repetition time = 4s, echo train length = 8, echo spacing = 15 ms, effective echo time = 60 ms, number of averages = 8, total acquisition time = 8 minutes 40 s. All data were processed using the LCModel software developed by Provencher [4]. This software calculates the best fit to the acquired data of a linear combination of model spectra acquired from *in vitro* solutions of all the brain metabolites of interest. This basis set of the model

spectra has the same echo time, sequence acquisition and field strength as the acquired data of the study. The LCModel software outputs the estimated concentration along with estimated standard deviations (Cramer-Rao lower bounds) expressed in percent of the estimated concentration, which can be used as a quantitative measure of reliability. To improve statistical significance, Miller et al. recently demonstrated the use of weighted averaging in NMR spectroscopic studies (*82*). In this current study, we also used weighted averaging to calculate the standard unequal variance t-test (Welch's t-test) as outlined by Miller [(82)] and in the reference manual of the LCModel software (*83*). All data used in the final analysis had Cramer-Rao lower bounds of 20% or less. The metabolites measured were: alanine(Ala), aspartate (Asp), creatine (Cr), phosphocreatine (PCr), ɣ-Aminobutyric Acid (GABA), glucose (Glc), glutamine (Gln), glutamate (Glu), glycerophosphocholine (GPC), phosphocholine (PCh), glutathione (GSH), myo-inositol (Ins), lactate (Lac), N-Acetylaspartate (NAA), N-Acetylaspartateglutamate (NAAG) and taurine (Tau). It is often quite difficult to resolve Glu from Gln, NAA from NAAG and PCh from GPC, particularly if the spectral quality is poor due to an inadequate shim. So, in addition to the principal metabolites the total of Glu and Gln, NAA and NAAG and PCh and GPC are also reported. These total concentrations are thought to be a more reliable metric. An unsuppressed water signal was also used for absolute concentration calculation and eddy current correction. This internal reference method assumes known values of water concentrations of gray and white matter[5-7].

There are several limitations to ^{1}H NMR spectroscopy which can make reliable measures particularly challenging. One such limitation is that is that ^{1}H NMR metabolite measures are inherently low in signal to noise. The metabolite signals measured are approximately 10,000-fold less than the proton signal used in imaging. The EC is also a small structure and thus requires a small VOI which reduces the measured signal strength. However, at 7T with shim values in the range 8 – 15 Hz and a short echo time of 8 ms, the spectral peaks were reasonably separated, allowing for direct and reliable measures of metabolite concentrations. For metabolites which have significant spectral overlap, total values (e.g. Glu and Gln) are also reported. Another error source is chemical shift displacement. The bandwidth of the 180º RF pulse is 5 kHz, which would give a displacement error of 0.3 mm in the vertical and horizontal directions over the

range of 0.2 to 4.2 ppm. However, this displacement was relatively small and still allowed for sufficient specificity. Despite the challenges of in vivo mouse brain ^{1}H NMR, we were able to achieve high quality spectra in this difficult region with high quantification accuracy.

Data Availability

The transcriptomics datasets are available in the NCBI Gene Expression Omnibus (GEO) repository: https://www.ncbi.nlm.nih.gov/geo/query/acc.cgi?acc=GSE102334. The metabolomics datasets are available in the MetaboLights repository: http://www.ebi.ac.uk/metabolights/MTBLS530

ACKNOWLEDGEMENTS

We acknowledge Drs. Wai-Haung Yu and Natura Myeku for advice on this manuscript, as well as Laidon Piroli for assistance with genotyping. We also acknowledge Dr. Paul Mathews for providing the APOE mice that were used in the ^{1}H NMR experiment. This work was supported by grants from NIA and NINDS to K.E.D. (AG048408 and NS071836), grants from NIA to E.A.G. (AG045335 and AG056387), grants from NICHD and NHLBI to S.S.G. (HD67244 and HL87062), grants from NIA and NINDS to E.F. (AG057331 and NS089076), a grant from NCCR (1S10RR023534-01) for the 7T rodent scanner at Nathan Kline Institute, grants from the U.S. Dept. of Defense to D.L., (W911NF-12-1-9159 and W911F-15-1-0169), funding from the Cure Alzheimer's Fund to KD and TN, and fellowships from NIA (AG047797) and the Brightfocus Foundation to T.N. In addition, this work was supported in part by the Intramural Research Program of the NIH, National Institute on Aging.

AUTHOR CONTRIBUTIONS

This study was designed and managed by T.N., E.A.G., and K.E.D. Animal care and breeding was performed by H.F. Transcriptomic analysis was performed by A.A.D., in the laboratory of M.R.C. Metabolomic analysis was performed by Q.C. and T.N., in the laboratory of S.S.G. Seahorse analysis was performed by D.L. and M.P., in the laboratory of E.A.G. PIUMet analysis was performed by L.P., in the laboratory of E.F. ^{1}H NMR spectroscopy was performed by K.S. and D.G. Additional molecular biology experiments and bioinformatics were performed by T.N., A.A. and H.A. Manuscript preparation was performed by T.N. and E.A.G., with input from K.E.D.

COMPETING FINANCIAL INTERESTS

K.E.D is on the board of directors of Ceracuity LLC. The authors declare no competing financial interests.

REFERENCES

1. R. W. Mahley, S. C. Rall, Jr., Apolipoprotein E: far more than a lipid transport protein. *Annual review of genomics and human genetics* **1**, 507-537 (2000).
2. X. Han, The role of apolipoprotein E in lipid metabolism in the central nervous system. *Cell Mol Life Sci* **61**, 1896-1906 (2004).
3. D. M. Holtzman, J. Herz, G. Bu, Apolipoprotein E and apolipoprotein E receptors: normal biology and roles in Alzheimer disease. *Cold Spring Harbor perspectives in medicine* **2**, a006312 (2012).
4. C. C. Liu, T. Kanekiyo, H. Xu, G. Bu, Apolipoprotein E and Alzheimer disease: risk, mechanisms and therapy. *Nat Rev Neurol* **9**, 106-118 (2013).
5. J. Davignon, R. E. Gregg, C. F. Sing, Apolipoprotein E polymorphism and atherosclerosis. *Arteriosclerosis* **8**, 1-21 (1988).
6. A. M. Cumming, F. W. Robertson, Polymorphism at the apoprotein-E locus in relation to risk of coronary disease. *Clin Genet* **25**, 310-313 (1984).
7. A. M. Saunders *et al.*, Association of apolipoprotein E allele epsilon 4 with late-onset familial and sporadic Alzheimer's disease. *Neurology* **43**, 1467-1472 (1993).
8. W. J. Strittmatter *et al.*, Apolipoprotein E: high-avidity binding to beta-amyloid and increased frequency of type 4 allele in late-onset familial Alzheimer disease. *Proc Natl Acad Sci U S A* **90**, 1977-1981 (1993).
9. L. A. Farrer *et al.*, Effects of age, sex, and ethnicity on the association between apolipoprotein E genotype and Alzheimer disease. A meta-analysis. APOE and Alzheimer Disease Meta Analysis Consortium. *JAMA* **278**, 1349-1356 (1997).
10. S. B. Sando *et al.*, APOE epsilon 4 lowers age at onset and is a high risk factor for Alzheimer's disease; a case control study from central Norway. *BMC neurology* **8**, 9 (2008).
11. D. C. Rubinsztein, D. F. Easton, Apolipoprotein E genetic variation and Alzheimer's disease. a meta-analysis. *Dementia and geriatric cognitive disorders* **10**, 199-209 (1999).
12. K. R. Bales *et al.*, Lack of apolipoprotein E dramatically reduces amyloid beta-peptide deposition. *Nat Genet* **17**, 263-264 (1997).
13. E. M. Castano *et al.*, Fibrillogenesis in Alzheimer's disease of amyloid beta peptides and apolipoprotein E. *Biochem J* **306 (Pt 2)**, 599-604 (1995).
14. G. W. Rebeck, J. S. Reiter, D. K. Strickland, B. T. Hyman, Apolipoprotein E in sporadic Alzheimer's disease: allelic variation and receptor interactions. *Neuron* **11**, 575-580 (1993).
15. D. E. Schmechel *et al.*, Increased amyloid beta-peptide deposition in cerebral cortex as a consequence of apolipoprotein E genotype in late-onset Alzheimer disease. *Proc Natl Acad Sci U S A* **90**, 9649-9653 (1993).
16. J. Ma, A. Yee, H. B. Brewer, Jr., S. Das, H. Potter, Amyloid-associated proteins alpha 1-antichymotrypsin and apolipoprotein E promote assembly of Alzheimer beta-protein into filaments. *Nature* **372**, 92-94 (1994).
17. J. M. Castellano *et al.*, Human apoE isoforms differentially regulate brain amyloid-beta peptide clearance. *Science translational medicine* **3**, 89ra57 (2011).

18. D. M. Holtzman *et al.*, Apolipoprotein E isoform-dependent amyloid deposition and neuritic degeneration in a mouse model of Alzheimer's disease. *Proc Natl Acad Sci U S A* **97**, 2892-2897 (2000).
19. Y. Huang, Abeta-independent roles of apolipoprotein E4 in the pathogenesis of Alzheimer's disease. *Trends in molecular medicine* **16**, 287-294 (2010).
20. A. B. Wolf *et al.*, Apolipoprotein E as a beta-amyloid-independent factor in alzheimer's disease. *Alzheimers Res Ther* **5**, 38 (2013).
21. E. M. Reiman *et al.*, Preclinical evidence of Alzheimer's disease in persons homozygous for the epsilon 4 allele for apolipoprotein E. *The New England journal of medicine* **334**, 752-758 (1996).
22. E. M. Reiman *et al.*, Functional brain abnormalities in young adults at genetic risk for late-onset Alzheimer's dementia. *Proc Natl Acad Sci U S A* **101**, 284-289 (2004).
23. E. M. Reiman *et al.*, Correlations between apolipoprotein E epsilon4 gene dose and brain-imaging measurements of regional hypometabolism. *Proc Natl Acad Sci U S A* **102**, 8299-8302 (2005).
24. Q. R. Ong, E. S. Chan, M. L. Lim, G. M. Cole, B. S. Wong, Reduced phosphorylation of brain insulin receptor substrate and Akt proteins in apolipoprotein-E4 targeted replacement mice. *Scientific reports* **4**, 3754 (2014).
25. N. Zhao *et al.*, Apolipoprotein E4 Impairs Neuronal Insulin Signaling by Trapping Insulin Receptor in the Endosomes. *Neuron* **96**, 115-129 e115 (2017).
26. L. A. Johnson *et al.*, Apolipoprotein E4 mediates insulin resistance-associated cerebrovascular dysfunction and the post-prandial response. *Journal of cerebral blood flow and metabolism : official journal of the International Society of Cerebral Blood Flow and Metabolism*, 271678X17746186 (2017).
27. L. A. Johnson, E. R. Torres, S. Impey, J. F. Stevens, J. Raber, Apolipoprotein E4 and Insulin Resistance Interact to Impair Cognition and Alter the Epigenome and Metabolome. *Scientific reports* **7**, 43701 (2017).
28. J. T. Keeney, S. Ibrahimi, L. Zhao, Human ApoE Isoforms Differentially Modulate Glucose and Amyloid Metabolic Pathways in Female Brain: Evidence of the Mechanism of Neuroprotection by ApoE2 and Implications for Alzheimer's Disease Prevention and Early Intervention. *Journal of Alzheimer's disease : JAD* **48**, 411-424 (2015).
29. L. Wu, X. Zhang, L. Zhao, Human ApoE Isoforms Differentially Modulate Brain Glucose and Ketone Body Metabolism: Implications for Alzheimer's Disease Risk Reduction and Early Intervention. *The Journal of neuroscience : the official journal of the Society for Neuroscience* **38**, 6665-6681 (2018).
30. S. Chang *et al.*, Lipid- and receptor-binding regions of apolipoprotein E4 fragments act in concert to cause mitochondrial dysfunction and neurotoxicity. *Proc Natl Acad Sci U S A* **102**, 18694-18699 (2005).
31. Y. Huang *et al.*, Apolipoprotein E fragments present in Alzheimer's disease brains induce neurofibrillary tangle-like intracellular inclusions in neurons. *Proc Natl Acad Sci U S A* **98**, 8838-8843 (2001).
32. T. Nakamura, A. Watanabe, T. Fujino, T. Hosono, M. Michikawa, Apolipoprotein E4 (1-272) fragment is associated with mitochondrial proteins and affects mitochondrial function in neuronal cells. *Mol Neurodegener* **4**, 35 (2009).

33. H. Braak, E. Braak, Neuropathological stageing of Alzheimer-related changes. *Acta neuropathologica* **82**, 239-259 (1991).
34. M. Bobinski *et al.*, MRI of entorhinal cortex in mild Alzheimer's disease. *Lancet* **353**, 38-40 (1999).
35. P. Shaw *et al.*, Cortical morphology in children and adolescents with different apolipoprotein E gene polymorphisms: an observational study. *Lancet neurology* **6**, 494-500 (2007).
36. G. A. Rodriguez, M. P. Burns, E. J. Weeber, G. W. Rebeck, Young APOE4 targeted replacement mice exhibit poor spatial learning and memory, with reduced dendritic spine density in the medial entorhinal cortex. *Learning & memory* **20**, 256-266 (2013).
37. X. Wang, M. L. Michaelis, E. K. Michaelis, Functional genomics of brain aging and Alzheimer's disease: focus on selective neuronal vulnerability. *Current genomics* **11**, 618-633 (2010).
38. S. Minoshima *et al.*, Metabolic reduction in the posterior cingulate cortex in very early Alzheimer's disease. *Ann Neurol* **42**, 85-94 (1997).
39. P. Giavalisco *et al.*, Elemental formula annotation of polar and lipophilic metabolites using (13) C, (15) N and (34) S isotope labelling, in combination with high-resolution mass spectrometry. *Plant J* **68**, 364-376 (2011).
40. V. Matyash, G. Liebisch, T. V. Kurzchalia, A. Shevchenko, D. Schwudke, Lipid extraction by methyl-tert-butyl ether for high-throughput lipidomics. *J Lipid Res* **49**, 1137-1146 (2008).
41. T. Nuriel *et al.*, The Endosomal-Lysosomal Pathway Is Dysregulated by APOE4 Expression in Vivo. *Front Neurosci* **11**, 702 (2017).
42. T. Nuriel *et al.*, Neuronal hyperactivity due to loss of inhibitory tone in APOE4 mice lacking Alzheimer's disease-like pathology. *Nature communications* **8**, 1464 (2017).
43. D. Speijer, Oxygen radicals shaping evolution: why fatty acid catabolism leads to peroxisomes while neurons do without it: FADH(2)/NADH flux ratios determining mitochondrial radical formation were crucial for the eukaryotic invention of peroxisomes and catabolic tissue differentiation. *BioEssays : news and reviews in molecular, cellular and developmental biology* **33**, 88-94 (2011).
44. S. P. Wang *et al.*, Metabolism as a tool for understanding human brain evolution: lipid energy metabolism as an example. *Journal of human evolution* **77**, 41-49 (2014).
45. P. Schonfeld, G. Reiser, Why does brain metabolism not favor burning of fatty acids to provide energy? Reflections on disadvantages of the use of free fatty acids as fuel for brain. *J Cereb Blood Flow Metab* **33**, 1493-1499 (2013).
46. K. A. Nalecz, D. Miecz, V. Berezowski, R. Cecchelli, Carnitine: transport and physiological functions in the brain. *Molecular aspects of medicine* **25**, 551-567 (2004).
47. D. Ebert, R. G. Haller, M. E. Walton, Energy contribution of octanoate to intact rat brain metabolism measured by 13C nuclear magnetic resonance spectroscopy. *J Neurosci* **23**, 5928-5935 (2003).
48. A. Panov, Z. Orynbayeva, V. Vavilin, V. Lyakhovich, Fatty acids in energy metabolism of the central nervous system. *BioMed research international* **2014**, 472459 (2014).

49. G. W. Rogers *et al.*, High throughput microplate respiratory measurements using minimal quantities of isolated mitochondria. *PLoS One* **6**, e21746 (2011).
50. M. D. Brand, D. G. Nicholls, Assessing mitochondrial dysfunction in cells. *Biochem J* **435**, 297-312 (2011).
51. L. Pirhaji *et al.*, Revealing disease-associated pathways by network integration of untargeted metabolomics. *Nature methods* **13**, 770-776 (2016).
52. A. M. Robinson, D. H. Williamson, Physiological roles of ketone bodies as substrates and signals in mammalian tissues. *Physiological reviews* **60**, 143-187 (1980).
53. Y. Zhang *et al.*, Ketosis proportionately spares glucose utilization in brain. *Journal of cerebral blood flow and metabolism : official journal of the International Society of Cerebral Blood Flow and Metabolism* **33**, 1307-1311 (2013).
54. A. L. Lin, W. Zhang, X. Gao, L. Watts, Caloric restriction increases ketone bodies metabolism and preserves blood flow in aging brain. *Neurobiology of aging* **36**, 2296-2303 (2015).
55. J. Thevenet *et al.*, Medium-chain fatty acids inhibit mitochondrial metabolism in astrocytes promoting astrocyte-neuron lactate and ketone body shuttle systems. *FASEB journal : official publication of the Federation of American Societies for Experimental Biology* **30**, 1913-1926 (2016).
56. N. Auestad, R. A. Korsak, J. W. Morrow, J. Edmond, Fatty acid oxidation and ketogenesis by astrocytes in primary culture. *Journal of neurochemistry* **56**, 1376-1386 (1991).
57. M. Guzman, C. Blazquez, Ketone body synthesis in the brain: possible neuroprotective effects. *Prostaglandins, leukotrienes, and essential fatty acids* **70**, 287-292 (2004).
58. M. G. Bixel, B. Hamprecht, Generation of ketone bodies from leucine by cultured astroglial cells. *Journal of neurochemistry* **65**, 2450-2461 (1995).
59. R. Murin, B. Hamprecht, Metabolic and regulatory roles of leucine in neural cells. *Neurochemical research* **33**, 279-284 (2008).
60. A. H. Emwas, The strengths and weaknesses of NMR spectroscopy and mass spectrometry with particular focus on metabolomics research. *Methods in molecular biology* **1277**, 161-193 (2015).
61. S. P. Bessman, The creatine phosphate energy shuttle--the molecular asymmetry of a "pool". *Analytical biochemistry* **161**, 519-523 (1987).
62. W. Chen, X. H. Zhu, G. Adriany, K. Ugurbil, Increase of creatine kinase activity in the visual cortex of human brain during visual stimulation: a 31P magnetization transfer study. *Magnetic resonance in medicine* **38**, 551-557 (1997).
63. A. Schousboe, L. K. Bak, H. S. Waagepetersen, Astrocytic Control of Biosynthesis and Turnover of the Neurotransmitters Glutamate and GABA. *Frontiers in endocrinology* **4**, 102 (2013).
64. M. Kreft, L. K. Bak, H. S. Waagepetersen, A. Schousboe, Aspects of astrocyte energy metabolism, amino acid neurotransmitter homoeostasis and metabolic compartmentation. *ASN neuro* **4**, (2012).
65. A. Falkowska *et al.*, Energy Metabolism of the Brain, Including the Cooperation between Astrocytes and Neurons, Especially in the Context of Glycogen Metabolism. *International journal of molecular sciences* **16**, 25959-25981 (2015).

66. A. B. Patel *et al.*, The contribution of GABA to glutamate/glutamine cycling and energy metabolism in the rat cortex in vivo. *Proc Natl Acad Sci U S A* **102**, 5588-5593 (2005).
67. R. Rossignol, M. Malgat, J. P. Mazat, T. Letellier, Threshold effect and tissue specificity. Implication for mitochondrial cytopathies. *J Biol Chem* **274**, 33426-33432 (1999).
68. A. M. Celotto, W. K. Chiu, W. Van Voorhies, M. J. Palladino, Modes of metabolic compensation during mitochondrial disease using the Drosophila model of ATP6 dysfunction. *PLoS One* **6**, e25823 (2011).
69. D. C. Chan, Mitochondria: dynamic organelles in disease, aging, and development. *Cell* **125**, 1241-1252 (2006).
70. B. E. Sansbury, S. P. Jones, D. W. Riggs, V. M. Darley-Usmar, B. G. Hill, Bioenergetic function in cardiovascular cells: the importance of the reserve capacity and its biological regulation. *Chemico-biological interactions* **191**, 288-295 (2011).
71. B. H. Goodpaster, L. M. Sparks, Metabolic Flexibility in Health and Disease. *Cell metabolism* **25**, 1027-1036 (2017).
72. F. Palmieri, The mitochondrial transporter family SLC25: identification, properties and physiopathology. *Molecular aspects of medicine* **34**, 465-484 (2013).
73. V. A. Saks *et al.*, Control of cellular respiration in vivo by mitochondrial outer membrane and by creatine kinase. A new speculative hypothesis: possible involvement of mitochondrial-cytoskeleton interactions. *Journal of molecular and cellular cardiology* **27**, 625-645 (1995).
74. I. Bratic, A. Trifunovic, Mitochondrial energy metabolism and ageing. *Biochimica et biophysica acta* **1797**, 961-967 (2010).
75. G. Yellen, Fueling thought: Management of glycolysis and oxidative phosphorylation in neuronal metabolism. *The Journal of cell biology* **217**, 2235-2246 (2018).
76. H. Eichenbaum, A cortical-hippocampal system for declarative memory. *Nat Rev Neurosci* **1**, 41-50 (2000).
77. L. M. Frank, E. N. Brown, M. Wilson, Trajectory encoding in the hippocampus and entorhinal cortex. *Neuron* **27**, 169-178 (2000).
78. A. V. Egorov, B. N. Hamam, E. Fransen, M. E. Hasselmo, A. A. Alonso, Graded persistent activity in entorhinal cortex neurons. *Nature* **420**, 173-178 (2002).
79. P. M. Sullivan, B. E. Mace, N. Maeda, D. E. Schmechel, Marked regional differences of brain human apolipoprotein E expression in targeted replacement mice. *Neuroscience* **124**, 725-733 (2004).
80. P. M. Sullivan *et al.*, Targeted replacement of the mouse apolipoprotein E gene with the common human APOE3 allele enhances diet-induced hypercholesterolemia and atherosclerosis. *J Biol Chem* **272**, 17972-17980 (1997).
81. Q. Chen *et al.*, Untargeted plasma metabolite profiling reveals the broad systemic consequences of xanthine oxidoreductase inactivation in mice. *PLoS One* **7**, e37149 (2012).
82. J. J. Miller, L. Cochlin, K. Clarke, D. J. Tyler, Weighted averaging in spectroscopic studies improves statistical power. *Magnetic resonance in medicine* **78**, 2082-2094 (2017).
83. S. W. Provencher, Estimation of metabolite concentrations from localized in vivo proton NMR spectra. *Magnetic resonance in medicine* **30**, 672-679 (1993).

FIGURE LEGENDS

Fig. 1. Transcriptomics analysis reveals an upregulation of electron transport chain genes in the EC of aged *APOE4* mice. RNA-sequencing was performed in order to analyze the effects of differential *APOE* isoform expression on RNA levels in the EC and PVC of aged *APOE* mice (19 *APOE3/4* males vs. 10 *APOE3/3* males). (A) Shown here are the significantly enriched KEGG pathways observed in the EC of *APOE3/4* vs. *APOE3/3* mice, using Cytoscape's ClueGo application, with the ten differentially expressed electron transport chain (ETC) genes circled. (B) Graphs of the differentially regulated ETC genes in the EC of the *APOE3/4* vs. *APOE3/3* mice. (** denotes $p < 0.01$; *** denotes $p < 0.001$; **** denotes $p < 0.0001$)

Fig. 2. Metabolomics analysis reveals differential expression of energy-related metabolites and fatty acids in the EC of aged *APOE4* mice. An untargeted metabolomics analysis was performed in order to analyze the effects of differential *APOE* isoform expression on small-molecule metabolite levels in the EC and PVC of aged *APOE* mice (8 *APOE3/3*, 9 *APOE3/4* and 7 *APOE4/4* males). (A-C) Shown here are graphs of the bioenergetics-related metabolite groups that were shown to be differentially expressed in the EC of the *APOE4/4* vs. *APOE3/3* mice: (A) General energy-related metabolites and (B) Fatty acids. (C) We have also calculated the ratio of ATP:ADP in each genotype group from the EC and PVC of the aged *APOE* mice. (* denotes $p < 0.05$; ** denotes $p < 0.01$; **** denotes $p < 0.0001$)

Fig. 3. Seahorse analysis reveals decreased mitochondrial respiration in the cortex and hippocampus, but not in the EC, of aged *APOE4* mice. Seahorse analysis was performed in order to analyze the effects of differential *APOE* isoform expression on mitochondrial respiration in mitochondria that were purified from the cortex (Ctx), hippocampus (Hip) and EC of aged *APOE* mice (2 *APOE4/4* males, tissues pooled vs. 2 *APOE3/3* males, tissues pooled). (A) The complex I- and complex II-driven ETC activity from each region shows decreased mitochondrial respiration in the mitochondria purified from the cortex and hippocampus, but not the EC of the aged *APOE4/4* mice. (B-C) Bar graphs showing the average oxygen consumption rate (OCR) from (B) State 3 and for (C) the Respiration Control Ratio (RCR; state 3u/state 4o) in mitochondria purified from each region of the *APOE4/4* mice, as a percentage of the *APOE3/3* OCR from the equivalent tissues. The dotted blue line represents the normalized levels in the *APOE3/3* tissues. (* denotes $p < 0.05$; ** denotes $p < 0.01$; *** denotes $p < 0.001$; **** denotes $p < 0.0001$)

Fig. 4. Proton nuclear magnetic resonance spectroscopy reveals differential expression of phosphocreatine, glutamate and GABA in the EC of aged *APOE4* mice. ^{1}H NMR spectroscopy was performed in order to analyze the effects of differential *APOE* isoform expression on the levels of high-abundance metabolites in the EC of anesthetized *APOE* mice (7 *APOE4/4* males vs. 7 *APOE3/3* males). (A) A representative coronal anatomical image used in the analysis, with the volume of interest, highlighted in green, shown over the EC. (B) A typical spectrum from the EC showing the spectral position of some major metabolites: N-Acetylaspartic acid (NAA), glutamate (Glu), total creatine (tCr) and total choline (tCho). The raw spectrum is shown in black (with no smoothing), and the software fit of the model spectra shown in red. The top of the figure shows the difference between the raw spectrum and the fit, with a "good fit" showing random oscillations with little noise. The solid black line at bottom of the figure is the baseline. (C) The metabolite concentrations in the EC of aged *APOE3/3* and *APOE4/4* mice. The metabolites reported are: alanine (Ala), aspartate (Asp), creatine (Cr), phosphocreatine (PCr), gamma-aminobutyric acid (GABA), glucose (Glc), glutamine (Gln), glutamate (Glu), glycerophosphocholine (GPC), phosphocholine (PCh), glutathione (GSH), myo-inositol (Ins), lactate (Lac), N-Acetylaspartate (NAA), N-Acetylaspartateglutamate (NAAG), taurine (Tau), total choline (GPC and PCh), total NAA (NAA and NAAG), total creatine (Cr and PCr) and total glutamate and glutamine (Glu and Gln). (* denotes $p < 0.05$; ** denotes $p < 0.01$; *** denotes $p < 0.001$; **** denotes $p < 0.0001$)

Fig. 5. Identification of differentially expressed bioenergetic genes and metabolites in the EC of aged *APOE4* mice. A schematic of the bioenergetics genes and metabolites that have been predicted to be altered by differential *APOE* isoform expression in this study, as depicted in a simplified manner with respect to their relationships to each other and their location inside or outside of mitochondria. Genes or metabolites that were putatively identified as increased in aged *APOE4* mice, as compared to aged *APOE3* mice, are marked with a green arrow, and those that are decreased are marked with a red arrow.

Fig. 6. Targeted lipidomics reveals differential expression of diacyglycerols and bis(monacylglycero)phosphates in the EC of aged *APOE4* mice. A targeted lipidomic analysis was performed in order to analyze the effects of differential *APOE* isoform expression on lipid levels in the EC and PVC of aged *APOE* mice (8 *APOE3/3*, 9 *APOE3/4* and 7 *APOE4/4* males). (A-C) Shown here are graphs of the three primary groups of lipids that were shown to be differentially expressed in the EC of the *APOE4/4* vs. *APOE3/3* mice: (A) Diacylglycerols, (B) Bis(monoacylglycero)phosphates, and (C) Hexosylceramides, which include both glucosylceramides and galactosylceramides. (* denotes $p < 0.05$; ** denotes $p < 0.01$; *** denotes $p < 0.001$; **** denotes $p < 0.0001$)

Fig. 1

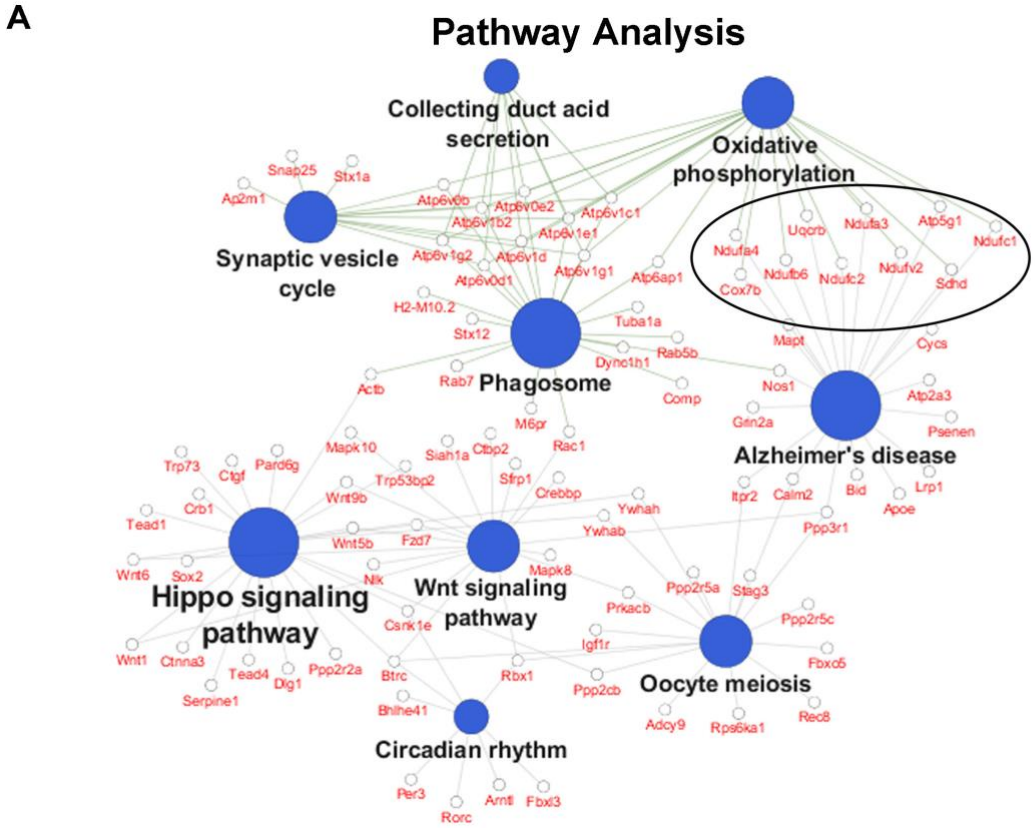
A
Pathway Analysis
Collecting duct acid secretion
Oxidative phosphorylation
Synaptic vesicle cycle
Phagosome
Alzheimer's disease
Hippo signaling pathway
Wnt signaling pathway
Oocyte meiosis
Circadian rhythm

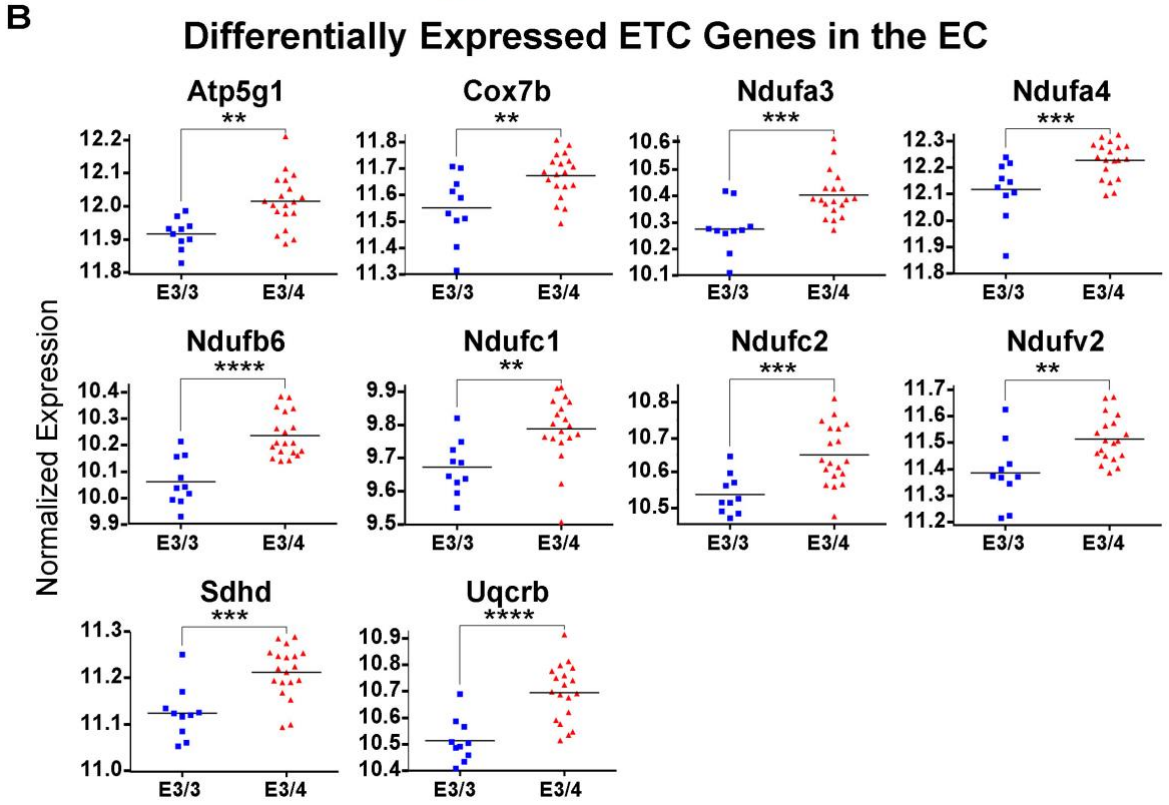
B
Differentially Expressed ETC Genes in the EC
Normalized Expression
Atp5g1
Cox7b
Ndufa3
Ndufa4
Ndufb6
Ndufc1
Ndufc2
Ndufv2
Sdhd
Uqcrb
E3/3
E3/4

Fig. 2

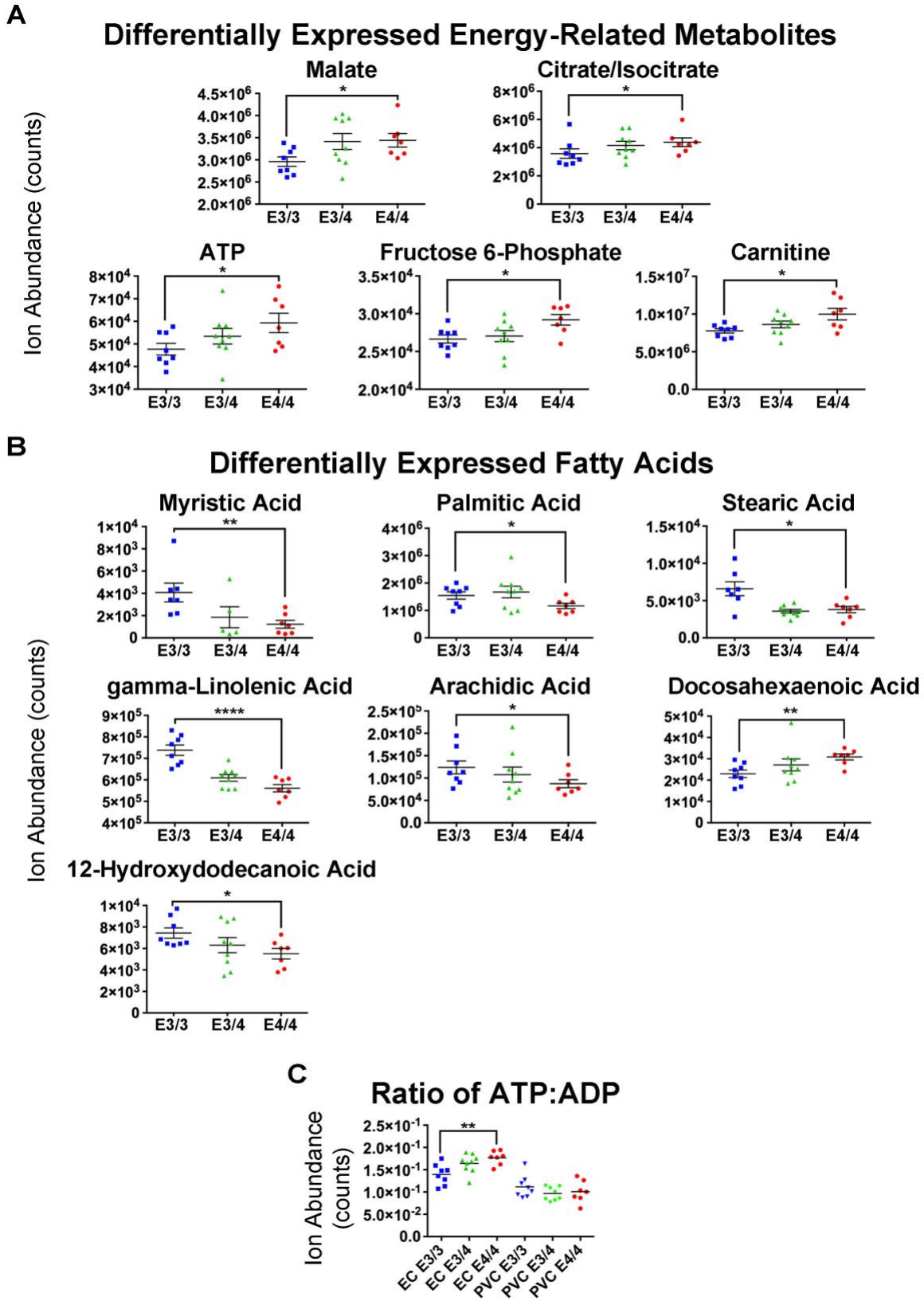
A
Differentially Expressed Energy-Related Metabolites
Malate
Citrate/Isocitrate
ATP
Fructose 6-Phosphate
Carnitine
Ion Abundance (counts)
E3/3
E3/4
E4/4
B
Differentially Expressed Fatty Acids
Myristic Acid
Palmitic Acid
Stearic Acid
gamma-Linolenic Acid
Arachidic Acid
Docosahexaenoic Acid
12-Hydroxydodecanoic Acid
Ion Abundance (counts)
C
Ratio of ATP:ADP
Ion Abundance (counts)
EC E3/3
EC E3/4
EC E4/4
PVC E3/3
PVC E3/4
PVC E4/4

Fig. 3

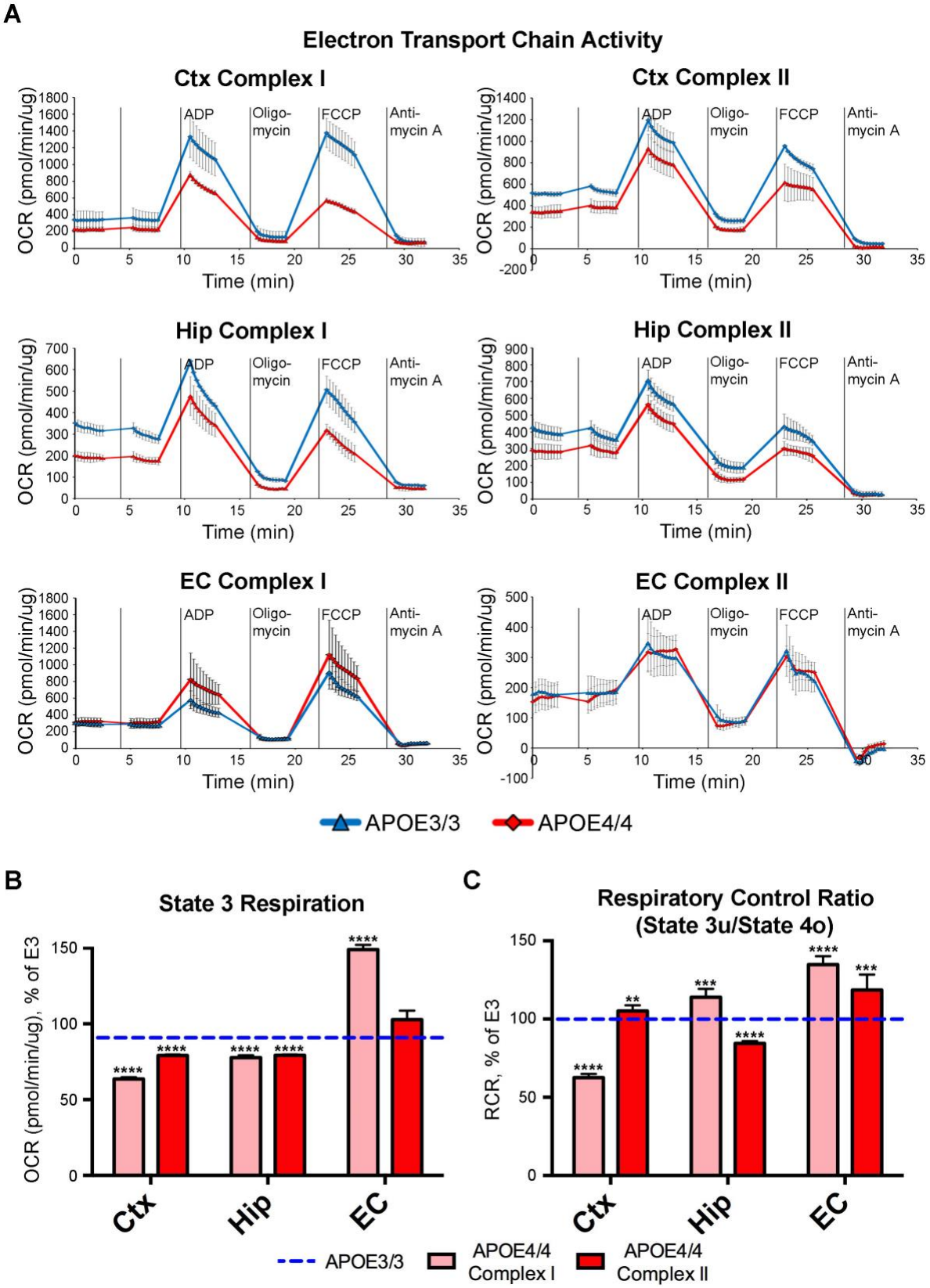
A
Electron Transport Chain Activity
Ctx Complex I
Ctx Complex II
Hip Complex I
Hip Complex II
EC Complex I
EC Complex II
OCR (pmol/min/ug)
Time (min)
ADP
Oligo-mycin
FCCP
Anti-mycin A
APOE3/3
APOE4/4
B
State 3 Respiration
OCR (pmol/min/ug), % of E3
Ctx
Hip
EC
C
Respiratory Control Ratio (State 3u/State 4o)
RCR, % of E3
APOE3/3
APOE4/4 Complex I
APOE4/4 Complex II

Fig. 4

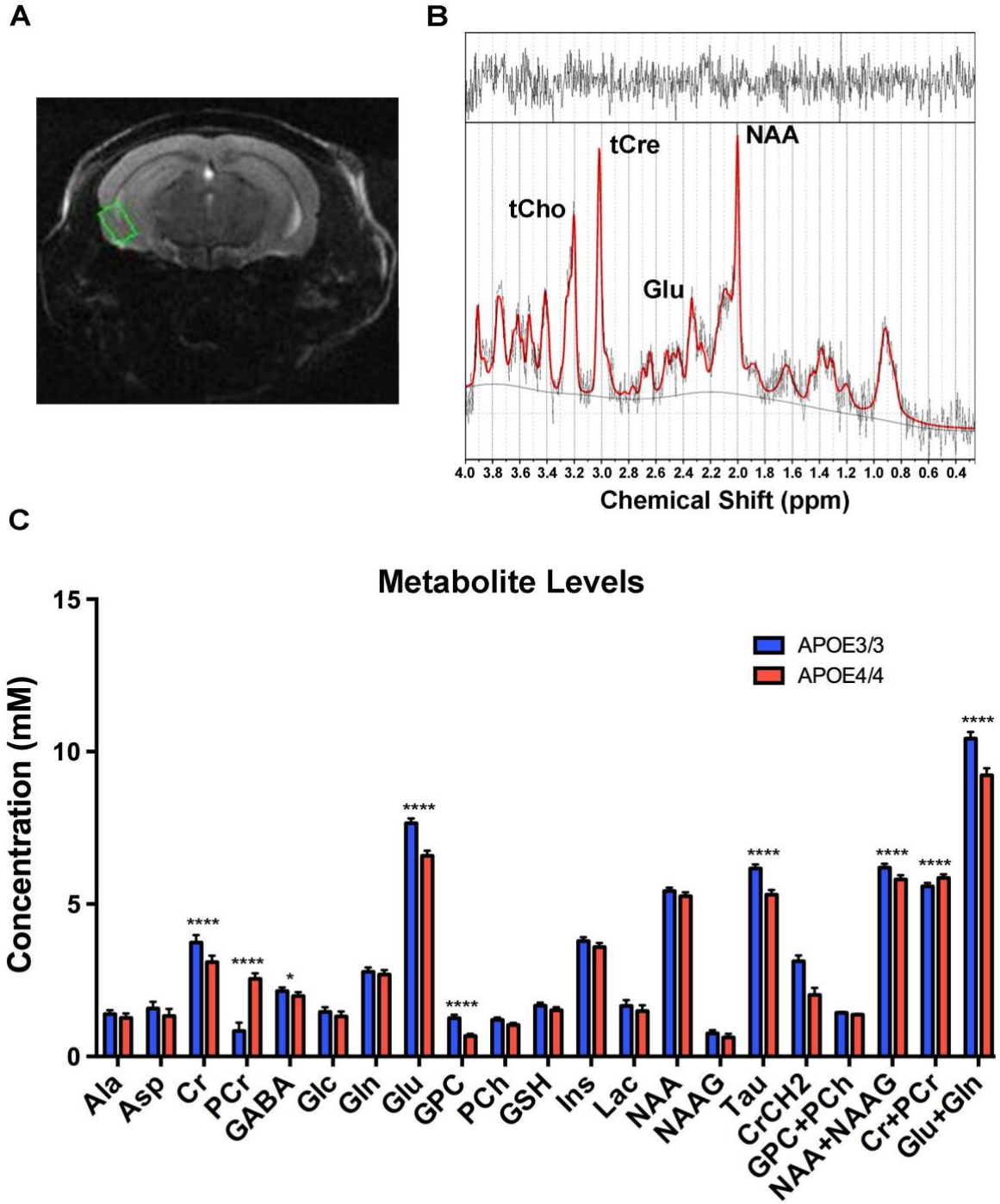
A
B
tCre
NAA
tCho
Glu
4.0 3.8 3.6 3.4 3.2 3.0 2.8 2.6 2.4 2.2 2.0 1.8 1.6 1.4 1.2 1.0 0.8 0.6 0.4
Chemical Shift (ppm)
C
Metabolite Levels
Concentration (mM)
0
5
10
15
APOE3/3
APOE4/4
Ala
Asp
Cr
PCr
GABA
Glc
Gln
Glu
GPC
PCh
GSH
Ins
Lac
NAA
NAAG
Tau
CrCH2
GPC+PCh
NAA+NAAG
Cr+PCr
Glu+Gln

Fig. 5

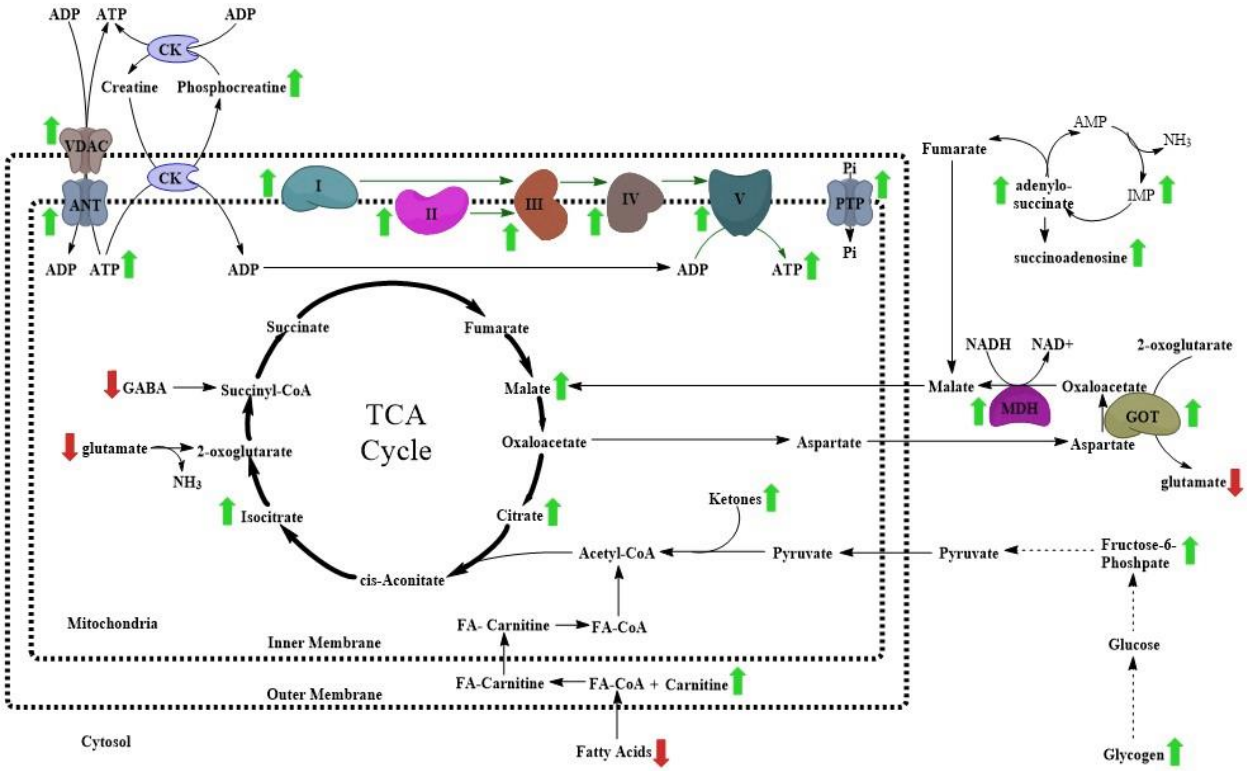
ADP
ATP
ADP
CK
Creatine
Phosphocreatine
VDAC
ANT
CK
I
II
III
IV
V
Pi
PTP
Pi
ADP
ATP
ADP
ADP
ATP
Fumarate
AMP
NH3
adenylo-
succinate
IMP
succinoadenosine
Succinate
Fumarate
GABA
Succinyl-CoA
Malate
TCA
Cycle
glutamate
2-oxoglutarate
NH3
Oxaloacetate
Aspartate
Isocitrate
Citrate
Ketones
Acetyl-CoA
Pyruvate
cis-Aconitate
Mitochondria
Inner Membrane
FA- Carnitine
FA-CoA
Outer Membrane
FA-Carnitine
FA-CoA + Carnitine
Cytosol
Fatty Acids
NADH
NAD+
2-oxoglutarate
Malate
Oxaloacetate
MDH
GOT
Aspartate
glutamate
Pyruvate
Fructose-6-
Phoshpate
Glucose
Glycogen

Table 1. Differentially expressed targeted metabolites from the EC of APOE3 vs. E4 mice

Metabolite	Regulation in E4/4	Fold Change	p-value	FDR	Detection Mode	CAS Number
Fatty Acids						
gamma-Linolenic Acid	down	1.31	1.19E-03	0.093	positive	506-26-3
Myristic Acid	down	3.92	0.004	0.118	positive	544-63-8
Docosahexaenoic Acid	up	1.36	0.011	0.154	positive	6217-54-5
Stearic Acid	down	1.69	0.011	0.154	positive	57-11-4
12-Hydroxydodecanoic Acid	down	1.36	0.021	0.213	positive	505-95-3
Arachidic Acid	down	1.40	0.037	0.230	negative	506-30-9
Palmitic Acid	down	1.32	0.049	0.243	negative	57-10-3
Oligosaccharides						
trisaccharide	up	1.99	0.001	0.049	negative	512-69-6
tetrasaccharide	up	2.24	0.015	0.169	negative	10094-58-3
disaccharide	up	2.20	0.015	0.169	negative	63-42-3
Vitamin and Vitamin Derivatives						
Phylloquinone	up	1.47	0.003	0.102	positive	84-80-0
Tocopherol	up	2.74	0.005	0.123	negative	59-02-9
Dehydroascorbic acid	up	1.76	0.008	0.134	positive	490-83-5
Energy-Related Metabolites						
Inosine 5'-monophosphate (IMP)	up	2.26	0.003	0.0720	negative	131-99-7
D-Fructose 6-phosphate	up	1.10	0.011	0.169	negative	643-13-0
Succinoadenosine	up	1.47	0.011	0.169	negative	4542-23-8
Carnitine	up	1.27	0.021	0.213	positive	541-15-1
Citric Acid/Isocitric Acid	up	1.24	0.028	0.230	negative	77-92-9/ 1637-73-6
Malic Acid	up	1.16	0.037	0.230	negative	97-67-6
ATP	up	1.24	0.049	0.243	negative	56-65-5
Cholesterol Metabolites						
Lanosterol	up	2.27	0.015	0.169	negative	79-63-0
Cholesteryl Acetate	up	2.29	0.015	0.169	negative	604-35-3
Amino Acids						
Leucine	up	1.26	0.015	0.169	negative	61-90-5
Proline	up	1.12	0.037	0.230	negative	147-85-3
Glycine	up	1.10	0.037	0.230	negative	56-40-6
Tryptophan Metabolites						
Quinaldic Acid	up	1.68	0.001	0.049	negative	93-10-7
Kynurenine	up	2.49	0.015	0.169	negative	2922-83-0
Kynurenic Acid	up	1.32	0.049	0.243	negative	492-27-3

Cysteine and Methionine Metabolites						
S-Adenosylhomocysteine	up	1.15	0.021	0.213	positive	979-92-0
Histidine Metabolism						
Carnosine	up	1.31	0.037	0.230	negative	305-84-0
Arginine and Proline Metabolites						
4-Oxoproline	up	1.30	0.003	0.102	positive	4347-18-6
Tyrosine Metabolites						
Vanylglycol (MHPG)	up	1.64	0.011	0.169	negative	67423-45-4
Tyramine	up	1.06	0.028	0.216	positive	51-67-2
Thymidine	down	1.49	0.028	0.216	positive	50-89-5
Uracil	down	1.38	0.049	0.243	negative	66-22-8
Purine Metabolism						
GMP	up	1.14	0.028	0.230	negative	85-32-5
Miscellaneous						
Hydroxybutyric acid	up	1.35	0.002	0.055	negative	5094-24-6
Methylglutarylcarnitine	up	2.42	0.005	0.134	positive	102673-95-0
Trimethylamine N-oxide	up	2.65	0.021	0.213	positive	1184-78-7
2-Hydroxypyridine	up	1.36	0.037	0.275	positive	142-08-5
N-Acetylneuraminic Acid	up	1.23	0.037	0.230	negative	131-48-6

Table 2. Differentially expressed targeted metabolites from the PVC of APOE3 vs. E4 mice

Metabolite	Regulation in E4/4	Fold Change	p-value	FDR	Detection Mode	CAS Number
Fatty Acids						
gamma-Linolenic Acid	down	1.19	0.003	0.068	positive	506-26-3
Palmitic Acid	down	1.32	0.021	0.212	negative	57-10-3
10-Hydroxydecanoate	up	2.22	0.015	0.195	positive	1679-53-4
Docosahexaenoic Acid	down	2.03	0.021	0.212	negative	6217-54-5
Arachidonic acid	down	1.45	0.021	0.212	negative	506-32-1
Oligosaccharides						
trisaccharide	up	1.82	0.015	0.212	negative	
tetrasaccharide	up	2.70	0.021	0.212	negative	
Vitamin and Vitamin Derivatives						
Dehydroascorbic acid	up	2.03	0.001	0.062	positive	490-83-5
Phylloquinone	up	1.90	0.001	0.062	positive	84-80-0
Ascorbic acid	up	105.84	0.005	0.192	negative	50-81-7
Tocopherol	up	2.28	0.008	0.192	negative	59-02-9
Energy-Related Metabolites						
Acetylcarnitine	up	1.40	0.003	0.068	positive	3040-38-8
Carnitine	up	1.31	0.011	0.154	positive	541-15-1
Coenzyme A (CoA)	up	2.82	0.028	0.282	positive	85-61-0
Pyruvate	up	1.43	0.028	0.238	negative	127-17-3
Acetoacetic Acid	up	1.40	0.028	0.238	negative	541-50-4
Cholesterol Metabolites						
Taurodeoxycholate	up	1.94	0.003	0.068	positive	516-50-7
Cholesteryl Acetate	up	2.24	0.008	0.192	negative	604-35-3
Lanosterol	up	2.50	0.011	0.192	negative	79-63-0
Amino Acids						
Tyrosine	up	1.25	0.037	0.270	negative	60-18-4
Serine	down	1.18	0.049	0.270	negative	56-45-1
Glutamate	down	1.08	0.049	0.282	positive	56-86-0
Cysteine and Methionine Metabolites						
Pterin	down	3.91	0.002	0.192	negative	2236-60-4
Histidine Metabolites						
Urocanic acid	down	1.34	0.021	0.212	negative	104-98-3
Carnosine	up	1.32	0.028	0.282	positive	305-84-0
Arginine and Proline Metabolites						

Phosphocreatine	up	1.62	0.037	0.282	positive	67-07-2
4-Guanidinobutyric Acid	down	1.09	0.049	0.270	negative	463-00-3
Threonine Metabolites						
2-Ketobutyric Acid	up	1.43	0.021	0.212	negative	600-18-0
Tyrosine Metabolites						
Homovanillic Acid	down	1.30	0.049	0.270	negative	306-08-1
Riboflavin Metabolites						
2,4-Dihydroxypteridine (Lumazine)	up	2.07	0.008	0.154	positive	487-21-8
Flavin adenine dinucleotide (FAD)	up	1.19	0.021	0.212	negative	146-14-5
Lumichrome	down	1.71	0.049	0.282	positive	1086-80-2
Pyrimidine Metabolites						
2-Aminoisobutyric acid	up	1.38	0.011	0.154	positive	62-57-7
UMP	up	1.22	0.049	0.270	negative	58-97-9
CMP	up	1.29	0.049	0.282	positive	63-37-6
Miscellaneous						
Lipoic Acid	up	3.76	0.005	0.192	negative	1077-28-7
Thiourea	down	1.45	0.008	0.192	negative	62-56-6
Butyrylcarnitine	up	1.24	0.011	0.154	positive	25576-40-6
Hydroxybutyric Acid	up	1.49	0.011	0.192	negative	
Indoxyl Sulfate	down	2.12	0.021	0.212	negative	2642-37-7
3-Hydroxymethylglutaric Acid	up	1.27	0.028	0.238	negative	503-49-1
2-Hydroxypyridine	up	1.45	0.037	0.282	positive	142-08-5
Maleic acid	up	1.92	0.037	0.270	negative	110-16-7
N-Acetylneuraminic Acid	up	1.17	0.037	0.282	positive	131-48-6
N-Methylglutamic Acid	down	1.19	0.049	0.270	negative	35989-16-3
2-Aminoadipic Acid	down	1.17	0.049	0.270	negative	542-32-5
Cytidine diphosphate choline (CDPcholine)	down	1.17	0.049	0.282	positive	987-78-0
Glutathione	up	1.49	0.049	0.282	positive	70-18-8

Table 3. GO biological processes observed in the PIUMet analysis of differentially expressed untargeted metabolites from the EC of *APOE4/4* vs. *APOE3/3* mice

GO Term	Enrichment	p-value	FDR
carboxylic acid transport	12.35	9.80E-20	1.43E-16
carboxylic acid transmembrane transport	22.34	1.36E-16	1.04E-13
long-chain fatty acid metabolic process	18.08	2.77E-13	1.50E-10
fatty acid metabolic process	7.8	1.45E-11	5.40E-09
indolalkylamine metabolic process	44.68	2.48E-09	6.68E-07
disaccharide metabolic process	63.29	6.92E-09	1.77E-06
IMP metabolic process	48.69	3.47E-08	7.43E-06
steroid metabolic process	6.87	1.78E-07	3.24E-05
maltose metabolic process	126.58	4.81E-07	8.06E-05
kynurenine metabolic process	50.63	7.51E-07	1.18E-04
IMP biosynthetic process	50.63	7.51E-07	1.19E-04
tryptophan catabolic process	50.63	7.51E-07	1.20E-04
'de novo' IMP biosynthetic process	63.29	9.46E-06	1.13E-03
ketone catabolic process		3.90E-05	3.92E-03
dopamine metabolic process	20.25	4.12E-05	4.06E-03
neurotransmitter catabolic process	37.97	5.54E-05	5.25E-03
keratan sulfate catabolic process	31.65	1.00E-04	8.37E-03
vitamin metabolic process	6.38	3.60E-04	2.35E-02

Table 4. Metabolite concentrations in the EC of *APOE3/3* and *APOE4/4* mice, as observed by ^{1}H NMR spectroscopy

Metabolite	*APOE3/3* concentration (mM)	*APOE4/4* concentration (mM)	p-value
Creatine (Cr)	3.73 +/- 0.25	3.09 +/- 0.21	3.04E-04
Phosphocreatine (PCr)	0.84 +/- 0.27	2.55 +/- 0.18	1.00E-05
Gamma-aminobutyrate (GABA)	2.14 +/- 0.12	1.98 +/- 0.13	0.036
Glutamate (Glu)	7.65 +/- 0.15	6.58 +/- 0.17	5.30E-05
Glycerophosphocholine (GPC)	1.25 +/- 0.12	0.67 +/- 0.07	2.90E-05
Taurine (Tau)	6.16 +/- 0.14	5.31 +/- 0.15	1.59E-05
Cr+PCr	5.58 +/- 0.11	5.85 +/- 0.12	8.90E-04
Glu+Gln	10.43 +/- 0.21	9.22 +/- 0.23	2.30E-05
NAA+NAAG	6.19 +/-0.14	5.81 +/- 0.12	8.90E-04

Table 5. Differentially expressed targeted lipids from the EC of APOE4/4 vs. APOE3/3 mice

Metabolite	Regulation in E4/4	Fold Change	p-value
Cholesteryl esters			
CE 18:0	down	1.44	0.039
Diacylglycerols			
DAG 28:0/14:0	down	1.33	0.003
DAG 30:0/14:0	down	1.50	0.002
DAG 32:0/16:0	down	1.30	0.006
DAG 32:1/16:0	down	1.45	0.001
DAG 32:2/16:1	down	1.38	0.031
DAG 34:1/16:0	down	1.28	0.011
DAG 34:2/16:0	down	1.38	0.016
DAG 38:3/18:0	down	1.24	0.032
DAG 38:4/18:1	down	1.32	0.022
DAG 40:6/18:0	down	1.19	0.013
Ceramides			
Cer 18:1	up	1.60	2.00E-04
Sphingomyelins			
SM 18:0	down	1.09	0.045
Hexosylceramides (glucosyl- and galactosyl-)			
HexCer 16:0	up	2.45	1.19E-05
HexCer 16:1	up	1.50	0.001
HexCer 18:0	up	1.43	0.020
HexCer 20:0	up	1.47	0.027
HexCer 26:0	up	2.08	0.049
Sulfatides			
Sulf(2OH) 18:0	up	1.31	0.028
Lactosylceramides			
LacCer 16:0	up	1.81	0.005
Phosphatidic acids			
PA 40:6	up	1.18	0.044
Phosphatidylcholines			
PC 30:0	down	1.14	0.045
PC 36:0	up	1.11	0.006
PC 42:7	up	1.28	0.020
Phosphatidylinositols			
PI 38:3	down	1.39	0.003
PI 38:4	down	1.32	0.033
Phosphatidylserines			

PS 42:4	up	1.33	0.022
PS 42:5	up	1.29	0.031
Lyso ether phosphatidylcholines			
LPCe 18:0	up	1.14	0.010
Lyso phosphatidylinositols			
LPI 16:0	down	1.15	0.002
Bis(monoacylglycero) phosphates, LBPA			
BMP 32:0	up	1.41	0.003
BMP 34:0	up	1.39	0.014
BMP 34:1	up	1.37	0.013
BMP 36:0	up	1.75	0.011
BMP 36:1	up	1.44	0.014
BMP 38:4	up	1.95	0.011

Table 6. Differentially expressed targeted lipids from the PVC of APOE4/4 vs. APOE3/3 mice

Metabolite	Regulation in E4/4	Fold Change	p-value
Diacylglycerols			
DAG 38:3/18:1	down	1.47	0.023
DAG 40:5/18:0	down	1.41	0.014
Ceramides			
Cer 18:1	down	1.30	0.017
Sphingomyelins			
SM 16:0	down	1.30	0.015
SM 20:0	down	1.27	0.011
Dihydrosphingomyelins			
dhSM 16:0	down	1.64	0.020
Hexosylceramides (glucosyl- and galactosyl-)			
HexCer 16:1	down	1.56	3.16E-04
Ether phosphatidylcholines			
PCe 36:0	down	1.26	0.043
PCe 40:6	down	1.29	0.005
Lyso ether phosphatidylcholines			
LPCe 16:0	down	1.53	0.007
Bis(monoacylglycero) phosphates, LBPA			
BMP 32:0	up	1.66	0.041
BMP 32:1	up	1.54	0.031
BMP 34:0	up	1.62	0.035
BMP 34:2	up	1.36	0.007
N-acyl phosphatidylserines			
NAPS 38:4	up	2.09	0.024

Supplementary Material

APOE4 is Associated with Differential Regional Vulnerability to Bioenergetic Deficits in Aged *APOE* Mice

Tal Nuriel[1,2,*], Delfina Larrea[1,3], David N. Guilfoyle[4], Leila Pirhaji[5], Kathleen Shannon[6], Hirra Arain[1,2], Archana Ashok[1,2], Marta Pera[1,3], Qiuying Chen[7], Allissa A. Dillman[8], Helen Y. Figueroa[1,2], Mark R. Cookson[8], Steven S. Gross[7], Ernest Fraenkel[5,9], Karen E. Duff[1,2,10, †], and Estela Area-Gomez[1,3, †]

* Corresponding author: Tal Nuriel, email: tn2283@cumc.columbia.edu

[†]These two authors contributed equally to this work and are co-senior authors.

FIGURE LEGENDS

Supplementary Fig. S1. Seahorse analysis reveals decreased mitochondrial respiration in the PVC, but not in the EC, of aged *APOE4* mice. Seahorse analysis was performed in order to analyze the effects of differential *APOE* isoform expression on mitochondrial respiration in mitochondria that were purified from the PVC and EC of aged *APOE* mice (4 *APOE4/4* males, tissues pooled vs. 4 *APOE3/3* males, tissues pooled). (A) The complex I- and complex II-driven ETC activity from each region shows decreased mitochondrial respiration in the mitochondria purified from the PVC, but not the EC of the aged *APOE4/4* mice. (B-C) Bar graphs showing the average oxygen consumption rate (OCR) from (B) State 3 and for (C) the Respiration Control Ratio (RCR; state 3u/state 4o) in mitochondria purified from each region of the *APOE4/4* mice, as a percentage of the *APOE3/3* OCR from the equivalent tissues. The dotted blue line represents the normalized levels in the *APOE3/3* tissues. (* denotes $p < 0.05$; ** denotes $p < 0.01$; *** denotes $p < 0.001$; **** denotes $p < 0.0001$)

Supplementary Fig. S2. Western blot and qPCR analysis shows no significant effects of APOE4 on mitochondrial mass or ETC protein expression. Western blotting and qPCR analysis was performed in order to investigate the effects of differential APOE isoform expression on various markers of mitochondrial mass and ETC proteins in the EC, Hip and Ctx of 21-month-old *APOE4/4* vs. *APOE3/3* mice. (A-B) Western blot analysis did not reveal any unique differences in the levels of mitochondrial outer membrane protein Tom20 or in ETC complex subunits between genotypes in the EC. Likewise, (C) the ratio of Mitochondrial:Nuclear DNA, as well as (D) the levels of PGC1α RNA were unchanged between *APOE* genotypes in the EC of 21-month-old *APOE* mice. (* denotes $p < 0.05$; ** denotes $p < 0.01$)

Supplementary Fig. S3. Results network from the PIUMet analysis of differentially expressed untargeted metabolites from the EC of *APOE4/4* vs. *APOE3/3* mice. Shown here is the results-network that was generated from the PIUMet (Prize-collecting Steiner forest algorithm for Integrative Analysis of Untargeted Metabolomics) analysis. PIUMet was able to predict identities for the differential expressed unidentified metabolite features or peaks detected in the EC of aged *APOE4/4 vs. APOE3/3* mice (corrected p-value <0.05, 4 *APOE4/4* males, tissues pooled vs. 4 *APOE3/3* males, tissues pooled). The resulting network shows 242 nodes connected by 328 edges. Input metabolite peaks or features are shown as red triangles, while grey circles represent proteins and square nodes display the metabolites in the network. The metabolites directly connected to the differential metabolite features show their putative identities. The size of the nodes reflects the specificity score and the thickness of the edges the confidence of the interaction. In addition, the robustness score of each node is associated with the thickness of each node line width.

Supplementary Fig. S1

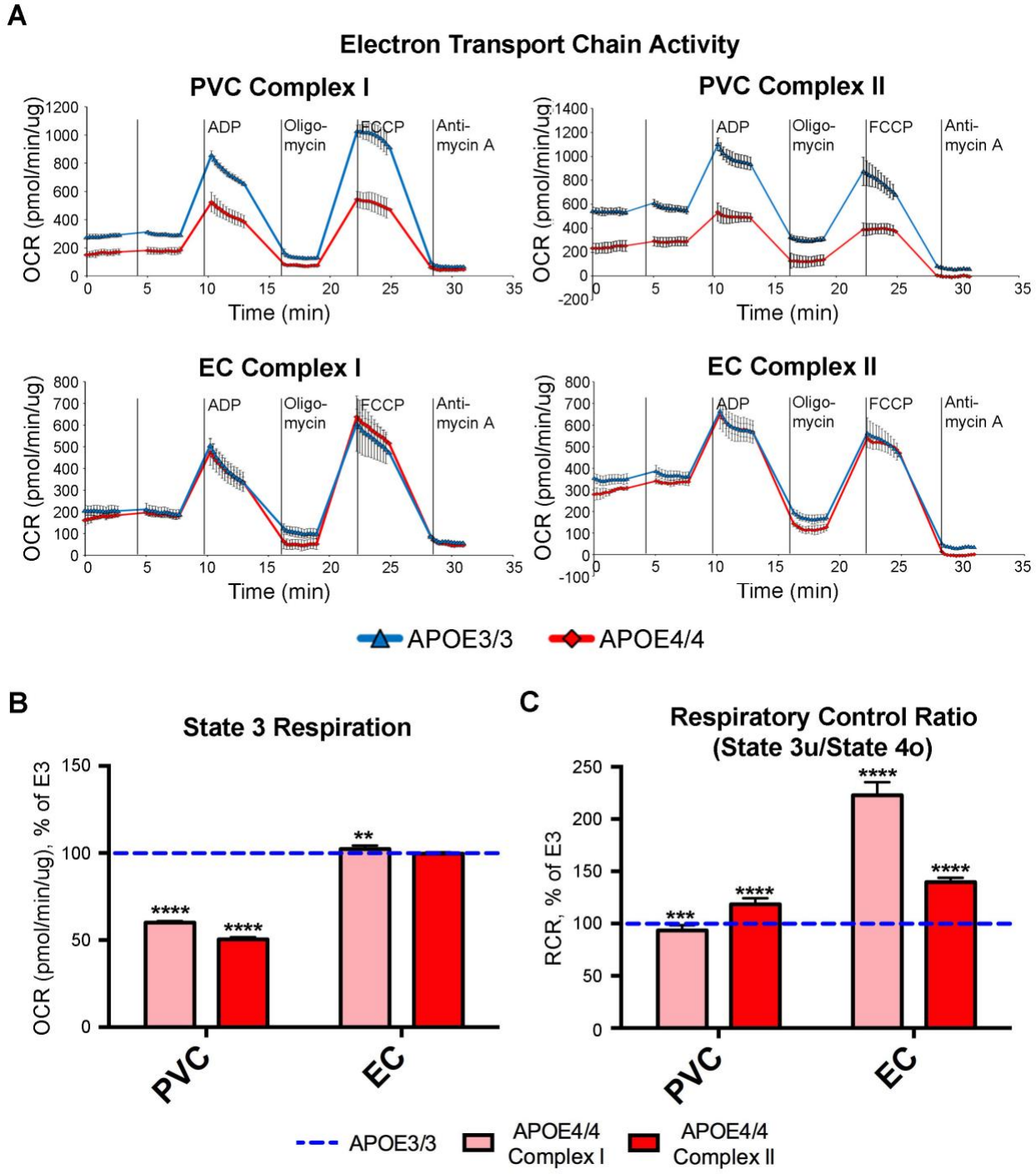

Supplementary Fig. S2

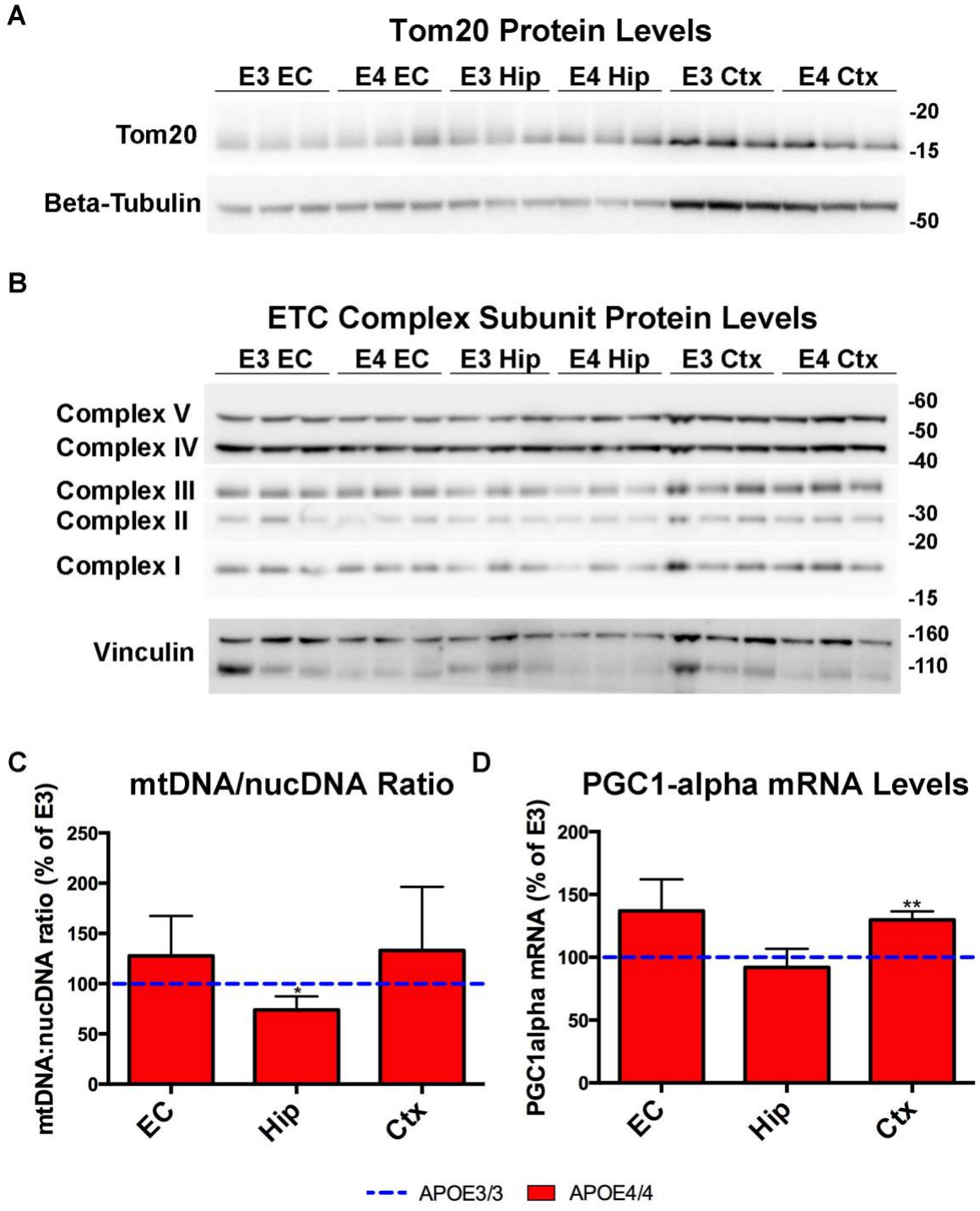

Supplementary Fig. S3 (high-res version available as supplemental file)

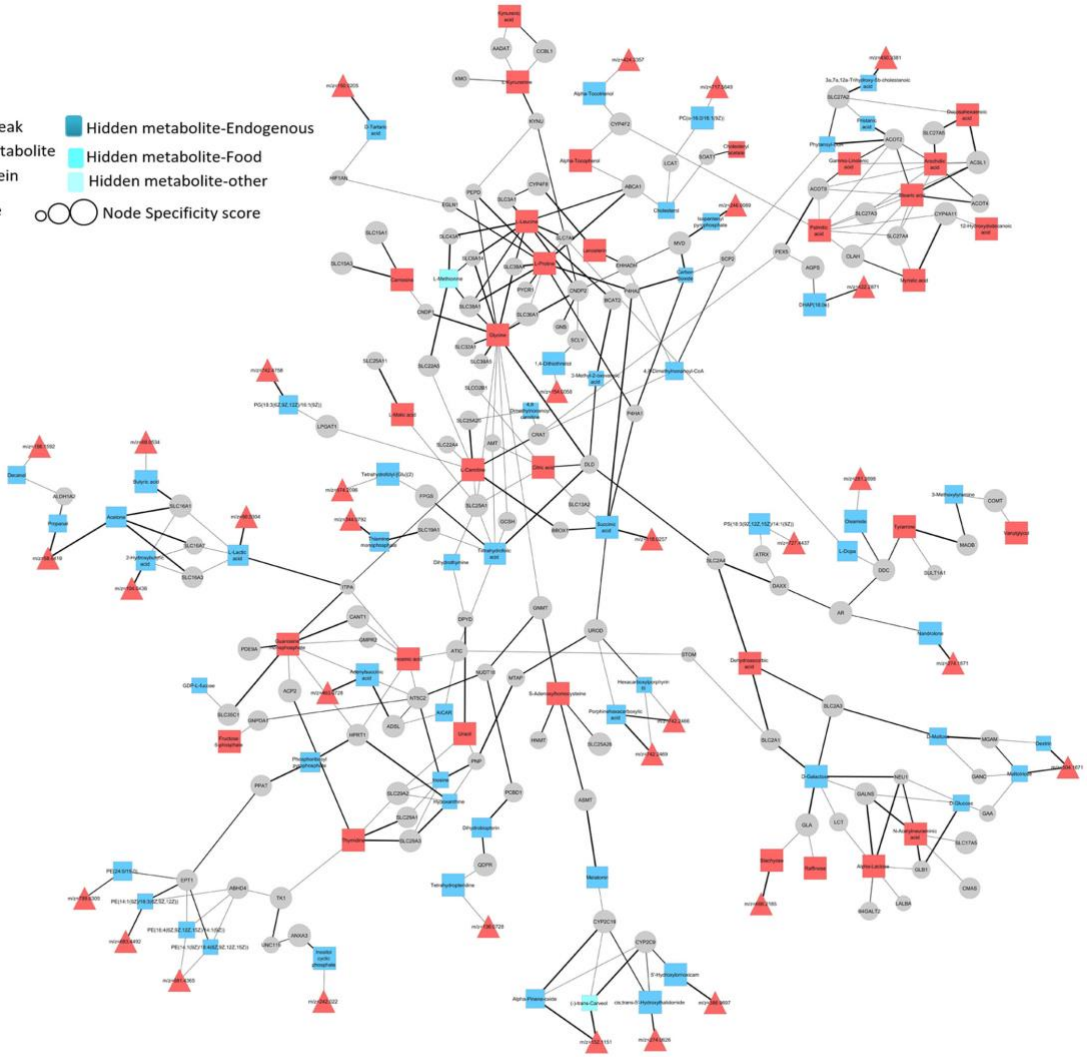

Supplementary Table S1. Differentially expressed genes from the EC of *APOE3/4* vs. *APOE3/3* mice

Gene Name	log2 FoldChange	p-value	FDR
Serpina3m	3.97	1.86E-166	3.41E-162
Serpina3n	1.95	4.65E-147	4.26E-143
Oscar	2.20	1.09E-60	6.67E-57
Rdh13	-0.44	1.37E-24	6.29E-21
Myadm	0.34	3.96E-14	1.45E-10
Thnsl1	0.50	4.69E-13	1.43E-09
Gm12762	1.14	4.52E-12	1.18E-08
Mboat7	0.21	6.98E-12	1.60E-08
Ica1	-0.35	1.55E-11	2.57E-08
Syngr3	0.26	1.38E-11	2.57E-08
Tmc4	0.62	1.42E-11	2.57E-08
Asprv1	-0.71	1.36E-10	1.92E-07
Fbxl2	0.18	1.35E-10	1.92E-07
Gm1082	1.04	1.76E-10	2.30E-07
Gm1078	-0.61	5.46E-10	6.67E-07
Wdfy1	-0.52	6.90E-10	7.90E-07
Srcap	-0.38	9.06E-10	9.63E-07
Zbtb20	-0.57	9.46E-10	9.63E-07
Dpysl2	-0.38	2.18E-09	2.00E-06
Pon2	-0.28	2.13E-09	2.00E-06
Gm15494	-0.59	3.57E-09	3.11E-06
Ccdc32	0.15	4.23E-09	3.37E-06
Mll2	-0.42	4.17E-09	3.37E-06

Fam103a1	0.22	4.86E-09	3.71E-06
Pkd1	-0.23	5.58E-09	4.09E-06
Atp6v1e1	0.16	6.86E-09	4.83E-06
Zfp652	-0.22	7.28E-09	4.94E-06
Dchs1	-0.27	9.22E-09	6.03E-06
Gm4723	0.61	1.53E-08	9.68E-06
1520402A15Rik	-0.52	1.85E-08	1.13E-05
Cml5	-0.74	2.63E-08	1.50E-05
Nfia	-0.33	2.59E-08	1.50E-05
Atp6v0e2	0.14	2.85E-08	1.53E-05
Trcg1	-0.92	2.79E-08	1.53E-05
AC154449.2	-0.40	3.01E-08	1.57E-05
Zfhx3	-0.43	3.13E-08	1.59E-05
Atp6v1g2	0.16	6.11E-08	3.02E-05
Mios	-0.31	6.36E-08	3.07E-05
Lrrc58	-0.37	8.70E-08	4.09E-05
Ppp6r2	-0.18	9.50E-08	4.24E-05
Trim72	-0.67	9.33E-08	4.24E-05
AC132303.1	-0.37	1.00E-07	4.27E-05
Cftr	-0.71	9.84E-08	4.27E-05
Cybrd1	-0.59	1.05E-07	4.35E-05
Ptprh	0.80	1.39E-07	5.67E-05
Cdh10	0.35	1.43E-07	5.69E-05
AC102195.1	-0.88	1.51E-07	5.78E-05
Mapt	0.12	1.51E-07	5.78E-05
Gm10931	-0.71	1.55E-07	5.81E-05
Gm3435	-0.35	1.59E-07	5.82E-05

BX537302.1	-0.53	1.67E-07	5.87E-05
Itpr2	-0.21	1.66E-07	5.87E-05
Rgs4	0.32	1.70E-07	5.87E-05
Tgfa	-0.23	1.93E-07	6.54E-05
Sbsn	-0.44	2.00E-07	6.66E-05
Gm11944	-0.51	2.10E-07	6.87E-05
Prdm11	-0.16	2.27E-07	7.30E-05
Tmem170b	-0.26	2.74E-07	8.65E-05
Plin4	-0.70	2.93E-07	9.09E-05
Ahsa1	0.17	3.39E-07	0.000102
Slco2a1	-0.70	3.37E-07	0.000102
Ksr2	-0.35	3.48E-07	0.000103
2010107E04Rik	0.17	3.65E-07	0.000106
Pan3	-0.24	4.46E-07	0.000128
RP24-161J8.2	-0.51	4.62E-07	0.00013
Nars	0.15	4.94E-07	0.000137
AC122417.1	-0.32	5.40E-07	0.000143
Spnb1	-0.29	5.24E-07	0.000143
Srp19	0.16	5.34E-07	0.000143
1500031L02Rik	0.18	6.00E-07	0.000151
Dctd	-0.32	5.81E-07	0.000151
Gm12116	-0.76	5.94E-07	0.000151
Gm16997	-0.83	5.93E-07	0.000151
Adcy9	-0.25	6.33E-07	0.000157
Acacb	-0.38	6.49E-07	0.000158
Igsf3	-0.36	6.54E-07	0.000158
Hif3a	-0.72	6.81E-07	0.000162

Syt11	0.15	7.71E-07	0.000181
Vopp1	0.26	8.24E-07	0.000191
Fmo2	-0.66	8.89E-07	0.000202
Ranbp17	-0.36	8.94E-07	0.000202
Srp54b	0.27	9.45E-07	0.000211
0610038L08Rik	-0.55	9.59E-07	0.000212
Mrpl36	0.20	9.74E-07	0.000212
Aff1	-0.32	9.95E-07	0.000214
Rdh9	-0.58	1.03E-06	0.000217
Synj2	0.33	1.03E-06	0.000217
Stmn1	0.24	1.05E-06	0.000218
Hbxip	0.19	1.08E-06	0.000221
Zc3h7b	0.22	1.09E-06	0.000221
Anxa4	0.62	1.12E-06	0.000222
Ndufb6	0.17	1.13E-06	0.000222
Yeats4	0.18	1.12E-06	0.000222
Ngrn	0.15	1.26E-06	0.000246
Bid	-0.28	1.35E-06	0.00026
Ncald	0.26	1.44E-06	0.000275
Flnc	-0.55	1.48E-06	0.00028
CT868690.1	-0.79	1.53E-06	0.000286
2410004B18Rik	0.18	1.61E-06	0.000298
Atf4	0.26	1.80E-06	0.00033
Icosl	-0.48	1.86E-06	0.000338
Tmem60	0.23	1.97E-06	0.00035
Zfp334	-0.13	1.97E-06	0.00035
Txndc12	0.18	2.08E-06	0.000367

Dync1h1	-0.17	2.11E-06	0.000369
Sdc4	-0.39	2.39E-06	0.000412
Scube2	-0.47	2.45E-06	0.000419
Agl	-0.15	2.48E-06	0.00042
Ahnak	-0.46	2.53E-06	0.000425
Pkp2	-0.64	2.64E-06	0.000435
Tmem85	0.13	2.62E-06	0.000435
Snrpd3	0.18	2.69E-06	0.00044
Celsr1	-0.33	2.77E-06	0.00045
Ahnak2	-0.44	2.80E-06	0.00045
Gm13375	-0.41	2.87E-06	0.000458
Zfand6	0.20	2.96E-06	0.000467
Selk	0.15	3.07E-06	0.000481
Gpnmb	-0.47	3.15E-06	0.000487
Gpr182	-0.50	3.17E-06	0.000487
Zhx3	-0.26	3.19E-06	0.000487
Rab7	0.10	3.32E-06	0.000503
Zbtb44	-0.32	3.38E-06	0.000507
RP23-388P16.8	-0.78	3.46E-06	0.000515
Ncbp2	0.13	3.54E-06	0.000523
Slc25a22	0.18	3.88E-06	0.000568
Cobl	0.27	3.93E-06	0.000572
Cd99l2	0.13	4.05E-06	0.000585
Ndfip1	0.20	4.44E-06	0.000626
Slc1a4	0.16	4.39E-06	0.000626
Trp73	-0.70	4.42E-06	0.000626
Ankrd7	-0.79	4.57E-06	0.00064

Prdx2	0.10	4.62E-06	0.000641
Agxt2l2	-0.21	4.78E-06	0.000651
Ly6e	0.23	4.76E-06	0.000651
Pm20d1	-0.45	4.80E-06	0.000651
Dhdh	-0.26	5.03E-06	0.000677
Gm15594	-0.73	5.33E-06	0.000712
Ppp1r16b	-0.29	5.42E-06	0.000719
Med1	-0.17	5.67E-06	0.000733
Pak1	0.18	5.68E-06	0.000733
Uqcrb	0.22	5.68E-06	0.000733
Wnk1	-0.16	5.64E-06	0.000733
Gm10151	-0.62	5.85E-06	0.000749
Isca2	0.15	6.19E-06	0.000787
4631405J19Rik	-0.62	6.80E-06	0.000859
Nlk	0.22	7.22E-06	0.000906
Gm10595	-0.73	7.72E-06	0.000962
Atp6v1b2	0.14	8.34E-06	0.000991
Atp6v1g1	0.17	8.39E-06	0.000991
Cldnd1	0.13	8.13E-06	0.000991
Cyb5	0.19	8.32E-06	0.000991
Dnajb6	0.14	8.05E-06	0.000991
Fxyd4	-0.61	8.41E-06	0.000991
Lonrf3	-0.36	8.50E-06	0.000991
Nicn1	0.14	8.40E-06	0.000991
Stx12	0.15	8.51E-06	0.000991
Tspyl4	0.18	8.55E-06	0.000991
Ube2e1	0.13	8.51E-06	0.000991

BC046401	-0.55	8.84E-06	0.001018
Rab28	0.14	8.90E-06	0.001019
Map1lc3b	0.19	9.11E-06	0.001037
Lefty1	-0.67	9.18E-06	0.001038
Ube2b	0.18	9.52E-06	0.00107
Lama1	-0.47	9.77E-06	0.001092
Sntb2	-0.33	9.87E-06	0.001096
Gm15082	-0.73	9.96E-06	0.001099
Cd2bp2	0.10	1.00E-05	0.0011
Mtap1a	-0.16	1.02E-05	0.001114
Slc2a9	-0.57	1.03E-05	0.001118
Rexo2	0.14	1.06E-05	0.001143
Atcay	0.15	1.07E-05	0.001144
Otud1	0.25	1.07E-05	0.001144
Slc25a3	0.12	1.12E-05	0.001186
Arl6ip5	0.13	1.13E-05	0.001193
Lysmd4	0.13	1.17E-05	0.001222
Ywhah	0.14	1.17E-05	0.001222
Atp6ap1	0.11	1.24E-05	0.001274
Fnbp1l	0.26	1.24E-05	0.001274
Stab2	-0.36	1.24E-05	0.001274
Fbxl18	-0.20	1.28E-05	0.001298
Letmd1	0.12	1.38E-05	0.001389
Txnl4a	0.21	1.38E-05	0.001389
Lysmd2	0.17	1.40E-05	0.001405
Nup98	-0.17	1.43E-05	0.001423
Gm12394	-0.46	1.48E-05	0.001465

7SK.295	-0.70	1.49E-05	0.001469
Atg5	0.15	1.53E-05	0.001496
Ndfip2	0.23	1.58E-05	0.001541
Elmo3	-0.28	1.65E-05	0.001601
Stx8	0.19	1.71E-05	0.001644
AC159277.1	-0.47	1.74E-05	0.001654
Col6a6	-0.64	1.74E-05	0.001654
Trpm3	-0.42	1.74E-05	0.001654
SNORD38.1	-0.65	1.78E-05	0.001676
Prox1	-0.63	1.84E-05	0.001728
2610507B11Rik	-0.11	1.95E-05	0.001805
Ndrg4	0.15	1.93E-05	0.001805
Rasgef1b	0.24	1.95E-05	0.001805
Notch2	-0.29	2.03E-05	0.001861
Snrnp27	0.15	2.02E-05	0.001861
Mrrf	0.14	2.05E-05	0.001869
Hipk2	-0.26	2.08E-05	0.001882
Lpp	-0.35	2.09E-05	0.001883
Arpp19	0.26	2.20E-05	0.001957
Gm15893	-0.41	2.20E-05	0.001957
Rbm18	0.15	2.18E-05	0.001957
1700021F05Rik	0.16	2.29E-05	0.00201
Slc24a4	-0.30	2.29E-05	0.00201
Ubr4	-0.15	2.28E-05	0.00201
AI413582	0.19	2.38E-05	0.002073
Slc39a10	0.22	2.45E-05	0.00213
Spcs2	0.13	2.48E-05	0.002147

1110054O05Rik	0.13	2.54E-05	0.002151
Hsp90b1	0.20	2.53E-05	0.002151
Nup214	-0.16	2.50E-05	0.002151
Patz1	-0.18	2.53E-05	0.002151
Galntl2	-0.68	2.56E-05	0.002164
Zfp783	-0.25	2.73E-05	0.002293
Got1	0.16	2.87E-05	0.002403
Maml2	-0.30	2.89E-05	0.00241
Qrfpr	0.48	2.92E-05	0.002422
Cd200	0.23	2.97E-05	0.002448
Sra1	0.16	3.00E-05	0.002464
Cpne4	0.23	3.05E-05	0.002481
Serf1	0.23	3.04E-05	0.002481
Igsf10	-0.35	3.15E-05	0.002547
Ralyl	0.21	3.17E-05	0.002547
Tsku	-0.48	3.17E-05	0.002547
Foxo3	-0.24	3.22E-05	0.002577
Crebbp	-0.21	3.24E-05	0.002579
Pnpla7	-0.28	3.32E-05	0.002622
Ykt6	0.12	3.32E-05	0.002622
B230120H23Rik	-0.35	3.35E-05	0.002637
Lrrc29	-0.41	3.44E-05	0.002682
Rgs20	0.23	3.44E-05	0.002682
Klhl11	-0.29	3.48E-05	0.002688
Ptprn2	0.23	3.47E-05	0.002688
Cisd2	0.14	3.57E-05	0.002734
Pacsin2	0.22	3.57E-05	0.002734

Gm15609	-0.41	3.75E-05	0.002862
Hnrnph2	0.17	3.86E-05	0.00292
Nf1	-0.21	3.84E-05	0.00292
Nap1l3	0.26	3.94E-05	0.002969
AL662835.2	-0.63	3.99E-05	0.002981
Tmem14c	0.18	3.99E-05	0.002981
Ube2e2	0.13	4.12E-05	0.003067
Gm6588	-0.56	4.17E-05	0.003092
4933425O20Rik	-0.34	4.32E-05	0.003178
R3hdm2	0.19	4.34E-05	0.003178
Ttc28	-0.37	4.33E-05	0.003178
Npepps	0.12	4.40E-05	0.00321
Gm12576	-0.64	4.47E-05	0.003246
Ssbp1	0.15	4.48E-05	0.003246
Kctd21	0.18	4.56E-05	0.003268
Tk1	-0.40	4.56E-05	0.003268
Tmem9b	0.13	4.57E-05	0.003268
Pitpna	0.14	4.59E-05	0.00327
Crb1	0.58	4.66E-05	0.003311
Nt5dc2	-0.39	4.74E-05	0.003326
Pfdn1	0.14	4.73E-05	0.003326
Vdac1	0.10	4.73E-05	0.003326
Ostc	0.17	4.76E-05	0.003329
Cmpk1	0.20	4.79E-05	0.003339
Mapre2	0.09	4.86E-05	0.003369
Apbb2	-0.14	5.01E-05	0.00346
Vta1	0.13	5.05E-05	0.003476

Pfkp	0.15	5.22E-05	0.003581
2210020M01Rik	-0.47	5.24E-05	0.003585
Tmub2	0.14	5.26E-05	0.003585
Tet2	-0.20	5.36E-05	0.003629
Ythdf1	0.11	5.37E-05	0.003629
Spdef	-0.62	5.43E-05	0.003659
Slc14a1	-0.30	5.53E-05	0.003705
Timm22	0.14	5.54E-05	0.003705
Golm1	-0.24	5.66E-05	0.00377
A930024N18Rik	-0.41	5.70E-05	0.003771
Muc6	-0.52	5.70E-05	0.003771
Siglec1	-0.45	5.81E-05	0.003831
Morf4l1	0.15	5.97E-05	0.003889
Proca1	-0.24	5.94E-05	0.003889
Ror1	-0.58	5.96E-05	0.003889
Lifr	-0.27	6.01E-05	0.003908
AC125486.1	-0.54	6.30E-05	0.00401
B3galnt1	0.19	6.30E-05	0.00401
Pde6h	-0.46	6.27E-05	0.00401
Polh	-0.23	6.26E-05	0.00401
Tnfrsf19	0.20	6.27E-05	0.00401
Tspan18	-0.56	6.21E-05	0.00401
Mff	0.12	6.33E-05	0.004016
Grinl1a	0.11	6.43E-05	0.004061
Tulp3	-0.20	6.49E-05	0.004083
Leprotl1	0.14	6.62E-05	0.004153
Gm11721	-0.47	6.67E-05	0.00417

Mkks	0.21	6.76E-05	0.004211
Plec	-0.24	6.98E-05	0.00432
Rbx1	0.11	6.98E-05	0.00432
Tgfbr3	-0.27	7.09E-05	0.004376
Nt5c1a	-0.33	7.19E-05	0.004391
Slc1a2	-0.19	7.17E-05	0.004391
Tbcd	-0.10	7.19E-05	0.004391
Calm2	0.16	7.23E-05	0.004398
Exd2	0.18	7.42E-05	0.004502
Lca5l	-0.32	7.51E-05	0.004524
Ywhab	0.12	7.49E-05	0.004524
6330527O06Rik	0.36	7.55E-05	0.004533
D430018E03Rik	-0.42	7.62E-05	0.004533
Plce1	-0.43	7.62E-05	0.004533
Vps24	0.11	7.60E-05	0.004533
BC031181	0.11	7.69E-05	0.004547
P2ry1	-0.49	7.72E-05	0.004547
Sema5a	-0.28	7.70E-05	0.004547
Sdccag8	0.15	7.75E-05	0.004552
A330049M08Rik	-0.55	7.96E-05	0.004662
Zfp365	0.17	8.03E-05	0.004687
Slmo2	0.12	8.14E-05	0.004734
Napg	0.14	8.19E-05	0.004744
Tor3a	-0.16	8.21E-05	0.004744
Ace	-0.27	8.36E-05	0.004816
Rec8	-0.63	8.50E-05	0.004881
Ppp2cb	0.11	8.53E-05	0.004886

Rc3h2	-0.29	8.71E-05	0.00497
Ppfia1	-0.15	8.82E-05	0.00502
Cyp3a13	-0.64	8.87E-05	0.00503
Rbm15	-0.25	8.97E-05	0.005073
Stk32a	-0.46	9.11E-05	0.005136
Bcs1l	0.15	9.20E-05	0.00517
4833412C05Rik	0.60	9.40E-05	0.005172
B430010I23Rik	-0.67	9.37E-05	0.005172
Dlx1	0.19	9.24E-05	0.005172
Gm16201	-0.67	9.29E-05	0.005172
Ict1	0.16	9.38E-05	0.005172
P2ry13	0.22	9.32E-05	0.005172
Ppp2r5c	0.13	9.31E-05	0.005172
Fkbp5	-0.42	9.44E-05	0.00518
Ccdc6	-0.23	9.58E-05	0.005191
Chac2	0.26	9.53E-05	0.005191
Hat1	0.23	9.51E-05	0.005191
Pkd2l2	0.16	9.55E-05	0.005191
Ube2j2	0.11	9.68E-05	0.005229
1700121F15Rik	-0.36	9.74E-05	0.005246
1500003O03Rik	0.11	9.99E-05	0.005365
Dctn3	0.15	0.0001	0.005377
Ccdc72	0.19	0.000101	0.00539
Trappc2	0.23	0.000101	0.00539
Eif1	0.12	0.000102	0.005403
Slc35f4	0.17	0.000102	0.005403
Bet1	0.24	0.000103	0.005433

Gm15478	-0.52	0.000103	0.005433
4933401P06Rik	-0.55	0.000105	0.005494
Eif2ak1	0.11	0.000105	0.005494
Ssh1	-0.14	0.000105	0.005494
Ttc13	-0.12	0.000106	0.005523
Arpc3	0.14	0.000107	0.005529
4831426I19Rik	-0.43	0.000109	0.005615
Agbl2	-0.55	0.000109	0.005615
Zbtb1	-0.15	0.000109	0.005619
Grin2a	-0.33	0.00011	0.005625
4921513D23Rik	-0.18	0.000111	0.005651
Hcfc1r1	0.18	0.000111	0.005651
Aldh3a1	-0.49	0.000112	0.005691
Fnip2	-0.22	0.000112	0.005691
Man2a2	-0.12	0.000114	0.005748
Dnahc9	-0.51	0.000115	0.005829
Naip1	-0.50	0.000117	0.005864
Fam168b	0.07	0.000118	0.005893
Zfp398	-0.17	0.000118	0.005893
Elk4	-0.15	0.000119	0.005961
Gm16183	-0.32	0.000121	0.006002
Prkacb	0.18	0.000122	0.006039
Atp6v0d1	0.13	0.000123	0.006049
Gm15835	-0.46	0.000123	0.006049
Morn1	-0.25	0.000122	0.006049
Slc2a4	-0.49	0.000123	0.006049
Fat1	-0.38	0.000125	0.006118

Tnxb	-0.47	0.000125	0.006118
1500011B03Rik	0.14	0.000126	0.006119
Gm16982	-0.40	0.000127	0.006146
Rabgef1	0.15	0.000127	0.006146
Lmo4	0.28	0.000128	0.006206
Amn1	0.19	0.000129	0.006233
AC123699.1	-0.29	0.00013	0.00626
Agt	-0.37	0.000131	0.006274
Gm12592	-0.26	0.000132	0.006274
Gm15892	-0.51	0.000132	0.006274
Svil	-0.23	0.000132	0.006274
Gm15651	-0.62	0.000135	0.006382
Gm16854	-0.62	0.000135	0.006382
Rpl7l1	0.11	0.000136	0.006402
Trp53inp2	0.13	0.000137	0.006473
Tulp4	-0.16	0.000138	0.006473
Ero1lb	0.18	0.000138	0.006486
Gm16626	-0.46	0.000139	0.006487
Ube2f	0.12	0.000142	0.006602
Gm15869	-0.61	0.000142	0.006607
Gm16534	-0.59	0.000144	0.006687
Arhgap25	0.53	0.000145	0.006688
Pam16	0.14	0.000145	0.00669
Gm16334	-0.59	0.000146	0.006733
B230319C09Rik	-0.43	0.000148	0.006781
1110007A13Rik	-0.16	0.000153	0.007
Gde1	0.14	0.000154	0.007028

Arhgef12	-0.12	0.000157	0.007135
Rnft2	0.14	0.000157	0.007137
Fam133b	0.13	0.000157	0.007139
Shisa6	-0.53	0.000158	0.007144
AA986860	-0.30	0.00016	0.007201
Cyp2d22	-0.18	0.000161	0.007231
Fanci	-0.38	0.000161	0.007231
4930404I05Rik	-0.35	0.000163	0.007302
Sept8	0.16	0.000163	0.007302
Dok5	0.24	0.000164	0.00732
5830444B04Rik	-0.53	0.000165	0.007341
A2m	-0.62	0.000166	0.007342
Sema3a	0.36	0.000167	0.007385
Golgb1	-0.11	0.000168	0.00742
Oplah	-0.22	0.000169	0.007422
C030046E11Rik	-0.13	0.00017	0.007474
AC122296.1	-0.58	0.000171	0.007475
Cyp2u1	-0.20	0.000172	0.00752
Dap3	0.10	0.000177	0.007682
Dnajc8	0.11	0.000177	0.007682
Gng11	0.37	0.000177	0.007682
Nsd1	-0.16	0.000177	0.007682
Rad54l	-0.40	0.000178	0.007682
AC163296.1	-0.41	0.00018	0.007777
Fam151b	0.24	0.000181	0.007802
Tmem65	0.20	0.000182	0.007823
Fbxw7	0.18	0.000187	0.007968

Gm14286	-0.40	0.000187	0.007968
Mdh1	0.15	0.000187	0.007968
Rab6	0.21	0.000187	0.007968
Nova2	-0.19	0.000188	0.007988
Slco1c1	0.18	0.000191	0.008098
Ppp2r2a	0.14	0.000193	0.008138
Dnaja1	0.18	0.000196	0.008172
F630040L22Rik	-0.54	0.000196	0.008172
Gm12216	-0.53	0.000196	0.008172
Nav2	-0.18	0.000196	0.008172
Nkiras1	0.14	0.000195	0.008172
Stmn2	0.14	0.0002	0.008326
BC060267	-0.29	0.000201	0.008337
Fscn2	-0.49	0.000201	0.008337
6530402F18Rik	-0.24	0.000202	0.008357
Dnaja3	0.09	0.000203	0.008394
Ehmt1	-0.12	0.000205	0.008443
Psma5	0.13	0.000206	0.008443
Mdk	-0.26	0.000209	0.008535
Tshb	-0.62	0.000209	0.008535
Ubl4	0.11	0.000209	0.008535
Zxdc	-0.12	0.000211	0.008597
C230096C10Rik	-0.13	0.000213	0.008627
Cpxm1	-0.28	0.000213	0.008627
Snap25	0.14	0.000213	0.008627
Idh3a	0.14	0.000214	0.008655
Cckbr	0.29	0.000215	0.008657

8030462N17Rik	-0.18	0.000217	0.008737
Sat1	0.23	0.000219	0.008774
Chst2	-0.22	0.000222	0.008899
AC148089.1	-0.53	0.000223	0.008906
Pde4b	0.15	0.000224	0.008906
2610001J05Rik	0.15	0.000227	0.008983
Als2cr4	0.15	0.000228	0.008983
Fndc4	0.12	0.000227	0.008983
Gcnt7	-0.43	0.000227	0.008983
Tead1	-0.23	0.000229	0.009022
Chd4	-0.14	0.000232	0.00906
Eef2k	-0.16	0.000232	0.00906
Kctd20	0.09	0.000231	0.00906
Ppp2r5a	0.13	0.000232	0.00906
Gpr161	-0.56	0.000232	0.009061
Bcas2	0.10	0.000233	0.00907
7SK.49	-0.48	0.000239	0.009277
Rbm47	-0.52	0.00024	0.009302
Tnfaip8l1	0.21	0.000244	0.009411
Wdr62	-0.30	0.000245	0.00943
Gm11827	-0.63	0.000245	0.009432
Uchl5	0.19	0.000247	0.009501
Gm16575	-0.61	0.000251	0.009616
Prkar2b	0.19	0.000252	0.009625
9830001H06Rik	-0.40	0.000257	0.009775
Gm711	-0.46	0.000257	0.009775
Zfyve26	-0.12	0.000257	0.009775

Itga11	-0.37	0.000259	0.009832
Acvr2b	-0.27	0.000261	0.009887
Mpeg1	0.17	0.000262	0.009892
Btrc	0.09	0.000265	0.009896
Ncrna00081	0.15	0.000264	0.009896
Nutf2	0.13	0.000265	0.009896
Prr5	-0.42	0.000264	0.009896
Sardh	-0.22	0.000263	0.009896
Zan	-0.47	0.000265	0.009896
Cyb5r4	0.18	0.00027	0.010057
Invs	-0.12	0.000271	0.010057
Ntrk3	-0.20	0.000271	0.010057
Actr1a	0.10	0.000275	0.010173
Atg12	0.14	0.000281	0.010392
Gm16896	-0.44	0.000284	0.010464
Gm14372	-0.47	0.000286	0.010492
Nsmce2	0.14	0.000286	0.010492
Slc16a12	-0.36	0.000286	0.010492
Gm15774	-0.32	0.000288	0.010501
Rab14	0.15	0.000288	0.010501
Trrap	-0.14	0.000288	0.010501
Dctn5	0.10	0.000289	0.010517
Sipa1l3	-0.24	0.000292	0.01058
Hsp90ab1	0.10	0.000293	0.010603
Mrps14	0.15	0.000294	0.010625
Pole	-0.39	0.000295	0.010625
Rab1	0.13	0.0003	0.010789

Csnk1e	0.20	0.000301	0.010799
Rabif	0.12	0.000302	0.010831
Tbck	-0.23	0.000304	0.010876
Vti1a	0.09	0.000305	0.010878
AC131761.1	-0.30	0.000312	0.011082
C130071C03Rik	0.19	0.000311	0.011082
9130011J15Rik	0.10	0.000312	0.011095
Yaf2	0.14	0.000314	0.011142
Mrps36	0.22	0.000316	0.011189
Il12a	0.55	0.00032	0.01128
D4Wsu53e	0.13	0.000321	0.011301
Iars	0.10	0.000321	0.011301
Pamr1	0.36	0.000327	0.011437
Pcmt1	0.12	0.000326	0.011437
Bag2	0.17	0.000328	0.01147
1700084C01Rik	0.24	0.000329	0.011471
N28178	0.17	0.000329	0.011471
Nap1l1	0.15	0.000331	0.011514
Pla1a	-0.41	0.000333	0.011569
Megf6	-0.36	0.000336	0.011622
AC137156.2	-0.49	0.000337	0.011652
Lmln	-0.15	0.000338	0.011673
Baalc	0.13	0.00034	0.011722
Syt13	0.15	0.000342	0.011765
Nynrin	-0.25	0.000344	0.011812
Ndufc1	0.13	0.000346	0.01185
Klhdc8a	0.31	0.000348	0.011909

Gm12227	-0.54	0.000349	0.011914
Atxn1	-0.21	0.000354	0.011998
Chordc1	0.23	0.000354	0.011998
Ndufa3	0.17	0.000354	0.011998
Pcp4	0.28	0.000355	0.011998
Tomm34	0.12	0.000355	0.011998
Gpr88	0.34	0.00036	0.0121
Myo7a	-0.16	0.000359	0.0121
Nif3l1	0.12	0.000359	0.0121
Dnaja2	0.14	0.000371	0.012432
Lyst	-0.23	0.000371	0.012438
Svep1	-0.59	0.000373	0.01248
Fam81a	0.18	0.000374	0.012489
Fbxl3	0.15	0.000375	0.012489
Cap2	0.18	0.000382	0.012658
Gm16316	-0.52	0.000382	0.012658
Igf2bp3	-0.28	0.000382	0.012658
Gm16738	-0.32	0.000383	0.01267
Cacng3	0.20	0.000388	0.012807
BC067074	-0.42	0.000391	0.012869
Pram1	-0.30	0.000394	0.012945
2900011O08Rik	0.10	0.000397	0.013025
Col18a1	-0.54	0.000397	0.013026
Atp6v1c1	0.13	0.000401	0.013028
Cfdp1	0.13	0.0004	0.013028
Dusp27	-0.52	0.0004	0.013028
Eif2b1	0.10	0.0004	0.013028

Sdhd	0.09	0.000401	0.013028
AC121121.1	-0.27	0.000404	0.013051
Ankrd61	-0.32	0.000404	0.013051
Bnip3l	0.14	0.000404	0.013051
Rab2b	0.13	0.000405	0.013072
Cnnm4	-0.20	0.000409	0.013168
5730403B10Rik	0.08	0.00041	0.013183
Mef2c	0.28	0.000411	0.013202
Bbs1	0.10	0.000414	0.013258
Bhlhe41	-0.22	0.000416	0.013293
Kcng2	-0.55	0.000418	0.013347
AC117232.2	-0.36	0.000421	0.01335
Cct2	0.09	0.000421	0.01335
Drd5	-0.60	0.000421	0.01335
Tpcn2	-0.38	0.000419	0.01335
B3galt5	-0.35	0.000422	0.013361
Cuta	0.20	0.000423	0.013361
Hdac9	0.23	0.000424	0.013383
Rasl11b	0.29	0.000425	0.013383
Mrpl21	0.15	0.000426	0.013384
5730455O13Rik	0.21	0.000431	0.013526
Dnahc17	-0.32	0.000432	0.013543
Khdrbs3	0.21	0.000433	0.013547
Tomm22	0.11	0.000435	0.01357
Capn11	0.48	0.000438	0.013575
Cyp4f18	-0.49	0.000437	0.013575
Mtap1b	-0.21	0.000436	0.013575

Ndufc2	0.12	0.000438	0.013575
Paip2	0.13	0.000439	0.013575
Ap3s1	0.21	0.00044	0.013583
Trp53bp2	-0.18	0.000441	0.013608
Dnmt3a	-0.14	0.000442	0.013613
Aloxe3	-0.32	0.000453	0.01392
Nudt4	0.20	0.000454	0.01392
Obscn	-0.38	0.000455	0.013946
Ctgf	0.39	0.000457	0.013972
AA408865	-0.37	0.000461	0.014088
Pgk1	0.13	0.000466	0.01421
Gm1698	-0.60	0.000471	0.014346
Tmem52	-0.59	0.000475	0.014435
4933423P22Rik	-0.54	0.000481	0.014582
Unc50	0.11	0.000483	0.014624
Ctbp2	-0.34	0.000487	0.014687
Rint1	-0.13	0.000487	0.014687
Znrf3	-0.23	0.000488	0.014703
Sec62	0.13	0.00049	0.014753
Gm11202	-0.53	0.000492	0.014762
Gm15965	-0.57	0.000493	0.014768
Mrpl42	0.18	0.000493	0.014768
C78339	0.19	0.000497	0.014794
Inpp4a	-0.13	0.000496	0.014794
Mrps27	0.12	0.000496	0.014794
Tdgf1	-0.58	0.000501	0.014898
Airn	-0.53	0.000502	0.014902

Lrp1	-0.17	0.000505	0.014956
Sfxn3	0.17	0.000508	0.015024
5830432E09Rik	-0.57	0.000512	0.015125
Atg4b	0.07	0.000513	0.015127
Pdcd5	0.13	0.000514	0.015127
Tmem49	0.14	0.000514	0.015127
Oxct1	0.15	0.000518	0.015198
6720456B07Rik	0.12	0.000521	0.015223
Klhl22	0.07	0.000521	0.015223
Sdhaf2	0.10	0.00052	0.015223
Cab39	0.13	0.000525	0.015315
Tert	-0.29	0.000526	0.015323
Itgb7	-0.54	0.000529	0.015371
Naa38	-0.17	0.000532	0.015449
Msh4	-0.25	0.000533	0.015451
Slc36a2	-0.51	0.000536	0.015503
Lrrtm3	0.18	0.00054	0.01559
Cnot8	0.08	0.000544	0.015688
Atp5g1	0.12	0.000545	0.015691
2310003L22Rik	0.12	0.000549	0.015724
9230117E06Rik	-0.57	0.00055	0.015724
Arfip2	0.07	0.000552	0.015724
Mt2	-0.33	0.000548	0.015724
Ndel1	0.11	0.000553	0.015724
Nphs2	-0.48	0.000549	0.015724
Pef1	0.15	0.000552	0.015724
Tnrc6c	-0.12	0.000549	0.015724

Gm10561	0.25	0.000554	0.015726
Slain1	0.12	0.000555	0.015727
Gm13110	-0.30	0.000556	0.015731
Dpy30	0.14	0.000561	0.01585
Gm14471	-0.47	0.000566	0.015956
Tdo2	-0.59	0.000566	0.015956
Arhgap21	-0.13	0.00057	0.015962
Farsb	0.11	0.00057	0.015962
Scamp5	0.09	0.00057	0.015962
Tbc1d4	-0.40	0.000569	0.015962
Mir494	-0.58	0.000572	0.015983
Trpv4	-0.35	0.000572	0.015983
Ankrd55	-0.33	0.000576	0.01603
Rabl2	0.15	0.000577	0.01603
Rtn4	0.18	0.000576	0.01603
Mpped2	0.23	0.000581	0.016119
Lamb3	-0.47	0.000584	0.016183
Ocel1	0.14	0.000586	0.016211
Fxyd7	0.32	0.000589	0.016275
Tceal8	0.19	0.000598	0.016501
Lrrc8a	-0.21	0.000602	0.016585
4930521C21Rik	-0.38	0.000608	0.016701
St18	-0.57	0.000609	0.016701
Ucp2	-0.32	0.000608	0.016701
Fbxo5	0.40	0.000616	0.016864
Cpne8	0.21	0.000624	0.017019
Ier3ip1	0.16	0.000624	0.017019

Stx1a	0.25	0.000623	0.017019
Ctnna3	-0.53	0.000626	0.017031
Cml2	0.49	0.000632	0.01712
Ebf3	-0.52	0.00063	0.01712
Mkrn1	0.09	0.000633	0.01712
Rala	0.14	0.000631	0.01712
Alpk1	-0.24	0.000635	0.017123
Spen	-0.16	0.000635	0.017123
Chst10	0.14	0.000638	0.017159
Igf2r	-0.13	0.000639	0.017159
Trim62	-0.39	0.000638	0.017159
Enkur	0.35	0.000645	0.017288
RP23-145O4.5	-0.58	0.000649	0.017375
Shmt1	-0.28	0.00065	0.017375
Tspan4	-0.29	0.000651	0.017375
Sh3gl2	0.20	0.000654	0.017449
2810025M15Rik	0.20	0.000659	0.017547
Ada	-0.38	0.000671	0.017781
Dlg1	0.11	0.00067	0.017781
Gm10564	-0.40	0.000669	0.017781
Il34	0.20	0.000675	0.017861
Wnt1	-0.37	0.000678	0.01793
Dnmbp	-0.19	0.000684	0.018049
Ppara	-0.29	0.000686	0.018091
Rufy3	0.11	0.000688	0.018111
Slc12a3	-0.54	0.000692	0.018202
Pion	-0.20	0.000695	0.018229

Tmem201	-0.17	0.000698	0.018295
Grb14	0.26	0.000702	0.01836
Fam164a	0.19	0.000705	0.018394
Fam192a	0.09	0.000705	0.018394
Tpm3	0.11	0.000714	0.018612
Aatf	-0.13	0.000717	0.018655
SNORA17.403	-0.58	0.000718	0.018655
Crtc3	-0.16	0.000721	0.01872
Fbxl7	-0.42	0.000735	0.019037
4921522P10Rik	-0.50	0.000738	0.019062
Arhgap31	-0.19	0.000738	0.019062
1110049F12Rik	0.11	0.000743	0.019143
Gm15816	-0.42	0.000742	0.019143
Ilf2	0.09	0.00075	0.019283
Stag3	-0.36	0.00075	0.019283
Rnf11	0.18	0.000755	0.019359
Txn1	0.14	0.00076	0.01948
Gm11750	-0.58	0.000762	0.019484
Lrrc20	0.11	0.000768	0.019583
Npas3	-0.22	0.000767	0.019583
Zc3h15	0.16	0.000769	0.019586
Heg1	-0.20	0.000771	0.019607
Cd27	-0.51	0.000776	0.019713
Map3k1	-0.28	0.000781	0.019793
Serinc3	0.15	0.000781	0.019793
Slc9a2	-0.44	0.000783	0.019803
Angptl7	-0.47	0.000785	0.01983

Angptl2	-0.41	0.000791	0.019943
Fam159b	0.39	0.000791	0.019943
Casc1	-0.44	0.000798	0.020073
Rtn3	0.14	0.000801	0.020137
Reep5	0.13	0.000804	0.020173
Gm15800	-0.12	0.000807	0.0202
Gm15813	-0.40	0.000807	0.0202
1700112E06Rik	0.57	0.000812	0.020283
Ostm1	0.12	0.000815	0.020339
Tusc3	0.14	0.00082	0.020427
2810006K23Rik	0.19	0.000822	0.020452
Slc22a12	-0.52	0.000823	0.020466
Ttl	0.14	0.000825	0.020486
Loxhd1	-0.55	0.000833	0.020622
Tmem2	-0.20	0.000832	0.020622
Klf6	0.27	0.000837	0.020671
Tmem55a	0.11	0.000836	0.020671
Fam40b	-0.44	0.000844	0.020786
Pappa	-0.57	0.000844	0.020786
Acr	-0.35	0.000846	0.020795
Ncam1	-0.15	0.000847	0.020795
3830431G21Rik	-0.54	0.000859	0.021037
M6pr	0.10	0.000858	0.021037
Slitrk6	-0.53	0.000868	0.021223
Pvrl4	-0.35	0.000871	0.021246
RP23-389D15.1	-0.52	0.00087	0.021246
Vapa	0.14	0.000874	0.021256

Zbtb42	-0.48	0.000873	0.021256
Mrpl9	0.10	0.000877	0.021317
Ccdc56	0.15	0.000887	0.0215
Fryl	-0.15	0.000887	0.0215
Rab15	0.15	0.00089	0.021542
Bex1	0.19	0.000893	0.021591
Dgkg	-0.28	0.000899	0.021702
Hnrnpa2b1	0.13	0.000901	0.021725
Ksr1	-0.31	0.000906	0.021811
Timp1	-0.36	0.000911	0.021903
Zcrb1	0.14	0.000914	0.021936
Bclp2	-0.56	0.000918	0.021972
Muc19	-0.42	0.000917	0.021972
Nlgn3	-0.17	0.00092	0.021972
Slc4a4	-0.19	0.00092	0.021972
Spats2l	0.17	0.000923	0.022022
Ryr1	-0.33	0.000926	0.022043
Tuba1a	0.15	0.000926	0.022043
Fank1	-0.24	0.000928	0.022048
Dlst	0.08	0.000929	0.022053
Rnf14	0.15	0.000932	0.022077
AC160104.2	-0.25	0.000941	0.022278
Foxm1	-0.32	0.000946	0.022342
Ubap1	0.11	0.000946	0.022342
Adamts18	-0.56	0.000952	0.022365
Ap3m2	0.10	0.000957	0.022365
Ep400	-0.09	0.000949	0.022365

Fxyd6	0.18	0.000956	0.022365
Gmps	-0.23	0.000953	0.022365
Lnx2	-0.31	0.000957	0.022365
Sema4b	-0.23	0.000952	0.022365
Zfp568	-0.30	0.000956	0.022365
Lrp4	-0.23	0.00097	0.022636
Hnrnpul2	0.08	0.000972	0.022645
Timm23	0.09	0.000973	0.022645
4933431E20Rik	0.13	0.000976	0.022693
Pdhb	0.09	0.000988	0.022931
Tmem44	0.30	0.000989	0.022931
C4b	-0.30	0.000996	0.023034
Gm14252	-0.56	0.000996	0.023034
Parva	-0.15	0.000998	0.023056
Ap2m1	0.12	0.001	0.023062
Stmn4	0.18	0.001003	0.023103
Spcs1	0.11	0.001017	0.023418
Gm16154	-0.49	0.00103	0.023677
A430105I19Rik	-0.25	0.001039	0.023842
Enoph1	0.11	0.001041	0.023865
Tmf1	-0.16	0.001045	0.023923
Cdc5l	0.11	0.001048	0.023975
Arsa	0.10	0.001052	0.024037
3110070M22Rik	-0.43	0.001063	0.024182
Gm11186	-0.56	0.001063	0.024182
Oat	0.09	0.001062	0.024182
Llph	0.16	0.001065	0.024214

6330577E15Rik	0.14	0.001069	0.024258
Odf2	-0.11	0.001072	0.024294
4930578G10Rik	-0.40	0.001081	0.024475
Batf3	-0.47	0.001083	0.024475
Cldn12	0.15	0.001083	0.024475
Atic	0.12	0.001086	0.024478
Thy1	0.12	0.001086	0.024478
4933427I04Rik	-0.20	0.001091	0.024523
A830093I24Rik	-0.25	0.001092	0.024523
Fahd1	0.15	0.001092	0.024523
AW011738	-0.26	0.001096	0.024537
Cacna1h	-0.27	0.001099	0.024537
Gm14376	-0.55	0.001099	0.024537
Mobkl2b	-0.32	0.001097	0.024537
Txnrd3	-0.29	0.0011	0.024537
Gm16197	-0.52	0.001104	0.024615
Basp1	0.16	0.001107	0.024647
Cyp4v3	-0.19	0.001123	0.024885
Gm14397	-0.56	0.001122	0.024885
Gm16907	-0.32	0.001122	0.024885
Usp29	-0.21	0.001123	0.024885
Snrpa	0.13	0.001129	0.02497
Tram1l1	0.12	0.001133	0.025008
Yars	0.10	0.001132	0.025008
Fam115a	0.13	0.001136	0.025042
Sdc1	-0.53	0.001137	0.025042
1300010F03Rik	-0.13	0.001144	0.025162

Rgag1	-0.29	0.001147	0.025193
Ivns1abp	0.14	0.001148	0.025195
Bsn	-0.19	0.001152	0.025243
Gm15863	-0.38	0.001153	0.025243
Gm15265	-0.29	0.00116	0.025353
Capns2	-0.38	0.001168	0.025501
Sybu	0.09	0.001169	0.025501
Gng5	0.13	0.001178	0.025663
Adam22	-0.16	0.00118	0.025664
Pdia3	0.15	0.001194	0.025944
Kif3a	0.10	0.0012	0.026007
Map6d1	0.15	0.001199	0.026007
Amica1	-0.55	0.001207	0.026051
Ptprk	0.19	0.001204	0.026051
Scarna9	-0.48	0.001206	0.026051
Xdh	-0.31	0.001206	0.026051
Dnase2a	-0.19	0.001218	0.026137
Hrh1	0.23	0.001217	0.026137
Ints3	0.09	0.001216	0.026137
Mir486	-0.55	0.001217	0.026137
Telo2	-0.16	0.001218	0.026137
Golga7	0.11	0.001225	0.026247
Rnf180	0.17	0.001228	0.02628
Abhd6	0.14	0.001232	0.026338
Ensa	0.11	0.001238	0.026429
Kdm2b	-0.15	0.001244	0.026536
Fry	-0.13	0.001248	0.026568

Gm7292	-0.16	0.001249	0.026568
Kdm5b	-0.11	0.001261	0.026792
4930594M22Rik	-0.45	0.001263	0.026802
Gm11681	-0.43	0.001265	0.026812
Gm10390	-0.52	0.001271	0.026924
Gabre	-0.49	0.001277	0.027016
St3gal1	0.23	0.001287	0.027187
4631416L12Rik	-0.17	0.001292	0.027196
Prom2	-0.54	0.001291	0.027196
Supt4h1	0.14	0.00129	0.027196
Asns	0.11	0.001294	0.02722
Txndc9	0.10	0.001297	0.02725
Rab5b	0.07	0.001308	0.02744
Ngfr	-0.47	0.001319	0.027643
Them4	0.18	0.001321	0.027667
Akr1b3	0.12	0.001324	0.027699
Nfib	-0.25	0.001326	0.027701
A3galt2	-0.52	0.001343	0.027902
Cmpk2	0.23	0.001343	0.027902
Lgmn	0.17	0.001341	0.027902
Lpin3	-0.49	0.001342	0.027902
Rps6ka5	-0.23	0.001343	0.027902
Gm15608	-0.34	0.001349	0.027948
Myo1e	0.27	0.001347	0.027948
9030617O03Rik	-0.18	0.001356	0.028009
Shank1	-0.29	0.001354	0.028009
Uap1	0.18	0.001357	0.028009

Usp54	-0.18	0.001358	0.028009
Hmgn3	0.11	0.001362	0.028032
Rc3h1	-0.19	0.001361	0.028032
Atp6v0b	0.14	0.001363	0.028033
Hmg20a	0.10	0.001375	0.028204
Lct	-0.47	0.001374	0.028204
Gm12977	-0.54	0.001383	0.028303
Myst3	-0.13	0.001383	0.028303
Fubp1	0.15	0.001387	0.028321
Trib2	0.28	0.001385	0.028321
2810004N23Rik	0.15	0.001391	0.028376
4930556I23Rik	-0.36	0.001402	0.028516
Cyb561	0.13	0.0014	0.028516
Entpd7	-0.17	0.001402	0.028516
Gm5901	-0.17	0.001408	0.028552
Slc22a4	-0.33	0.001409	0.028552
Zc3hav1	-0.22	0.001409	0.028552
Pde6b	-0.51	0.001411	0.028554
Copz1	0.10	0.001415	0.028604
Rnf181	0.10	0.001416	0.028604
Smad9	-0.18	0.001425	0.028751
Eif4e	0.14	0.001431	0.028839
Irgm1	0.22	0.001443	0.029052
Gchfr	-0.53	0.001448	0.029124
Git2	-0.18	0.001456	0.029247
Gm11126	-0.32	0.001458	0.029247
Enah	-0.15	0.00146	0.029271

Dusp14	0.22	0.001477	0.029572
7SK.5	0.54	0.001488	0.029755
1810063B07Rik	0.17	0.001494	0.029845
Sec16a	-0.09	0.001495	0.029845
Ceacam2	-0.44	0.001503	0.029901
Hprt	0.15	0.001503	0.029901
Qrsl1	0.14	0.001503	0.029901
Hnf1b	-0.50	0.001508	0.029903
Mrpl49	0.10	0.001508	0.029903
Snap47	0.10	0.001507	0.029903
3110035E14Rik	0.32	0.001515	0.030007
Arl1	0.12	0.001523	0.030093
Snx15	0.15	0.001522	0.030093
Acsf2	-0.14	0.001529	0.030127
Atg7	0.11	0.001529	0.030127
Tnrc18	-0.21	0.001528	0.030127
9130019P16Rik	-0.49	0.001545	0.030394
Atpaf1	0.13	0.00155	0.030406
Ghitm	0.11	0.001549	0.030406
Kif26b	-0.30	0.001549	0.030406
Apoe	0.16	0.001554	0.030441
Neb	-0.44	0.001561	0.03055
Mboat2	-0.16	0.001567	0.030638
Morf4l2	0.14	0.001571	0.030692
Arpp21	0.15	0.00158	0.030808
Creld1	0.17	0.001581	0.030808
9330154K18Rik	-0.52	0.001588	0.030878

Fzd7	-0.34	0.001591	0.030878
Mrpl19	0.12	0.001589	0.030878
Nr3c2	-0.26	0.001591	0.030878
Sult5a1	-0.53	0.001596	0.030907
Tomm5	0.15	0.001595	0.030907
Gm15631	0.25	0.0016	0.030954
Extl2	0.18	0.001603	0.030971
Gemin8	0.13	0.001608	0.030985
Nexn	-0.44	0.001608	0.030985
Tbc1d16	-0.18	0.001607	0.030985
Abcc12	-0.54	0.001615	0.031076
Psenen	0.14	0.001619	0.031114
Mzt1	0.18	0.001624	0.031126
Pdp2	-0.19	0.001622	0.031126
Tmem107	0.24	0.001623	0.031126
Gm16601	-0.26	0.001633	0.031261
Klhl3	-0.22	0.001642	0.03131
Pofut1	-0.14	0.001638	0.03131
Qrfp	-0.53	0.001639	0.03131
Trpa1	-0.54	0.001642	0.03131
P2ry12	0.17	0.001645	0.031318
Slc9a3	-0.53	0.00165	0.03138
4930547N16Rik	-0.46	0.001654	0.031405
Pdzd11	0.11	0.001653	0.031405
Chst15	-0.10	0.001661	0.031419
Gm1987	-0.54	0.001665	0.031419
Mmachc	0.14	0.001659	0.031419

Pip4k2b	0.11	0.001661	0.031419
Tbr1	0.25	0.001663	0.031419
Tmem50b	0.11	0.001665	0.031419
Fam83d	-0.53	0.001681	0.03169
Hexdc	-0.10	0.001691	0.031808
Igf1r	-0.18	0.00169	0.031808
Ndufa4	0.13	0.001694	0.031833
2510003E04Rik	0.07	0.001699	0.031882
4930422G04Rik	-0.23	0.001712	0.032077
Snrpb2	0.18	0.001712	0.032077
Cycs	0.14	0.001727	0.032324
Comp	-0.54	0.001731	0.032359
7SK.312	-0.54	0.001737	0.032443
R3hdm1	0.14	0.001746	0.032565
Ppid	0.13	0.001749	0.032597
Pknox2	0.15	0.001752	0.032623
Olfm2	0.32	0.001756	0.03266
Kctd8	-0.36	0.001776	0.032786
Mcts1	0.16	0.001775	0.032786
Nos1	-0.31	0.001777	0.032786
Pitpnm2	-0.23	0.001774	0.032786
Smarcd2	-0.22	0.001773	0.032786
Sod3	-0.22	0.001768	0.032786
Tardbp	0.15	0.00177	0.032786
Tex11	-0.51	0.001771	0.032786
Mtmr6	0.13	0.001782	0.032809
Stk39	0.13	0.001781	0.032809

4930534B04Rik	-0.20	0.001788	0.032843
AC118017.1	-0.29	0.001798	0.032843
Barx2	0.32	0.0018	0.032843
Dimt1	0.14	0.001794	0.032843
Elavl4	0.24	0.00179	0.032843
Gpr12	0.23	0.001789	0.032843
Ltbp3	-0.26	0.001795	0.032843
Mapk10	0.13	0.001798	0.032843
Sfrp1	0.33	0.001798	0.032843
Gm15787	-0.30	0.001805	0.032895
AC044864.2	-0.20	0.00181	0.032934
Klf13	-0.21	0.001809	0.032934
Dazap2	0.09	0.001814	0.03297
Wnk4	-0.32	0.001821	0.033057
Col17a1	-0.53	0.001827	0.033134
Megf11	-0.33	0.00183	0.033169
Necap1	0.11	0.001837	0.033254
Alkbh5	-0.15	0.001842	0.033279
Atp6v1d	0.11	0.001841	0.033279
Uba3	0.18	0.001848	0.033347
Cdc123	0.09	0.001855	0.033422
Wnt5b	-0.37	0.001855	0.033422
Man2b2	-0.17	0.001861	0.033494
Txndc15	0.09	0.001866	0.033539
Cpt2	-0.18	0.001879	0.033742
SNORA17.514	-0.51	0.001883	0.033784
Atp6ap2	0.16	0.001888	0.033826

Tfg	0.10	0.001889	0.033826
Gm10925	0.25	0.001891	0.033827
Gm13405	-0.53	0.001898	0.033923
Arntl	0.19	0.001909	0.034
Chn1	0.10	0.001912	0.034
Dctn6	0.10	0.001911	0.034
Hsd17b12	0.11	0.001905	0.034
Mras	0.11	0.001909	0.034
Tmem194	-0.21	0.001917	0.034065
Aanat	-0.32	0.001922	0.034125
Pard6g	-0.26	0.001933	0.034288
Grin3a	-0.15	0.001945	0.034466
Atl1	0.11	0.001949	0.034475
Nxn	-0.26	0.001951	0.034475
Uros	0.11	0.001951	0.034475
Rbmxrt	0.11	0.001954	0.034478
A430071A18Rik	-0.52	0.001959	0.034547
Golph3	0.12	0.001968	0.034669
Add1	0.08	0.001974	0.034737
Fam107b	-0.47	0.001976	0.034737
Tusc2	0.12	0.001992	0.034991
AL929166.1	0.25	0.001996	0.035033
Gm13069	-0.47	0.001999	0.03504
Ppp3r1	0.16	0.002011	0.035221
Kcnk10	-0.33	0.002017	0.035296
9330162012Rik	-0.24	0.00202	0.035312
1700015E13Rik	-0.45	0.002024	0.035342

H2-M10.2	-0.29	0.002042	0.035622
Rps6ka1	-0.35	0.002044	0.035622
Chsy3	0.25	0.002048	0.035626
Gca	0.18	0.002047	0.035626
Fam174a	0.12	0.002051	0.035641
Ndufv2	0.12	0.002062	0.035801
Cerkl	-0.37	0.002069	0.035889
1810063B05Rik	0.18	0.002076	0.035911
Gm15722	-0.53	0.002075	0.035911
Tekt4	-0.53	0.002075	0.035911
Gm16952	-0.47	0.002078	0.035917
Ddo	-0.29	0.002084	0.035984
L1cam	0.12	0.002093	0.0361
Kit	-0.27	0.0021	0.036198
Otx1	0.37	0.002112	0.036346
Sv2c	-0.20	0.002113	0.036346
2310040G07Rik	-0.43	0.002117	0.036375
Cadps2	-0.38	0.002123	0.036389
Gm11201	-0.47	0.002123	0.036389
Zwint	0.12	0.002122	0.036389
Ppargc1b	-0.24	0.002126	0.036394
B3gat1	0.13	0.002143	0.036622
Dpf3	-0.47	0.002142	0.036622
Rere	-0.13	0.002147	0.03665
Atp1a4	-0.44	0.002158	0.036817
Itpkb	-0.23	0.002164	0.036855
Slc6a5	-0.42	0.002165	0.036855

Zranb2	0.18	0.002169	0.036894
Kif3b	0.09	0.002179	0.037026
AC163094.1	0.25	0.002208	0.037478
Npb	-0.52	0.002209	0.037478
Echdc2	-0.27	0.002221	0.03758
Gatad2b	-0.17	0.002225	0.03758
Mrpl40	0.15	0.002226	0.03758
Stk11ip	0.14	0.002218	0.03758
Zfp111	-0.12	0.002226	0.03758
Fam123c	-0.15	0.002237	0.037732
Ttc36	-0.50	0.002251	0.037934
Gatc	0.10	0.002261	0.038043
Per3	-0.31	0.00226	0.038043
Bptf	-0.11	0.002267	0.038095
Fkbp3	0.16	0.002274	0.038125
Olfr544	-0.52	0.002277	0.038125
Spns3	-0.42	0.002275	0.038125
Vps4a	0.08	0.002272	0.038125
1110002B05Rik	0.14	0.002283	0.038204
Slc22a18	-0.39	0.002287	0.038222
Cpe	0.11	0.002297	0.038357
1110008P14Rik	0.31	0.002303	0.038396
A930001C03Rik	-0.52	0.002303	0.038396
Uck1	0.11	0.002311	0.038486
Pxn	-0.26	0.002313	0.038486
Gm11738	-0.52	0.002321	0.038582
Klhl18	0.11	0.002331	0.038683

Lamb2	-0.24	0.002331	0.038683
Clmn	-0.17	0.002336	0.03871
Pcdha1	0.12	0.002337	0.03871
Rbm17	0.08	0.00234	0.038732
Fat4	-0.28	0.002344	0.038754
Phyhipl	0.11	0.002347	0.038773
Stard3nl	0.11	0.002354	0.038817
Wls	0.22	0.002353	0.038817
Cebpg	0.14	0.002359	0.038871
Egr1	0.47	0.00238	0.039144
Siah1a	0.11	0.00238	0.039144
Prr12	-0.22	0.002387	0.039227
Slc22a15	-0.22	0.00239	0.039227
Sgtb	0.19	0.002399	0.03935
2310046A06Rik	0.17	0.002417	0.03951
B3gat2	-0.16	0.002415	0.03951
Gm9754	-0.44	0.002419	0.03951
Nfya	0.17	0.002424	0.03951
P2rx1	-0.50	0.002423	0.03951
Pcsk2	0.15	0.00242	0.03951
Wnt6	-0.45	0.002424	0.03951
C1ql2	-0.52	0.002429	0.039521
Pskh1	-0.14	0.002429	0.039521
AI480653	0.15	0.002441	0.039672
Commd3	0.11	0.002459	0.039943
Lyrm1	0.14	0.002463	0.039959
Prx	-0.32	0.002487	0.040292

Tmem127	0.09	0.002486	0.040292
Vps45	0.11	0.00249	0.040294
Srsf6	0.11	0.002495	0.040345
Fkbp10	-0.22	0.002519	0.040656
Sox2	0.21	0.002518	0.040656
Cd163	-0.39	0.00253	0.040751
Gm16267	-0.37	0.002531	0.040751
Tmem170	-0.27	0.002531	0.040751
Cdc42	0.14	0.002544	0.040877
Hdac4	-0.16	0.002542	0.040877
2010002N04Rik	-0.33	0.002555	0.040932
Alms1	-0.25	0.002552	0.040932
Tra2a	0.17	0.002556	0.040932
Znrf1	0.14	0.002551	0.040932
Ghrl	-0.23	0.002566	0.041023
Sycp2	-0.28	0.002566	0.041023
Rtp1	-0.51	0.002582	0.041232
Ntn1	-0.34	0.002586	0.041267
H2afz	0.11	0.002602	0.041449
Prrt4	-0.31	0.002601	0.041449
Glrx5	0.15	0.002607	0.041501
Arf2	0.10	0.002631	0.041514
BC018473	-0.44	0.002618	0.041514
C130039O16Rik	-0.13	0.002614	0.041514
Cldn1	0.38	0.002628	0.041514
Gm15345	-0.50	0.002629	0.041514
Kifc2	0.16	0.002616	0.041514

Mpp4	-0.41	0.002621	0.041514
Rac1	0.09	0.002619	0.041514
Snx3	0.11	0.002629	0.041514
Wwc2	-0.12	0.002627	0.041514
Fam136a	0.14	0.002635	0.041546
Cdc42bpg	-0.37	0.002661	0.041888
Gas2l3	-0.31	0.002664	0.041888
Tspyl1	0.08	0.002662	0.041888
RP23-353F16.2	-0.52	0.002668	0.04192
Psap	0.09	0.002686	0.042132
Serpine1	-0.43	0.002686	0.042132
Mrpl50	0.14	0.002694	0.042223
Zic2	-0.48	0.002704	0.042344
Reep1	0.13	0.002721	0.042562
Pfn2	0.12	0.002731	0.04269
Ebna1bp2	0.09	0.002735	0.042717
Gtf2h5	0.10	0.002742	0.042785
Pfas	-0.13	0.002754	0.042863
Rorc	-0.36	0.002754	0.042863
Sgsh	-0.17	0.002751	0.042863
Adamts14	-0.51	0.002761	0.042897
Polg2	-0.23	0.00276	0.042897
Dhtkd1	-0.15	0.002766	0.042913
Dsg2	0.34	0.002765	0.042913
Plcg2	-0.22	0.00277	0.042939
Zdbf2	-0.30	0.002781	0.043069
Fndc1	-0.30	0.002788	0.043137

Rap1gap2	0.11	0.002797	0.043241
Hexa	0.13	0.002804	0.043308
Dopey2	-0.10	0.002811	0.043347
Mapk8	0.23	0.00281	0.043347
Rab9	0.10	0.002826	0.043536
1700061G19Rik	-0.40	0.002831	0.043579
Syce2	-0.25	0.002835	0.043612
6430562O15Rik	-0.32	0.002843	0.043653
Pcna	0.09	0.002843	0.043653
A930028C08Rik	-0.32	0.002851	0.043742
4921518J05Rik	-0.27	0.002858	0.043816
Atg2b	-0.11	0.002863	0.043849
Cox7b	0.13	0.002868	0.043892
1700056N10Rik	-0.22	0.002888	0.044118
Acyp1	0.20	0.00289	0.044118
Gm14015	0.51	0.002888	0.044118
Hnrnpm	0.11	0.002893	0.044128
Glt8d2	0.24	0.002897	0.044157
Atp2a3	-0.49	0.002901	0.044176
Bloc1s3	0.16	0.002904	0.044186
Mterfd1	0.15	0.002923	0.044433
Dusp22	0.10	0.002931	0.044527
Gm14169	0.17	0.00295	0.044777
Slc6a7	0.15	0.002959	0.044872
Ccdc78	-0.37	0.002962	0.044889
Akr1b8	-0.37	0.002965	0.04489
Ribc1	-0.37	0.00297	0.044926

AC151908.1	-0.17	0.002977	0.044996
Elmod3	-0.13	0.002982	0.045041
Gm10818	-0.35	0.002992	0.045115
Ston1	-0.27	0.00299	0.045115
Mtor	-0.10	0.003011	0.045302
Nhsl2	-0.13	0.003012	0.045302
Pyroxd2	-0.25	0.003011	0.045302
1700026J04Rik	-0.34	0.003026	0.04548
Uts2	-0.51	0.003038	0.045625
Bbs12	0.23	0.003055	0.045756
Cacng8	-0.28	0.003054	0.045756
P2rx5	-0.44	0.00305	0.045756
Cdca7l	0.28	0.003062	0.045825
Bzw1	0.16	0.003076	0.045998
Btg2	0.37	0.003092	0.046198
1700094C10Rik	-0.51	0.003095	0.046203
Plxnb1	-0.16	0.003101	0.046203
Prrg3	0.13	0.003102	0.046203
Vps29	0.13	0.003098	0.046203
Gm16719	-0.51	0.003109	0.046234
Tcp11	-0.40	0.003108	0.046234
Mkl2	-0.14	0.003115	0.046278
Mir665	-0.48	0.003123	0.046362
Dhdpsl	-0.35	0.003127	0.046385
Ccdc67	-0.46	0.003137	0.046493
4921536K21Rik	-0.43	0.003149	0.046559
Gm5077	-0.40	0.003149	0.046559

Tns1	-0.17	0.003146	0.046559
Nptn	0.11	0.003174	0.046897
Atp2c2	-0.41	0.003185	0.046927
Pqlc1	-0.18	0.003187	0.046927
Tmem177	0.14	0.00318	0.046927
Zcchc18	0.11	0.003182	0.046927
Tpo	-0.50	0.00319	0.04694
Tead4	-0.50	0.003196	0.046989
Hinfp	-0.14	0.003212	0.047186
Tcf25	0.09	0.003223	0.04731
Mat2b	0.14	0.003227	0.047317
St3gal6	0.13	0.003229	0.047317
Xrcc3	-0.21	0.003235	0.047381
Snrpd1	0.16	0.003248	0.047529
Cybasc3	0.15	0.003252	0.047541
Syn2	0.09	0.003283	0.047962
9130017K11Rik	0.49	0.003292	0.048037
Elp3	0.08	0.003296	0.048037
Mov10	-0.22	0.003296	0.048037
Abhd2	-0.17	0.003311	0.048222
Wbp4	0.09	0.003318	0.048276
Ccdc25	0.14	0.003323	0.048282
Gpd1l	0.09	0.003325	0.048282
Slc25a4	0.08	0.003326	0.048282
Kdm1a	0.07	0.003331	0.048319
Dffa	0.09	0.00334	0.048376
Ftsjd2	0.10	0.00334	0.048376

4930443O20Rik	-0.49	0.003366	0.048568
Aurkc	-0.49	0.003359	0.048568
Fgfr1op2	0.15	0.003361	0.048568
Mir1942	-0.50	0.003367	0.048568
Trem3	0.50	0.003366	0.048568
Dcxr	-0.25	0.003372	0.048608
Bnip3	0.18	0.003382	0.048625
Dusp6	0.36	0.003384	0.048625
Nphs1as	-0.50	0.003378	0.048625
Wnt9b	-0.49	0.003383	0.048625
Arhgap17	-0.13	0.003389	0.048656
Ank1	-0.31	0.003399	0.048726
Cep164	-0.14	0.003399	0.048726
Gon4l	-0.06	0.003416	0.04893
Osbpl1a	0.23	0.003419	0.04894
Abca2	-0.14	0.003423	0.048958
Ppp2r3c	0.16	0.003431	0.049028
Gm15489	-0.32	0.003438	0.049093
Shisa5	0.15	0.003441	0.049093
Abcc5	0.13	0.00345	0.049177
Gm10565	-0.48	0.003452	0.049177
CT030259.3	-0.31	0.003455	0.049179
BB114351	-0.41	0.003465	0.04929
Colq	-0.50	0.003478	0.049394
Tnrc6b	-0.13	0.003478	0.049394
Actb	-0.11	0.003515	0.049877

Supplementary Table S2. Differentially expressed genes from the PVC of *APOE3/4* vs. *APOE3/3* mice

Gene Name	log2 FoldChange	p-value	FDR
Serpina3m	1.86	1.00E-36	1.66E-32
Oscar	1.60	5.49E-29	4.55E-25
Serpina3n	1.53	4.45E-28	2.46E-24
Rdh13	-0.53	1.91E-26	7.90E-23
Ptprh	1.13	1.84E-14	6.09E-11
Thnsl1	0.49	3.19E-12	8.82E-09
Tmc4	0.71	5.55E-11	1.31E-07
Dctd	-0.57	9.84E-11	2.04E-07
Wdfy1	-0.54	1.12E-09	2.07E-06
Zc3h7b	0.25	2.11E-09	3.49E-06
Gm15494	-0.81	2.63E-09	3.96E-06
BC060267	-0.46	5.93E-09	8.18E-06
Fmo2	-0.77	1.96E-08	2.49E-05
Gm8759	0.48	2.29E-08	2.71E-05
2210404J11Rik	-0.31	3.78E-08	4.17E-05
Serpina3g	0.74	1.63E-07	0.000168
Asprv1	-0.62	4.73E-07	0.00046
RP24-161J8.2	-0.62	7.13E-07	0.000656
Gm1082	0.72	8.29E-07	0.000657
Hif3a	-0.67	8.33E-07	0.000657
Psg16	-0.23	7.59E-07	0.000657
Fbxo5	0.59	9.36E-07	0.000705
Ica1	-0.35	1.46E-06	0.001051

Maml3	0.46	5.88E-06	0.003894
Nrbp2	-0.26	5.76E-06	0.003894
1700048O20Rik	-0.46	9.66E-06	0.005928
Gm10931	-0.59	9.33E-06	0.005928
Gm1078	-0.46	1.30E-05	0.007719
Gm15594	-0.64	1.43E-05	0.008191
Pisd	-0.28	1.63E-05	0.009001
Gm16854	-0.61	1.77E-05	0.009452
Rps14	0.24	1.94E-05	0.010054
Gm5506	0.39	2.05E-05	0.010293
Gm10094	0.57	2.13E-05	0.010379
Rpa3	-0.34	2.53E-05	0.011949
C8g	-0.35	3.31E-05	0.014492
Gm10654	-0.40	3.32E-05	0.014492
Rpl30	0.20	3.16E-05	0.014492
Cdkn2c	0.45	4.27E-05	0.018126
Akt2	0.27	4.82E-05	0.019952
Tcea2	-0.23	4.96E-05	0.020029
Gm9846	0.45	5.45E-05	0.021494
Mtmr4	-0.16	7.52E-05	0.028961
Zfp629	-0.13	8.44E-05	0.031786
Irak1	-0.19	9.10E-05	0.03349
Srp54b	0.27	0.000108	0.039036
Gm10268	0.41	0.000122	0.042921
Nhlh1	-0.56	0.000131	0.044114
Otud1	0.28	0.000129	0.044114
2500003M10Rik	0.13	0.000133	0.044169

Gm12394	-0.46	0.000139	0.045173
Rps3a	0.19	0.000144	0.045888
Large	0.18	0.000158	0.048456
Nudt3	0.18	0.000158	0.048456
Snrpd3	0.21	0.000161	0.048456

Table S3. Differentially expressed untargeted metabolites from the EC of APOE3 vs. E4 mice

Mass (Da) @ Retention Time (min)	Regulation in E4/4	Fold Change	p-value	FDR	Detection Mode
386.186@1.277	up	3.25	0.001	0.012	positive
191.151@9.700	up	1.48	0.001	0.012	positive
295.251@1.347	down	1.31	0.001	0.012	positive
403.209@1.277	up	2.72	0.001	0.012	positive
772.707@1.277	up	3.55	0.001	0.012	positive
279.254@1.379	down	1.38	0.001	0.012	positive
789.398@1.275	up	6.27	0.001	0.012	positive
173.140@9.690	up	1.66	0.001	0.012	positive
281.270@1.379	down	1.55	0.001	0.012	positive
681.437@1.328	up	2.26	0.001	0.012	positive
330.121@1.276	up	2.78	0.001	0.012	positive
667.456@1.355	up	2.25	0.001	0.012	positive
665.441@1.363	up	2.43	0.001	0.012	positive
297.264@1.344	down	1.33	0.001	0.012	positive
556.448@1.344	down	1.28	0.001	0.012	positive
387.356@1.276	up	3.75	0.001	0.012	positive
683.449@1.329	up	2.05	0.001	0.012	positive
97.088@9.700	up	1.47	0.001	0.012	positive
472.270@1.247	up	6.65	0.001	0.012	positive
472.280@1.211	down	13.97	0.001	0.012	positive
136.073@2.354	up	4.07	0.001	0.012	positive
508.230@2.083	up	3.37	0.001	0.012	positive
386.779@1.279	up	3.85	0.001	0.012	positive
467.184@1.436	up	2.49	0.001	0.012	positive
701.462@1.432	up	4.04	0.001	0.012	positive
200.046@5.028	up	1.98	0.001	0.012	positive
742.247@1.458	up	1.87	0.001	0.012	positive
536.526@1.393	down	1.78	0.001	0.012	positive
251.224@1.397	down	1.24	0.001	0.012	positive
900.685@1.443	up	2.73	0.001	0.012	positive
155.130@9.692	up	1.63	0.001	0.012	positive
640.135@10.140	up	1.74	0.001	0.012	positive
697.432@1.323	up	2.25	0.001	0.012	positive
180.019@1.418	up	1.84	0.001	0.012	positive
699.446@1.385	up	2.89	0.001	0.012	positive

574.210@9.700	up	1.68	0.001	0.012	positive
269.238@1.355	down	1.41	0.001	0.012	positive
580.217@1.283	up	2.48	0.001	0.012	positive
667.457@1.355	up	2.25	0.001	0.012	positive
574.318@9.703	up	1.66	0.001	0.012	positive
900.690@1.443	up	2.40	0.001	0.012	positive
772.944@1.276	up	12.77	0.001	0.012	positive
506.475@1.386	down	1.54	0.001	0.012	positive
118.063@2.355	up	3.65	0.001	0.012	positive
403.206@1.539	up	4.48	0.001	0.012	positive
653.402@1.344	up	3.62	0.001	0.012	positive
262.227@1.379	down	1.35	0.001	0.012	positive
403.381@1.274	up	3.49	0.001	0.012	positive
80.062@1.379	down	1.29	0.001	0.012	positive
789.631@1.270	up	9.38	0.001	0.012	positive
261.192@9.629	up	1.35	0.001	0.012	positive
794.355@1.275	up	5.83	0.001	0.012	positive
246.221@9.299	up	1.87	0.001	0.012	positive
683.271@2.120	up	5.47	0.001	0.012	positive
560.518@1.380	down	1.97	0.001	0.012	positive
695.423@1.342	up	2.59	0.001	0.012	positive
710.620@1.386	down	1.70	0.001	0.012	positive
776.853@1.271	up	4.02	0.001	0.012	positive
655.428@1.334	up	2.08	0.001	0.012	positive
990.823@1.282	up	2.22	0.001	0.012	positive
990.829@1.282	up	2.56	0.001	0.012	positive
576.823@9.699	up	1.58	0.001	0.012	positive
277.222@9.631	up	2.85	0.001	0.012	positive
889.205@1.346	down	1.43	0.001	0.012	positive
566.508@1.426	down	1.43	0.001	0.012	positive
886.688@1.341	down	1.45	0.001	0.012	positive
854.355@1.441	up	8.56	0.001	0.012	positive
858.465@1.285	up	10.13	0.001	0.012	positive
265.227@1.385	down	1.60	0.001	0.012	positive
519.763@9.689	up	1.79	0.001	0.012	positive
120.089@1.368	down	1.22	0.001	0.012	positive
544.316@1.208	up	2.43	0.001	0.012	positive
333.213@1.354	down	3.14	0.001	0.012	positive
266.206@9.705	up	3.73	0.001	0.012	positive
307.198@9.729	up	1.72	0.001	0.012	positive
637.414@1.375	up	3.77	0.001	0.012	positive

636.165@1.273	up	2.33	0.001	0.012	positive
774.084@1.278	up	6.45	0.001	0.012	positive
508.493@1.369	down	2.16	0.001	0.012	positive
534.509@1.370	down	2.18	0.001	0.012	positive
241.213@1.375	down	1.64	0.001	0.012	positive
655.422@1.333	up	2.05	0.001	0.012	positive
323.273@1.334	down	1.74	0.001	0.012	positive
533.252@1.445	up	8.86	0.001	0.012	positive
917.339@1.443	up	6.10	0.001	0.012	positive
789.735@1.279	up	17.67	0.001	0.012	positive
629.372@1.971	up	9.18	0.001	0.012	positive
576.958@9.702	up	1.63	0.001	0.012	positive
274.063@1.281	up	2.84	0.001	0.012	positive
667.675@1.356	up	2.72	0.001	0.012	positive
731.430@1.422	up	2.26	0.001	0.012	positive
677.407@1.334	up	2.66	0.001	0.012	positive
713.422@1.350	up	2.26	0.001	0.012	positive
729.425@1.402	up	2.67	0.001	0.012	positive
316.093@2.535	up	3.74	0.001	0.012	positive
562.939@1.379	down	1.78	0.001	0.012	positive
660.673@1.274	up	8.95	0.001	0.012	positive
442.254@1.200	up	5.47	0.001	0.012	positive
807.153@1.274	up	2.96	0.001	0.012	positive
183.155@1.382	down	1.90	0.001	0.012	positive
934.369@1.435	up	2.23	0.001	0.012	positive
681.748@1.321	up	2.71	0.001	0.012	positive
657.447@1.374	up	3.02	0.001	0.012	positive
797.387@1.282	up	14.72	0.001	0.012	positive
731.437@1.422	up	2.14	0.001	0.012	positive
403.447@1.275	up	4.17	0.001	0.012	positive
627.413@1.356	up	5.36	0.001	0.012	positive
429.395@7.778	up	2.58	0.001	0.012	positive
684.237@1.451	up	2.08	0.001	0.012	positive
627.415@1.363	up	4.08	0.001	0.012	positive
485.278@9.312	up	1.86	0.001	0.012	positive
807.152@1.274	up	3.31	0.001	0.012	positive
700.137@1.418	up	1.80	0.001	0.012	positive
229.233@8.620	up	1.24	0.001	0.012	positive
178.166@1.379	down	1.70	0.001	0.012	positive
385.281@1.410	down	1.56	0.001	0.012	positive
422.163@1.266	up	3.10	0.001	0.012	negative

424.161@1.266	up	3.19	0.001	0.012	negative
446.206@1.268	up	4.25	0.001	0.012	negative
200.044@5.046	up	1.62	0.001	0.012	negative
450.158@1.415	up	2.17	0.001	0.012	negative
492.135@5.046	up	1.66	0.001	0.012	negative
742.247@1.458	up	1.86	0.001	0.012	negative
424.336@1.266	up	4.37	0.001	0.012	negative
449.181@1.261	up	3.08	0.001	0.012	negative
404.196@1.422	up	4.10	0.001	0.012	negative
264.014@7.119	up	1.81	0.001	0.012	negative
446.206@1.262	up	4.48	0.001	0.012	negative
191.916@5.047	up	1.59	0.001	0.012	negative
422.783@1.268	up	5.40	0.001	0.012	negative
334.046@10.373	up	4.27	0.001	0.012	negative
200.168@5.048	up	1.66	0.001	0.012	negative
514.093@1.270	up	2.60	0.001	0.012	negative
450.338@1.416	up	2.55	0.001	0.012	negative
286.119@4.311	up	4.87	0.001	0.012	negative
416.028@10.351	up	4.10	0.001	0.012	negative
333.238@1.351	down	1.44	0.001	0.012	negative
200.044@7.119	up	1.56	0.001	0.012	negative
374.073@10.325	up	4.61	0.001	0.012	negative
356.174@1.269	up	2.62	0.001	0.012	negative
424.780@1.260	up	5.60	0.001	0.012	negative
331.228@1.331	down	1.42	0.001	0.012	negative
434.038@10.351	up	4.78	0.001	0.012	negative
374.010@5.049	up	1.50	0.001	0.012	negative
850.822@1.268	up	5.98	0.001	0.012	negative
696.289@1.450	up	4.71	0.001	0.012	negative
556.106@7.113	up	1.81	0.001	0.012	negative
341.995@7.123	up	1.61	0.001	0.012	negative
235.997@2.353	up	5.60	0.001	0.012	negative
426.167@1.265	up	3.36	0.001	0.012	negative
349.234@1.379	down	1.25	0.001	0.012	negative
468.169@4.330	up	2.16	0.001	0.012	negative
196.090@2.343	up	4.98	0.001	0.012	negative
450.410@1.416	up	3.20	0.001	0.012	negative
191.917@7.124	up	1.74	0.001	0.012	negative
318.104@6.006	up	2.97	0.001	0.012	negative
386.186@1.269	up	3.57	0.001	0.012	negative
304.018@5.064	up	1.36	0.001	0.012	negative

432.198@1.265	up	10.65	0.001	0.012	negative
512.185@1.267	up	1.62	0.001	0.012	negative
254.132@1.229	up	1.94	0.001	0.012	negative
614.181@1.414	up	2.04	0.001	0.012	negative
610.197@6.008	up	7.45	0.001	0.012	negative
578.207@4.303	up	7.30	0.001	0.012	negative
742.476@1.460	up	2.04	0.001	0.012	negative
500.121@5.060	up	1.46	0.001	0.012	negative
594.088@4.925	up	1.96	0.001	0.012	negative
596.221@1.432	up	4.26	0.001	0.012	negative
490.203@1.294	up	5.00	0.001	0.012	negative
596.108@5.056	up	1.61	0.001	0.012	negative
586.201@1.249	up	2.04	0.001	0.012	negative
898.728@1.261	up	3.62	0.001	0.012	negative
218.013@2.383	up	1.89	0.001	0.012	negative
492.135@5.042	up	1.68	0.001	0.012	negative
336.074@4.992	up	2.22	0.001	0.012	negative
666.219@7.821	up	2.22	0.001	0.012	negative
614.182@1.414	up	2.03	0.001	0.012	negative
388.099@5.039	up	1.49	0.001	0.012	negative
382.075@7.279	up	2.29	0.001	0.012	negative
376.008@5.046	up	1.50	0.001	0.012	negative
386.041@4.301	up	3.56	0.001	0.012	negative
492.396@5.042	up	3.35	0.001	0.012	negative
431.105@5.042	up	1.53	0.001	0.012	negative
420.336@2.339	up	17.11	0.001	0.012	negative
510.233@1.225	up	4.37	0.001	0.012	negative
530.198@1.419	up	6.40	0.001	0.012	negative
451.990@5.046	up	1.83	0.001	0.012	negative
504.167@7.031	up	2.00	0.001	0.012	negative
642.203@6.955	up	1.67	0.001	0.012	negative
476.215@2.809	up	4.94	0.001	0.012	negative
192.119@5.045	up	1.72	0.001	0.012	negative
419.973@7.156	up	1.51	0.001	0.012	negative
764.188@7.811	up	2.57	0.001	0.012	negative
617.177@1.422	up	2.56	0.001	0.012	negative
184.050@4.293	up	1.97	0.001	0.012	negative
141.948@10.350	up	16.89	0.001	0.012	negative
780.203@1.449	up	2.53	0.001	0.012	negative
633.186@7.035	up	2.44	0.001	0.012	negative
596.179@2.361	up	4.24	0.001	0.012	negative

150.021@7.323	down	4.38	0.001	0.012	negative
795.160@1.430	up	3.81	0.001	0.012	negative
258.131@1.961	up	2.37	0.001	0.012	negative
828.275@8.413	up	3.07	0.001	0.012	negative
267.221@1.367	down	1.26	0.002	0.016	positive
255.254@1.404	down	1.33	0.002	0.016	positive
653.283@3.085	up	2.11	0.002	0.016	positive
574.706@9.701	up	1.73	0.002	0.016	positive
562.834@1.379	down	1.55	0.002	0.016	positive
886.824@1.347	down	1.56	0.002	0.016	positive
550.538@1.403	down	1.72	0.002	0.016	positive
371.174@8.148	up	2.87	0.002	0.016	positive
70.076@1.359	down	1.37	0.002	0.016	positive
800.543@1.198	up	1.65	0.002	0.016	positive
679.424@1.321	up	1.27	0.002	0.016	positive
551.281@1.285	up	1.97	0.002	0.016	positive
972.323@7.826	up	3.06	0.002	0.016	positive
802.076@1.364	down	1.36	0.002	0.016	positive
727.444@1.300	up	1.50	0.002	0.016	positive
459.226@7.870	up	1.71	0.002	0.016	positive
242.022@6.421	up	1.96	0.002	0.018	negative
534.110@6.421	up	2.12	0.002	0.018	negative
246.009@7.121	up	2.37	0.002	0.018	negative
524.092@1.410	up	1.74	0.002	0.018	negative
478.069@5.049	up	3.98	0.002	0.018	negative
250.219@1.350	down	1.33	0.003	0.021	positive
461.292@1.408	up	1.38	0.003	0.021	positive
717.565@1.398	down	1.34	0.003	0.021	positive
232.216@1.356	down	1.23	0.003	0.021	positive
260.210@1.362	down	1.23	0.003	0.021	positive
153.108@1.392	down	1.38	0.003	0.021	positive
465.170@1.438	up	1.71	0.003	0.021	positive
406.290@1.218	down	1.53	0.003	0.021	positive
521.198@7.040	up	1.98	0.003	0.021	positive
283.173@1.832	up	7.14	0.003	0.021	positive
665.662@1.360	up	3.05	0.003	0.021	positive
557.309@8.349	up	1.93	0.003	0.021	positive
835.103@1.346	down	1.31	0.003	0.021	positive
972.327@7.043	up	2.69	0.003	0.021	positive
622.794@1.402	down	1.28	0.003	0.021	positive
154.006@3.792	up	1.31	0.003	0.024	negative

335.239@1.357	down	1.27	0.003	0.024	negative
611.172@6.833	up	1.82	0.003	0.024	negative
104.044@2.228	up	1.31	0.003	0.024	negative
58.042@7.453	up	1.22	0.003	0.024	negative
321.212@1.368	up	2.89	0.003	0.024	negative
478.073@5.044	up	4.19	0.003	0.024	negative
482.181@1.290	up	2.02	0.003	0.024	negative
438.147@1.302	down	1.65	0.003	0.024	negative
749.941@1.160	up	1.25	0.004	0.028	positive
344.079@2.194	down	17.74	0.004	0.028	positive
327.199@2.027	up	14.61	0.004	0.028	positive
152.115@1.352	down	1.36	0.004	0.028	positive
574.604@9.700	up	1.66	0.004	0.028	positive
213.161@1.398	down	1.69	0.004	0.028	positive
118.064@5.030	up	1.61	0.004	0.028	positive
359.192@8.408	up	1.86	0.004	0.028	positive
463.073@10.792	up	1.48	0.004	0.028	positive
274.187@1.393	down	1.27	0.004	0.028	positive
448.144@1.438	up	1.66	0.004	0.028	positive
603.844@17.681	down	1.17	0.004	0.028	positive
118.026@1.376	down	1.42	0.004	0.032	negative
236.051@1.376	down	1.37	0.004	0.032	negative
464.101@10.288	down	1.63	0.004	0.032	negative
434.118@6.584	up	1.33	0.004	0.032	negative
612.175@1.435	up	1.95	0.004	0.032	negative
278.035@5.046	up	1.81	0.004	0.032	negative
617.173@1.417	up	2.04	0.004	0.032	negative
390.031@7.359	down	4.37	0.005	0.043	negative
194.115@2.535	up	1.82	0.005	0.036	positive
156.159@24.812	up	1.62	0.005	0.036	positive
150.088@2.295	up	1.75	0.005	0.036	positive
250.975@1.161	up	1.22	0.005	0.036	positive
386.970@1.279	up	2.56	0.005	0.036	positive
774.844@1.278	up	1.80	0.005	0.036	positive
422.287@2.533	up	1.72	0.005	0.036	positive
141.147@9.405	up	1.49	0.005	0.036	positive
241.219@1.382	down	1.36	0.005	0.036	positive
582.704@2.535	up	1.76	0.005	0.036	positive
612.477@1.440	down	1.41	0.005	0.036	positive
116.061@1.626	up	2.42	0.005	0.036	positive
618.595@1.554	down	2.74	0.005	0.036	positive

78.047@1.374	down	1.51	0.005	0.036	positive
150.135@1.369	down	1.34	0.005	0.036	positive
515.301@5.145	up	5.91	0.005	0.036	positive
90.030@7.680	up	1.15	0.005	0.043	negative
419.152@5.090	up	1.37	0.005	0.043	negative
500.174@1.273	up	3.96	0.005	0.043	negative
512.858@1.421	down	1.41	0.005	0.043	negative
523.049@6.882	up	1.15	0.005	0.043	negative
773.224@7.256	up	2.02	0.005	0.043	negative
511.103@9.165	up	1.34	0.005	0.043	negative
619.090@7.472	up	2.33	0.005	0.043	negative
238.142@2.995	up	1.87	0.008	0.048	positive
293.219@1.416	down	1.21	0.008	0.048	positive
277.234@1.439	down	1.18	0.008	0.048	positive
88.053@2.530	up	1.98	0.008	0.048	positive
311.245@1.415	down	1.19	0.008	0.048	positive
817.417@1.268	up	1.94	0.008	0.048	positive
82.044@1.285	up	1.59	0.008	0.048	positive
269.158@7.136	up	2.87	0.008	0.048	positive
714.828@2.990	up	2.05	0.008	0.048	positive
626.818@1.407	down	1.21	0.008	0.048	positive
443.326@1.386	down	1.79	0.008	0.048	positive
765.915@2.993	up	2.77	0.008	0.048	positive

Table S4. Differentially expressed untargeted metabolites from the PVC of APOE3 vs. E4 mice

Mass (Da) @ Retention Time (min)	Regulation in E4/4	Fold Change	p-value	FDR	Detection Mode
386.186@1.277	up	3.11	0.001	0.014	positive
191.151@9.700	up	1.51	0.001	0.014	positive
403.209@1.277	up	2.64	0.001	0.014	positive
772.707@1.277	up	3.55	0.001	0.014	positive
279.254@1.379	down	1.37	0.001	0.014	positive
789.398@1.275	up	6.08	0.001	0.014	positive
173.140@9.690	up	1.64	0.001	0.014	positive
281.270@1.379	down	1.43	0.001	0.014	positive
681.437@1.328	up	2.29	0.001	0.014	positive
330.121@1.276	up	2.60	0.001	0.014	positive
667.456@1.355	up	2.10	0.001	0.014	positive
665.441@1.363	up	2.15	0.001	0.014	positive
297.264@1.344	down	1.30	0.001	0.014	positive
387.356@1.276	up	3.69	0.001	0.014	positive
683.449@1.329	up	2.02	0.001	0.014	positive
97.088@9.700	up	1.51	0.001	0.014	positive
472.270@1.247	up	20.46	0.001	0.014	positive
810.327@1.275	up	5.15	0.001	0.014	positive
472.280@1.211	down	12.38	0.001	0.014	positive
255.254@1.404	down	1.27	0.001	0.014	positive
136.073@2.354	up	2.90	0.001	0.014	positive
508.230@2.083	up	3.89	0.001	0.014	positive
386.779@1.279	up	4.48	0.001	0.014	positive
467.184@1.436	up	2.81	0.001	0.014	positive
424.141@1.280	up	2.13	0.001	0.014	positive
701.462@1.432	up	3.64	0.001	0.014	positive
174.008@1.273	up	1.94	0.001	0.014	positive
536.526@1.393	down	1.59	0.001	0.014	positive
251.224@1.397	down	1.28	0.001	0.014	positive
900.685@1.443	up	8.45	0.001	0.014	positive
155.130@9.692	up	1.60	0.001	0.014	positive
697.432@1.323	up	2.17	0.001	0.014	positive
180.019@1.418	up	1.64	0.001	0.014	positive
699.446@1.385	up	2.57	0.001	0.014	positive
574.210@9.700	up	1.74	0.001	0.014	positive

269.238@1.355	down	1.36	0.001	0.014	positive
580.217@1.283	up	2.50	0.001	0.014	positive
250.975@1.161	up	1.14	0.001	0.014	positive
667.457@1.355	up	2.10	0.001	0.014	positive
574.318@9.703	up	1.68	0.001	0.014	positive
900.690@1.443	up	5.28	0.001	0.014	positive
772.944@1.276	up	10.49	0.001	0.014	positive
506.475@1.386	down	1.51	0.001	0.014	positive
118.063@2.355	up	2.75	0.001	0.014	positive
262.227@1.379	down	1.29	0.001	0.014	positive
403.381@1.274	up	3.62	0.001	0.014	positive
789.631@1.270	up	5.61	0.001	0.014	positive
246.221@9.299	up	1.76	0.001	0.014	positive
683.271@2.120	up	4.25	0.001	0.014	positive
560.518@1.380	down	1.96	0.001	0.014	positive
695.423@1.342	up	1.72	0.001	0.014	positive
710.620@1.386	down	2.26	0.001	0.014	positive
776.853@1.271	up	4.51	0.001	0.014	positive
655.428@1.334	up	1.81	0.001	0.014	positive
990.823@1.282	up	2.14	0.001	0.014	positive
574.706@9.701	up	1.70	0.001	0.014	positive
990.829@1.282	up	2.29	0.001	0.014	positive
576.823@9.699	up	1.61	0.001	0.014	positive
277.222@9.631	up	2.74	0.001	0.014	positive
566.508@1.426	down	1.53	0.001	0.014	positive
886.688@1.341	down	1.40	0.001	0.014	positive
854.355@1.441	up	6.49	0.001	0.014	positive
858.465@1.285	up	10.18	0.001	0.014	positive
562.834@1.379	down	1.54	0.001	0.014	positive
544.316@1.208	up	2.70	0.001	0.014	positive
266.206@9.705	up	2.65	0.001	0.014	positive
636.165@1.273	up	2.09	0.001	0.014	positive
241.219@1.382	down	1.27	0.001	0.014	positive
774.084@1.278	up	7.49	0.001	0.014	positive
508.493@1.369	down	2.10	0.001	0.014	positive
534.509@1.370	down	2.07	0.001	0.014	positive
655.422@1.333	up	1.80	0.001	0.014	positive
917.339@1.443	up	8.14	0.001	0.014	positive
789.735@1.279	up	14.76	0.001	0.014	positive
723.519@1.621	up	3.58	0.001	0.014	positive
576.958@9.702	up	1.68	0.001	0.014	positive

274.063@1.281	up	3.15	0.001	0.014	positive
800.543@1.198	up	1.72	0.001	0.014	positive
713.422@1.350	up	2.12	0.001	0.014	positive
729.425@1.402	up	2.37	0.001	0.014	positive
316.093@2.535	up	2.96	0.001	0.014	positive
679.424@1.321	up	1.38	0.001	0.014	positive
562.939@1.379	down	1.69	0.001	0.014	positive
660.673@1.274	up	11.80	0.001	0.014	positive
442.254@1.200	up	3.63	0.001	0.014	positive
807.153@1.274	up	4.24	0.001	0.014	positive
934.369@1.435	up	3.52	0.001	0.014	positive
938.270@1.439	up	5.64	0.001	0.014	positive
681.748@1.321	up	3.15	0.001	0.014	positive
146.105@1.305	up	1.42	0.001	0.014	positive
797.387@1.282	up	13.54	0.001	0.014	positive
731.437@1.422	up	2.44	0.001	0.014	positive
403.447@1.275	up	3.55	0.001	0.014	positive
627.413@1.356	up	4.23	0.001	0.014	positive
429.395@7.778	up	3.77	0.001	0.014	positive
485.278@9.312	up	1.88	0.001	0.014	positive
745.417@1.429	up	2.29	0.001	0.014	positive
807.152@1.274	up	4.64	0.001	0.014	positive
203.114@13.469	up	1.40	0.002	0.018	positive
742.247@1.458	up	2.34	0.002	0.018	positive
84.021@13.470	up	1.36	0.002	0.018	positive
261.192@9.629	up	1.49	0.002	0.018	positive
241.270@8.482	down	9.41	0.002	0.018	positive
886.824@1.347	down	1.31	0.002	0.018	positive
369.296@1.310	down	1.97	0.002	0.018	positive
203.238@13.469	up	1.48	0.002	0.018	positive
241.213@1.375	down	1.33	0.002	0.018	positive
550.538@1.403	down	1.39	0.002	0.018	positive
371.174@8.148	up	2.81	0.002	0.018	positive
592.920@1.348	down	1.44	0.002	0.018	positive
118.064@5.030	up	2.10	0.002	0.018	positive
677.407@1.334	up	1.94	0.002	0.018	positive
835.103@1.346	down	1.26	0.002	0.018	positive
684.237@1.451	up	2.80	0.002	0.018	positive
609.848@13.474	up	1.53	0.002	0.018	positive
295.251@1.347	down	1.22	0.003	0.023	positive
311.245@1.402	down	1.15	0.003	0.023	positive

200.046@5.028	up	2.27	0.003	0.023	positive
250.219@1.350	down	1.18	0.003	0.023	positive
243.186@9.691	up	1.16	0.003	0.023	positive
312.274@8.872	down	1.26	0.003	0.023	positive
575.489@1.357	up	1.22	0.003	0.023	positive
889.205@1.346	down	1.27	0.003	0.023	positive
637.414@1.375	up	3.05	0.003	0.023	positive
82.044@1.285	up	2.03	0.003	0.023	positive
144.043@13.472	up	1.39	0.003	0.023	positive
335.222@1.371	down	1.55	0.003	0.023	positive
731.430@1.422	up	1.87	0.003	0.023	positive
665.662@1.360	up	2.73	0.003	0.023	positive
557.309@8.349	up	2.01	0.003	0.023	positive
627.415@1.363	up	3.49	0.003	0.023	positive
422.163@1.266	up	3.31	0.001	0.026	negative
424.161@1.266	up	3.50	0.001	0.026	negative
446.206@1.268	up	4.12	0.001	0.026	negative
450.158@1.415	up	2.73	0.001	0.026	negative
424.336@1.266	up	4.79	0.001	0.026	negative
449.181@1.261	up	3.06	0.001	0.026	negative
446.206@1.262	up	4.46	0.001	0.026	negative
422.783@1.268	up	7.22	0.001	0.026	negative
422.730@1.268	up	5.75	0.001	0.026	negative
642.183@1.464	up	4.91	0.001	0.026	negative
450.338@1.416	up	3.42	0.001	0.026	negative
286.119@4.311	up	4.02	0.001	0.026	negative
416.028@10.351	up	3.24	0.001	0.026	negative
374.073@10.325	up	3.76	0.001	0.026	negative
356.174@1.269	up	4.59	0.001	0.026	negative
424.780@1.260	up	6.11	0.001	0.026	negative
434.038@10.351	up	3.60	0.001	0.026	negative
850.822@1.268	up	7.68	0.001	0.026	negative
235.997@2.353	up	4.04	0.001	0.026	negative
426.167@1.265	up	3.61	0.001	0.026	negative
468.169@4.330	up	1.90	0.001	0.026	negative
450.410@1.416	up	4.53	0.001	0.026	negative
386.186@1.269	up	4.89	0.001	0.026	negative
432.198@1.265	up	11.42	0.001	0.026	negative
500.174@1.273	up	4.45	0.001	0.026	negative
246.009@7.121	up	2.28	0.001	0.026	negative
479.888@10.357	up	3.39	0.001	0.026	negative

898.728@1.261	up	4.25	0.001	0.026	negative
460.091@4.301	up	14.40	0.001	0.026	negative
386.041@4.301	up	3.49	0.001	0.026	negative
478.073@5.044	up	6.00	0.001	0.026	negative
510.233@1.225	up	4.11	0.001	0.026	negative
210.004@3.861	down	3.46	0.001	0.026	negative
476.215@2.809	up	5.05	0.001	0.026	negative
305.992@3.872	down	2.58	0.001	0.026	negative
780.203@1.449	up	3.19	0.001	0.026	negative
466.138@7.514	up	4.02	0.001	0.026	negative
498.171@1.246	up	3.58	0.001	0.026	negative
478.069@5.049	up	4.88	0.001	0.026	negative
530.090@5.032	up	2.26	0.001	0.026	negative
795.160@1.430	up	3.44	0.001	0.026	negative
374.010@5.049	up	1.72	0.002	0.027	negative
110.998@2.919	down	1.53	0.002	0.027	negative
556.106@7.113	up	2.03	0.002	0.027	negative
403.089@2.912	down	1.56	0.002	0.027	negative
191.917@7.124	up	1.93	0.002	0.027	negative
318.104@6.006	up	2.95	0.002	0.027	negative
445.102@1.444	down	5.15	0.002	0.027	negative
614.181@1.414	up	2.28	0.002	0.027	negative
610.197@6.008	up	7.49	0.002	0.027	negative
58.042@7.453	up	1.31	0.002	0.027	negative
596.221@1.432	up	3.11	0.002	0.027	negative
492.135@5.042	up	1.93	0.002	0.027	negative
614.182@1.414	up	2.29	0.002	0.027	negative
388.099@5.039	up	1.78	0.002	0.027	negative
382.075@7.279	up	2.50	0.002	0.027	negative
514.127@4.986	up	2.70	0.002	0.027	negative
451.990@5.046	up	1.96	0.002	0.027	negative
524.092@1.410	up	1.92	0.002	0.027	negative
184.050@4.293	up	2.75	0.002	0.027	negative
258.131@1.961	up	1.95	0.002	0.027	negative
200.044@5.046	up	1.99	0.003	0.030	negative
492.135@5.046	up	1.95	0.003	0.030	negative
742.247@1.458	up	1.88	0.003	0.030	negative
88.015@2.780	up	2.43	0.003	0.030	negative
191.916@5.047	up	1.96	0.003	0.030	negative
413.833@17.826	up	1.05	0.003	0.030	negative
334.046@10.373	up	3.07	0.003	0.030	negative

112.015@1.554	up	2.45	0.003	0.030	negative
200.168@5.048	up	1.99	0.003	0.030	negative
106.026@3.856	down	2.55	0.003	0.030	negative
386.068@2.750	up	19.03	0.003	0.030	negative
304.018@5.064	up	1.79	0.003	0.030	negative
594.088@4.925	up	1.69	0.003	0.030	negative
218.013@2.383	up	2.12	0.003	0.030	negative
431.105@5.042	up	1.77	0.003	0.030	negative
419.973@7.156	up	1.77	0.003	0.030	negative
629.473@1.341	down	1.39	0.003	0.030	negative
278.035@5.046	up	2.70	0.003	0.030	negative
315.277@1.439	down	1.10	0.004	0.031	positive
431.232@1.255	down	1.72	0.004	0.031	positive
414.204@1.258	down	1.78	0.004	0.031	positive
556.448@1.344	down	1.18	0.004	0.031	positive
574.604@9.700	up	1.73	0.004	0.031	positive
774.844@1.278	up	2.39	0.004	0.031	positive
265.227@1.385	down	1.45	0.004	0.031	positive
134.075@1.259	down	1.42	0.004	0.031	positive
307.198@9.729	up	1.50	0.004	0.031	positive
465.170@1.438	up	1.31	0.004	0.031	positive
216.110@10.420	down	1.39	0.004	0.031	positive
183.155@1.382	down	1.59	0.004	0.031	positive
462.476@1.131	down	1.16	0.004	0.031	positive
264.014@7.119	up	1.95	0.004	0.039	negative
514.093@1.270	up	2.38	0.004	0.039	negative
509.820@17.860	up	1.05	0.004	0.039	negative
333.238@1.351	down	1.21	0.004	0.039	negative
200.044@7.119	up	1.87	0.004	0.039	negative
341.995@7.123	up	1.81	0.004	0.039	negative
272.001@1.128	down	1.07	0.004	0.039	negative
500.121@5.060	up	1.64	0.004	0.039	negative
596.108@5.056	up	1.95	0.004	0.039	negative
376.008@5.046	up	1.68	0.004	0.039	negative
398.996@8.771	down	1.17	0.004	0.039	negative
582.407@1.339	down	1.36	0.005	0.041	positive
280.137@1.253	down	1.77	0.005	0.041	positive
488.113@1.435	up	1.80	0.005	0.041	positive
532.242@9.096	up	1.07	0.005	0.041	positive
375.256@9.354	up	1.18	0.005	0.041	positive
231.143@11.714	up	1.26	0.005	0.041	positive

117.040@8.488	down	1.29	0.005	0.041	positive
90.047@1.263	down	2.69	0.005	0.041	positive
150.135@1.369	down	1.33	0.005	0.041	positive
700.137@1.418	up	1.67	0.005	0.041	positive
176.031@2.785	up	39.98	0.005	0.046	negative
684.009@1.538	up	62.14	0.005	0.046	negative
404.196@1.422	up	2.57	0.005	0.046	negative
100.015@1.534	up	1.80	0.005	0.046	negative
210.037@1.998	up	2.09	0.005	0.046	negative
275.956@2.798	up	21.38	0.005	0.046	negative
419.152@5.090	up	1.90	0.005	0.046	negative
726.066@1.393	up	6.12	0.005	0.046	negative
257.946@2.783	up	16.93	0.005	0.046	negative
271.986@2.887	down	1.59	0.005	0.046	negative
364.982@2.818	up	12.87	0.005	0.046	negative
586.201@1.249	up	2.15	0.005	0.046	negative
726.063@1.393	up	6.03	0.005	0.046	negative
337.993@4.729	down	1.50	0.005	0.046	negative
530.198@1.419	up	4.61	0.005	0.046	negative
642.203@6.955	up	1.91	0.005	0.046	negative
482.181@1.290	up	2.47	0.005	0.046	negative
630.182@1.478	up	3.10	0.005	0.046	negative
618.325@4.233	up	4.49	0.005	0.046	negative

Supplementary Table S5. Putative identities of untargeted metabolites from the EC of APOE3 vs. E4 mice by PIUMet analysis

mz-peak	Metabolite-Name	PIUMet-ID	HMDB-ID	monisotopic-molecular weight	Chemical-formula
m/z=82.0441	2-Methylfuran	Met20304	HMDB13749	82.04186481	C5H6O
m/z=82.0441	2,4-Pentadienal	Met11526	HMDB31597	82.04186481	C5H6O
m/z=828.2752	Maltopentaose	Met40535	HMDB12254	828.2746818	C30H52O26
m/z=88.0534	Butyric acid	Met4442	HMDB00039	88.0524295	C4H8O2
m/z=88.0534	Butyric acid	Met4435	HMDB00039	88.0524295	C4H8O2
m/z=88.0534	Butyric acid	Met4437	HMDB00039	88.0524295	C4H8O2
m/z=88.0534	Isobutyric acid	Met34213	HMDB01873	88.0524295	C4H8O2
m/z=88.0534	Methyl propionate	Met26873	HMDB30062	88.0524295	C4H8O2
m/z=88.0534	Ethyl acetate	Met42630	HMDB31217	88.0524295	C4H8O2
m/z=88.0534	1-Hydroxy-2-butanone	Met27352	HMDB31507	88.0524295	C4H8O2
m/z=88.0534	Propyl formate	Met12858	HMDB40253	88.0524295	C4H8O2
m/z=88.0534	Isopropyl formate	Met11917	HMDB40579	88.0524295	C4H8O2
m/z=90.0304	L-Lactic acid	Met2685	HMDB00190	90.03169406	C3H6O3
m/z=90.0304	L-Lactic acid	Met2690	HMDB00190	90.03169406	C3H6O3
m/z=90.0304	L-Lactic acid	Met2687	HMDB00190	90.03169406	C3H6O3
m/z=90.0304	L-Lactic acid	Met2688	HMDB00190	90.03169406	C3H6O3
m/z=90.0304	Hydroxypropionic acid	Met395	HMDB00700	90.03169406	C3H6O3
m/z=90.0304	Hydroxypropionic acid	Met383	HMDB00700	90.03169406	C3H6O3
m/z=90.0304	Glyceraldehyde	Met2434	HMDB01051	90.03169406	C3H6O3
m/z=90.0304	Glyceraldehyde	Met2900	HMDB01051	90.03169406	C3H6O3
m/z=90.0304	D-Lactic acid	Met77	HMDB01311	90.03169406	C3H6O3
m/z=90.0304	D-Lactic acid	Met71	HMDB01311	90.03169406	C3H6O3
m/z=90.0304	D-Lactic acid	Met69	HMDB01311	90.03169406	C3H6O3
m/z=90.0304	Dihydroxyacetone	Met3499	HMDB01882	90.03169406	C3H6O3
m/z=90.0304	Dihydroxyacetone	Met386	HMDB01882	90.03169406	C3H6O3
m/z=90.0304	Dimethyl carbonate	Met15485	HMDB29580	90.03169406	C3H6O3
m/z=90.0304	Monoethyl carbonate	Met13334	HMDB31232	90.03169406	C3H6O3
m/z=90.0304	Methoxyacetic acid	Met38392	HMDB41929	90.03169406	C3H6O3
m/z=104.0436	2-Hydroxybutyric acid	Met1435	HMDB00008	104.0473441	C4H8O3
m/z=104.0436	2-Hydroxybutyric acid	Met1439	HMDB00008	104.0473441	C4H8O3
m/z=104.0436	(R)-3-Hydroxybutyric acid	Met837	HMDB00011	104.0473441	C4H8O3
m/z=104.0436	(R)-3-Hydroxybutyric acid	Met831	HMDB00011	104.0473441	C4H8O3
m/z=104.0436	(R)-3-Hydroxybutyric acid	Met833	HMDB00011	104.0473441	C4H8O3
m/z=104.0436	(S)-3-Hydroxyisobutyric acid	Met1299	HMDB00023	104.0473441	C4H8O3
m/z=104.0436	(R)-3-Hydroxyisobutyric acid	Met41554	HMDB00336	104.0473441	C4H8O3

m/z=104.0436	3-Hydroxybutyric acid	Met31206	HMDB00357	104.0473441	C4H8O3
m/z=104.0436	(S)-3-Hydroxybutyric acid	Met34843	HMDB00442	104.0473441	C4H8O3
m/z=104.0436	4-Hydroxybutyric acid	Met38085	HMDB00710	104.0473441	C4H8O3
m/z=104.0436	Ethoxyacetic acid	Met9767	HMDB31212	104.0473441	C4H8O3
m/z=116.0607	2-Methyl-1-methylthio-2-butene	Met34744	HMDB32411	116.0659711	C6H12S
m/z=116.0607	1-Propenyl propyl sulfide	Met37762	HMDB40244	116.0659711	C6H12S
m/z=118.0257	Methylmalonic acid	Met39066	HMDB00202	118.0266087	C4H6O4
m/z=118.0257	Succinic acid	Met3924	HMDB00254	118.0266087	C4H6O4
m/z=118.0257	Succinic acid	Met2481	HMDB00254	118.0266087	C4H6O4
m/z=118.0257	Succinic acid	Met433	HMDB00254	118.0266087	C4H6O4
m/z=118.0257	Succinic acid	Met434	HMDB00254	118.0266087	C4H6O4
m/z=118.0257	Succinic acid	Met436	HMDB00254	118.0266087	C4H6O4
m/z=118.0257	Erythrono-1,4-lactone	Met6527	HMDB00349	118.0266087	C4H6O4
m/z=118.0257	Threonolactone	Met18515	HMDB00940	118.0266087	C4H6O4
m/z=118.0257	4-Hydroxy-2-oxobutanoic acid	Met27915	HMDB31204	118.0266087	C4H6O4
m/z=118.0257	xi-3-Hydroxy-2-oxobutanoic acid	Met19871	HMDB39324	118.0266087	C4H6O4
m/z=118.0634	3-Hydroxy-2-methyl-[R-(R,S)]-butanoic acid	Met31201	HMDB00351	118.0629942	C5H10O3
m/z=118.0634	2-Methyl-3-hydroxybutyric acid	Met31203	HMDB00354	118.0629942	C5H10O3
m/z=118.0634	2-Ethylhydracrylic acid	Met13611	HMDB00396	118.0629942	C5H10O3
m/z=118.0634	2-Hydroxy-3-methylbutyric acid	Met23796	HMDB00407	118.0629942	C5H10O3
m/z=118.0634	3-Hydroxy-2-methyl-[S-(R,R)]-butanoic acid	Met8473	HMDB00410	118.0629942	C5H10O3
m/z=118.0634	3-Hydroxyvaleric acid	Met18759	HMDB00531	118.0629942	C5H10O3
m/z=118.0634	Erythronilic acid	Met44489	HMDB00642	118.0629942	C5H10O3
m/z=118.0634	3-Hydroxyisovaleric acid	Met19003	HMDB00754	118.0629942	C5H10O3
m/z=118.0634	2-Hydroxyvaleric acid	Met9566	HMDB01863	118.0629942	C5H10O3
m/z=118.0634	2-Hydroxy-2-methylbutyric acid	Met12795	HMDB01987	118.0629942	C5H10O3
m/z=118.0634	4-Hydroxyisovaleric acid	Met18300	HMDB02011	118.0629942	C5H10O3
m/z=118.0634	Ethyl lactate	Met26153	HMDB40735	118.0629942	C5H10O3
m/z=118.0634	Methyl 3-hydroxybutyrate	Met40266	HMDB41603	118.0629942	C5H10O3
m/z=118.0635	3-Hydroxy-2-methyl-[R-(R,S)]-butanoic acid	Met31201	HMDB00351	118.0629942	C5H10O3
m/z=118.0635	2-Methyl-3-hydroxybutyric acid	Met31203	HMDB00354	118.0629942	C5H10O3
m/z=118.0635	2-Ethylhydracrylic acid	Met13611	HMDB00396	118.0629942	C5H10O3
m/z=118.0635	2-Hydroxy-3-methylbutyric acid	Met23796	HMDB00407	118.0629942	C5H10O3
m/z=118.0635	3-Hydroxy-2-methyl-[S-(R,R)]-butanoic acid	Met8473	HMDB00410	118.0629942	C5H10O3
m/z=118.0635	3-Hydroxyvaleric acid	Met18759	HMDB00531	118.0629942	C5H10O3
m/z=118.0635	Erythronilic acid	Met44489	HMDB00642	118.0629942	C5H10O3
m/z=118.0635	3-Hydroxyisovaleric acid	Met19003	HMDB00754	118.0629942	C5H10O3
m/z=118.0635	2-Hydroxyvaleric acid	Met9566	HMDB01863	118.0629942	C5H10O3
m/z=118.0635	2-Hydroxy-2-methylbutyric acid	Met12795	HMDB01987	118.0629942	C5H10O3
m/z=118.0635	4-Hydroxyisovaleric acid	Met18300	HMDB02011	118.0629942	C5H10O3
m/z=118.0635	Ethyl lactate	Met26153	HMDB40735	118.0629942	C5H10O3

m/z=118.0635	Methyl 3-hydroxybutyrate	Met40266	HMDB41603	118.0629942	C5H10O3
m/z=120.0888	1,2,4-Trimethylbenzene	Met23024	HMDB13733	120.0939004	C9H12
m/z=120.0888	Isopropylbenzene	Met33772	HMDB34029	120.0939004	C9H12
m/z=120.0888	1,2,4-Tris(methylene)cyclohexane	Met43086	HMDB40458	120.0939004	C9H12
m/z=136.0728	Tetrahydropteridine	Met19291	HMDB01216	136.0748963	C6H8N4
m/z=136.0728	N-Methylnicotinamide	Met42986	HMDB03152	136.0636629	C7H8N2O
m/z=136.0728	2-Methylerythritol	Met28115	HMDB11659	136.0735589	C5H12O4
m/z=136.0728	2-Acetyl-3-methylpyrazine	Met18135	HMDB30001	136.0636629	C7H8N2O
m/z=136.0728	3-Deoxy-D-arabinitol	Met27920	HMDB31201	136.0735589	C5H12O4
m/z=136.0728	2-Deoxy-D-ribitol	Met12863	HMDB33919	136.0735589	C5H12O4
m/z=136.0728	2-Aminobenzamide	Met8451	HMDB33947	136.0636629	C7H8N2O
m/z=136.0728	4-Acetyl-2-methylpyrimidine	Met28071	HMDB37819	136.0636629	C7H8N2O
m/z=136.0728	1-Deoxy-D-ribitol	Met18415	HMDB41486	136.0735589	C5H12O4
m/z=150.0205	Tartaric acid	Met43356	HMDB00956	150.0164379	C4H6O6
m/z=150.0205	2-(2-Thienyl)furan	Met13520	HMDB29715	150.0139355	C8H6OS
m/z=150.0205	D-Tartaric acid	Met18901	HMDB29878	150.0164379	C4H6O6
m/z=150.0205	2-Methyl-2-(methyldithio)propanal	Met43729	HMDB38889	150.0173063	C5H10OS2
m/z=150.0877	6-Methylnicotinamide	Met14204	HMDB13704	150.079313	C8H10N2O
m/z=150.0877	2-Acetyl-3-ethylpyrazine	Met26675	HMDB29410	150.079313	C8H10N2O
m/z=150.0877	7,8-Dihydro-3-methylpyrrolo[1,2-a]pyrimidin-2(6H)-one	Met23285	HMDB38513	150.079313	C8H10N2O
m/z=150.0877	2-Acetyl-3,6-dimethylpyrazine	Met27431	HMDB39998	150.079313	C8H10N2O
m/z=150.0877	2-Acetyl-3,5-dimethylpyrazine	Met27432	HMDB39999	150.079313	C8H10N2O
m/z=150.1352	Cystophorene	Met15805	HMDB30944	150.1408506	C11H18
m/z=150.1352	(E)-4,8-Dimethyl-1,3,7-nonatriene	Met13279	HMDB35792	150.1408506	C11H18
m/z=152.1151	(-)-trans-Carveol	Met2940	HMDB03450	152.1201151	C10H16O
m/z=152.1151	(-)-trans-Carveol	Met2934	HMDB03450	152.1201151	C10H16O
m/z=152.1151	Alpha-Pinene-oxide	Met3747	HMDB03667	152.1201151	C10H16O
m/z=152.1151	Alpha-Pinene-oxide	Met3745	HMDB03667	152.1201151	C10H16O
m/z=152.1151	p-Menth-3-en-9-al	Met9390	HMDB30892	152.1201151	C10H16O
m/z=152.1151	Isocitral	Met9391	HMDB30893	152.1201151	C10H16O
m/z=152.1151	3-Methyl-5-propyl-2-cyclohexen-1-one	Met23042	HMDB31854	152.1201151	C10H16O
m/z=152.1151	2,6-Dimethyl-1,7-octadien-3-one	Met21047	HMDB32120	152.1201151	C10H16O
m/z=152.1151	(E)-3,7-Dimethyl-1,5,7-octatrien-3-ol	Met41157	HMDB32242	152.1201151	C10H16O
m/z=152.1151	2-(trans-2-Pentenyl)cyclopentanone	Met26593	HMDB32536	152.1201151	C10H16O
m/z=152.1151	p-Mentha-1(6),8-dien-3-ol	Met24158	HMDB34715	152.1201151	C10H16O
m/z=152.1151	cis-2-Thujen-4-ol	Met39498	HMDB34916	152.1201151	C10H16O
m/z=152.1151	(R)-Campholenic aldehyde	Met29100	HMDB34973	152.1201151	C10H16O
m/z=152.1151	(R)-Carvotanacetone	Met29099	HMDB34974	152.1201151	C10H16O
m/z=152.1151	Piperitone	Met29098	HMDB34975	152.1201151	C10H16O
m/z=152.1151	(+)-Fenchone	Met26109	HMDB34985	152.1201151	C10H16O
m/z=152.1151	(1S,4R)-p-Mentha-2,8-dien-1-ol	Met23627	HMDB35054	152.1201151	C10H16O

m/z=152.1151	(1R,4R)-p-Mentha-2,8-dien-1-ol	Met16263	HMDB35077	152.1201151	C10H16O
m/z=152.1151	Geranial	Met13426	HMDB35078	152.1201151	C10H16O
m/z=152.1151	cis-Citral	Met44109	HMDB35092	152.1201151	C10H16O
m/z=152.1151	2-Pinen-10-ol	Met15975	HMDB35100	152.1201151	C10H16O
m/z=152.1151	Dehydrolinalool	Met26053	HMDB35120	152.1201151	C10H16O
m/z=152.1151	Darwinol	Met26048	HMDB35125	152.1201151	C10H16O
m/z=152.1151	1,2-Epoxy-p-menth-8-ene	Met21693	HMDB35158	152.1201151	C10H16O
m/z=152.1151	(S)-9,10-Cyclo-p-menth-1-en-4-ol	Met12817	HMDB35203	152.1201151	C10H16O
m/z=152.1151	(Z)-2-Methyl-6-methylene-2,7-octadien-1-ol	Met33119	HMDB35241	152.1201151	C10H16O
m/z=152.1151	(2S,4R)-p-Mentha-1(7),5-dien-2-ol	Met18660	HMDB35277	152.1201151	C10H16O
m/z=152.1151	Teresantalol	Met11534	HMDB35280	152.1201151	C10H16O
m/z=152.1151	(S)-Phellandral	Met38766	HMDB35600	152.1201151	C10H16O
m/z=152.1151	(R)-p-Menth-4(8)-en-3-one	Met38762	HMDB35604	152.1201151	C10H16O
m/z=152.1151	(+)-cis-Carveol	Met9427	HMDB35622	152.1201151	C10H16O
m/z=152.1151	3-Pinanone	Met32762	HMDB35656	152.1201151	C10H16O
m/z=152.1151	alpha-Cyclocitral	Met26503	HMDB35706	152.1201151	C10H16O
m/z=152.1151	(R)-Piperitone	Met41265	HMDB35737	152.1201151	C10H16O
m/z=152.1151	(S)-Piperitone	Met41258	HMDB35738	152.1201151	C10H16O
m/z=152.1151	(-)-trans-Isopulegone	Met7493	HMDB35741	152.1201151	C10H16O
m/z=152.1151	Pinocarveol	Met7491	HMDB35743	152.1201151	C10H16O
m/z=152.1151	(-)-Isopinocamphone	Met7498	HMDB35744	152.1201151	C10H16O
m/z=152.1151	Marmelo oxide A	Met33868	HMDB36044	152.1201151	C10H16O
m/z=152.1151	Dihydrocarvone	Met25035	HMDB36079	152.1201151	C10H16O
m/z=152.1151	(1S,4S)-Dihydrocarvone	Met24059	HMDB36080	152.1201151	C10H16O
m/z=152.1151	(-)-cis-Carveol	Met7749	HMDB36082	152.1201151	C10H16O
m/z=152.1151	Carveol	Met7748	HMDB36083	152.1201151	C10H16O
m/z=152.1151	Dehydro-1,8-cineole	Met7750	HMDB36085	152.1201151	C10H16O
m/z=152.1151	(R)-p-Mentha-1,8-dien-7-ol	Met7752	HMDB36087	152.1201151	C10H16O
m/z=152.1151	(S)-p-Mentha-1,8-dien-7-ol	Met7744	HMDB36088	152.1201151	C10H16O
m/z=152.1151	(+)-3-Thujone	Met35762	HMDB36113	152.1201151	C10H16O
m/z=152.1151	(-)-3-Thujone	Met35761	HMDB36114	152.1201151	C10H16O
m/z=152.1151	(-)-3-Isothujone	Met35760	HMDB36115	152.1201151	C10H16O
m/z=152.1151	(-)-Pinocamphone	Met22313	HMDB36127	152.1201151	C10H16O
m/z=152.1151	(-)-trans-Pinocarveol	Met11120	HMDB36128	152.1201151	C10H16O
m/z=152.1151	Verbenol	Met11121	HMDB36129	152.1201151	C10H16O
m/z=152.1151	(E,E)-2,4-Decadienal	Met23649	HMDB36598	152.1201151	C10H16O
m/z=152.1151	6,8-Epoxy-p-menth-2-ene	Met17005	HMDB37008	152.1201151	C10H16O
m/z=152.1151	Terpinolene oxide	Met17006	HMDB37009	152.1201151	C10H16O
m/z=152.1151	(2S,4R)-p-Mentha-1(7),8-dien-2-ol	Met31479	HMDB37010	152.1201151	C10H16O
m/z=152.1151	p-Mentha-1,8-dien-4-ol	Met31482	HMDB37015	152.1201151	C10H16O
m/z=152.1151	(R)-p-Mentha-1,8-dien-10-ol	Met31484	HMDB37017	152.1201151	C10H16O

m/z=152.1151	4-Acetyl-1,4-dimethyl-1-cyclohexene	Met27090	HMDB37024	152.1201151	C10H16O
m/z=152.1151	Hop ether	Met27091	HMDB37025	152.1201151	C10H16O
m/z=152.1151	Tetrahydro-5-isopropenyl-2-methyl-2-vinylfuran	Met21750	HMDB37172	152.1201151	C10H16O
m/z=152.1151	Junionone	Met14054	HMDB37280	152.1201151	C10H16O
m/z=152.1151	xi-p-Mentha-3,8-dien-1-ol	Met42772	HMDB37302	152.1201151	C10H16O
m/z=152.1151	xi-p-Mentha-1(7),2-dien-4-ol	Met42771	HMDB37303	152.1201151	C10H16O
m/z=152.1151	xi-Pinol	Met13963	HMDB38251	152.1201151	C10H16O
m/z=152.1151	Photocitral A	Met34260	HMDB38290	152.1201151	C10H16O
m/z=152.1151	xi-3,6-Dihydro-4-methyl-2-(2-methyl-1-propenyl)-2H-pyran	Met42277	HMDB38557	152.1201151	C10H16O
m/z=152.1151	3,4-Epoxy-p-menth-1(7)-ene	Met37711	HMDB39008	152.1201151	C10H16O
m/z=152.1151	2-Hexylfuran	Met25270	HMDB39816	152.1201151	C10H16O
m/z=152.1151	Anethofuran	Met28888	HMDB40766	152.1201151	C10H16O
m/z=152.1151	beta-Cyclocitral	Met43579	HMDB41011	152.1201151	C10H16O
m/z=152.1151	Isocyclocitral	Met43581	HMDB41013	152.1201151	C10H16O
m/z=152.1151	3-Thujanone	Met13671	HMDB41631	152.1201151	C10H16O
m/z=153.1077	psi-Pelletierine	Met12508	HMDB34580	153.1153641	C9H15NO
m/z=153.1077	2-Methyl-4-pentyloxazole	Met13683	HMDB37856	153.1153641	C9H15NO
m/z=153.1077	4-Methyl-2-pentyloxazole	Met13678	HMDB37857	153.1153641	C9H15NO
m/z=153.1077	5-Butyl-2-ethyloxazole	Met18237	HMDB37862	153.1153641	C9H15NO
m/z=153.1077	2-Ethyl-4-methyl-5-propyloxazole	Met32706	HMDB37872	153.1153641	C9H15NO
m/z=153.1077	4-Ethyl-2-methyl-5-propyloxazole	Met14624	HMDB37873	153.1153641	C9H15NO
m/z=153.1077	5-Ethyl-4-methyl-2-(1-methylethyl)oxazole	Met14641	HMDB37874	153.1153641	C9H15NO
m/z=153.1077	2-Butyl-4,5-dimethyloxazole	Met32710	HMDB37875	153.1153641	C9H15NO
m/z=153.1077	5-Ethyl-2-methyl-4-propyloxazole	Met32709	HMDB37876	153.1153641	C9H15NO
m/z=153.1077	4-Ethyl-5-methyl-2-(1-methylethyl)oxazole	Met32713	HMDB37878	153.1153641	C9H15NO
m/z=153.1077	4-Butyl-2,5-dimethyloxazole	Met32712	HMDB37879	153.1153641	C9H15NO
m/z=153.1077	2-Isobutyl-4,5-dimethyloxazole	Met25548	HMDB37880	153.1153641	C9H15NO
m/z=153.1077	4-Ethyl-5-methyl-2-propyloxazole	Met25549	HMDB37881	153.1153641	C9H15NO
m/z=153.1077	5-Butyl-2,4-dimethyloxazole	Met25546	HMDB37882	153.1153641	C9H15NO
m/z=154.0058	1,4-Dithiothreitol	Met915	HMDB13593	154.0122209	C4H10O2S2
m/z=154.0058	1-(2-Thienyl)-1,2-propanedione	Met17124	HMDB40002	154.0088501	C7H6O2S
m/z=155.1303	Methylisopelletierine	Met35080	HMDB30326	155.1310142	C9H17NO
m/z=155.1303	2,2,6,6-Tetramethyl-4-piperidinone	Met6299	HMDB31179	155.1310142	C9H17NO
m/z=155.1303	3-(1-Pyrrolidinyl)-2-pentanone	Met17983	HMDB39833	155.1310142	C9H17NO
m/z=155.1303	2-(1-Pyrrolidinyl)-3-pentanone	Met17978	HMDB39834	155.1310142	C9H17NO
m/z=156.1592	Menthol	Met5210	HMDB03352	156.1514153	C10H20O
m/z=156.1592	Decanal	Met43897	HMDB11623	156.1514153	C10H20O
m/z=156.1592	(E)-3-decen-1-ol	Met44294	HMDB13810	156.1514153	C10H20O
m/z=156.1592	2-Decanone	Met39704	HMDB31409	156.1514153	C10H20O
m/z=156.1592	cis-4-Decenol	Met20669	HMDB32206	156.1514153	C10H20O

m/z=156.1592	3-Decanone	Met6196	HMDB32212	156.1514153	C10H20O
m/z=156.1592	3,7-Dimethyloctanal	Met41158	HMDB32241	156.1514153	C10H20O
m/z=156.1592	(+/-)-4-Ethyloctanal	Met16353	HMDB32274	156.1514153	C10H20O
m/z=156.1592	2-DECENOL	Met26589	HMDB32532	156.1514153	C10H20O
m/z=156.1592	Menthanol	Met24156	HMDB34717	156.1514153	C10H20O
m/z=156.1592	D-Citronellol	Met44108	HMDB35093	156.1514153	C10H20O
m/z=156.1592	L-Citronellol	Met44107	HMDB35094	156.1514153	C10H20O
m/z=156.1592	p-Menthan-4-ol	Met16455	HMDB35726	156.1514153	C10H20O
m/z=156.1592	(+)-Neomenthol	Met36747	HMDB35763	156.1514153	C10H20O
m/z=156.1592	(-)-Neoisomenthol	Met36742	HMDB35764	156.1514153	C10H20O
m/z=156.1592	p-Menthan-3-ol	Met36741	HMDB35765	156.1514153	C10H20O
m/z=156.1592	p-Menthan-1-ol	Met27086	HMDB37020	156.1514153	C10H20O
m/z=156.1592	alpha-Citronellol	Met26733	HMDB37171	156.1514153	C10H20O
m/z=156.1592	(±)-Carvomenthol	Met5330	HMDB37223	156.1514153	C10H20O
m/z=156.1592	Dihydrocitronellal	Met19268	HMDB37806	156.1514153	C10H20O
m/z=156.1592	1-Decen-3-ol	Met7693	HMDB39854	156.1514153	C10H20O
m/z=156.1592	(+)-Neoisomenthol	Met20995	HMDB41628	156.1514153	C10H20O
m/z=180.0193	2,4,6-Trimethyl-1,3,5-trithiane	Met24561	HMDB31671	180.0101125	C6H12S3
m/z=180.0193	1-(Methylthio)ethyl 2-propenyl disulfide	Met13906	HMDB32115	180.0101125	C6H12S3
m/z=180.0193	2,5-Dimethyl-1,4-dithiane-2,5-diol	Met32769	HMDB33556	180.027871	C6H12O2S2
m/z=180.0193	Ethyl 2-(methyldithio)propionate	Met28969	HMDB38896	180.027871	C6H12O2S2
m/z=184.0502	(+/-)-3-[(2-methyl-3-furyl)thio]-2-butanone	Met10146	HMDB32401	184.0558003	C9H12O2S
m/z=192.1189	2-Methyl-1-phenyl-2-propanyl acetate	Met43497	HMDB31571	192.1150298	C12H16O2
m/z=192.1189	4-Phenyl-2-butyl acetate	Met33335	HMDB31614	192.1150298	C12H16O2
m/z=192.1189	Ethyl 4-phenylbutanoate	Met33327	HMDB31618	192.1150298	C12H16O2
m/z=192.1189	Benzyl 3-methylbutanoate	Met38261	HMDB32043	192.1150298	C12H16O2
m/z=192.1189	3-Methylbutyl benzoate	Met11957	HMDB33380	192.1150298	C12H16O2
m/z=192.1189	2-Methylpropyl phenylacetate	Met42697	HMDB35010	192.1150298	C12H16O2
m/z=192.1189	2-Phenylethyl butanoate	Met42693	HMDB35014	192.1150298	C12H16O2
m/z=192.1189	2-Phenylethyl 2-methylpropanoate	Met42692	HMDB35015	192.1150298	C12H16O2
m/z=192.1189	5-Isopropyl-2-methylphenol acetate	Met35852	HMDB35447	192.1150298	C12H16O2
m/z=192.1189	3-Phenylpropyl propanoate	Met24154	HMDB36388	192.1150298	C12H16O2
m/z=192.1189	11,12,13-Trinor-1(10)-spirovetivene-2,7-dione	Met12301	HMDB36734	192.1150298	C12H16O2
m/z=192.1189	4-Methyl-2-(1-phenylethyl)-1,3-dioxolane, 9CI	Met36329	HMDB37165	192.1150298	C12H16O2
m/z=192.1189	4-Methylphenyl 3-methylbutanoate	Met29043	HMDB37709	192.1150298	C12H16O2
m/z=192.1189	1-Phenylethyl isobutyrate	Met42984	HMDB37716	192.1150298	C12H16O2
m/z=192.1189	1-Phenylethyl butyrate	Met14511	HMDB37717	192.1150298	C12H16O2
m/z=192.1189	1-Ethoxy-2-methoxy-4-(1-propenyl)benzene	Met37915	HMDB37792	192.1150298	C12H16O2
m/z=192.1189	2-(2-Hydroxy-4-methylphenyl)-3-pentanone	Met43220	HMDB38180	192.1150298	C12H16O2

m/z=192.1189	2-Ethoxy-1-methoxy-4-(1-propenyl)benzene	Met30335	HMDB39496	192.1150298	C12H16O2
m/z=192.1189	11,12,13-Trinor-1,3,5-bisabolatrien-10-oic acid	Met14609	HMDB39643	192.1150298	C12H16O2
m/z=192.1189	2-Benzyl-4,5-dimethyl-1,3-dioxolane	Met32417	HMDB39841	192.1150298	C12H16O2
m/z=192.1189	Butyl phenylacetate	Met37305	HMDB40427	192.1150298	C12H16O2
m/z=194.1152	Laccarin	Met32640	HMDB41440	194.1055277	C10H14N2O2
m/z=196.0903	2-(Ethylamino)-4,5-dihydroxybenzamide	Met16648	HMDB32852	196.0847923	C9H12N2O3
m/z=196.0903	5-Nitro-2-propoxyaniline	Met42666	HMDB37688	196.0847923	C9H12N2O3
m/z=196.0903	1-(2-Thienyl)-1-heptanone	Met37759	HMDB40241	196.0921858	C11H16OS
m/z=200.0438	Potassium 2-(1'-ethoxy) ethoxypropanoate	Met11645	HMDB37192	200.0450908	C7H13KO4
m/z=200.0438	Camalexin	Met12815	HMDB38631	200.040819	C11H8N2S
m/z=200.0443	Potassium 2-(1'-ethoxy) ethoxypropanoate	Met11645	HMDB37192	200.0450908	C7H13KO4
m/z=200.0443	Camalexin	Met12815	HMDB38631	200.040819	C11H8N2S
m/z=200.046	Potassium 2-(1'-ethoxy) ethoxypropanoate	Met11645	HMDB37192	200.0450908	C7H13KO4
m/z=200.046	Camalexin	Met12815	HMDB38631	200.040819	C11H8N2S
m/z=200.1675	2-Hexenoylcholine	Met9828	HMDB13162	200.165054	C11H22NO2
m/z=218.0129	Diphenyl disulfide	Met43013	HMDB31823	218.0223917	C12H10S2
m/z=236.0509	Aspartyl-Cysteine	Met40029	HMDB28750	236.0466922	C7H12N2O5S
m/z=236.0509	Cysteinyl-Aspartate	Met10784	HMDB28771	236.0466922	C7H12N2O5S
m/z=236.0509	Brassinin	Met17767	HMDB33350	236.0441898	C11H12N2S2
m/z=242.022	Inositol cyclic phosphate	Met38558	HMDB01125	242.0191538	C6H11O8P
m/z=246.0089	Dimethylallylpyrophosphate	Met2437	HMDB01120	246.0058258	C5H12O7P2
m/z=246.0089	Dimethylallylpyrophosphate	Met2439	HMDB01120	246.0058258	C5H12O7P2
m/z=246.0089	Isopentenyl pyrophosphate	Met2405	HMDB01347	246.0058258	C5H12O7P2
m/z=246.0089	Isopentenyl pyrophosphate	Met2418	HMDB01347	246.0058258	C5H12O7P2
m/z=246.0089	Isopentenyl pyrophosphate	Met2413	HMDB01347	246.0058258	C5H12O7P2
m/z=246.2208	8,8-Diethoxy-2,6-dimethyl-2-octanol	Met6723	HMDB34557	246.2194948	C14H30O3
m/z=251.2239	Herculin	Met9833	HMDB30275	251.2249146	C16H29NO
m/z=254.1321	Homoanserine	Met5820	HMDB05767	254.1378905	C11H18N4O3
m/z=254.1321	Histidinyl-Valine	Met7272	HMDB28898	254.1378905	C11H18N4O3
m/z=254.1321	Valyl-Histidine	Met32174	HMDB29129	254.1378905	C11H18N4O3
m/z=254.1321	L-Furosine	Met9726	HMDB29390	254.1266571	C12H18N2O4
m/z=254.1321	L-Pyridosine	Met20884	HMDB29443	254.1266571	C12H18N2O4
m/z=254.1321	Isoeugenol benzyl ether	Met37709	HMDB32058	254.1306798	C17H18O2
m/z=254.1321	Isoeugenyl benzyl ether	Met10391	HMDB32349	254.1306798	C17H18O2
m/z=254.1321	Pyrraline	Met35129	HMDB33143	254.1266571	C12H18N2O4
m/z=254.1321	(+)-Setoclavine	Met11401	HMDB33428	254.1419132	C16H18N2O
m/z=254.1321	4-[(2-Methyl-3-furanyl)thio]-5-nonanone	Met7189	HMDB37141	254.1340506	C14H22O2S
m/z=254.1321	2,6-Dimethyl-3-[(2-methyl-3-furanyl)thio]-4-heptanone	Met31892	HMDB37154	254.1340506	C14H22O2S
m/z=254.1321	(S)-Argpyrimidine	Met26147	HMDB37180	254.1378905	C11H18N4O3

m/z=254.1321	Aldosine	Met28069	HMDB37817	254.1266571	C12H18N2O4
m/z=255.2543	Palmitic amide	Met11268	HMDB12273	255.2562147	C16H33NO
m/z=258.131	Strobilurin A	Met43837	HMDB30420	258.1255944	C16H18O3
m/z=258.131	gamma-L-Glutamyl-L-pipecolic acid	Met42048	HMDB38614	258.1215717	C11H18N2O5
m/z=258.131	(2S,2'S)-Pyrosaccharopine	Met31799	HMDB38676	258.1215717	C11H18N2O5
m/z=262.2268	6,10,14-Trimethyl-5,9,13-pentadecatrien-2-one	Met9412	HMDB34495	262.2296656	C18H30O
m/z=262.2268	2-(5,8-Tetradecadienyl)cyclobutanone	Met38859	HMDB37519	262.2296656	C18H30O
m/z=264.0141	5,8-Dihydro-6-(4-methyl-3-pentenyl)-1,2,3,4-tetrathiocin	Met10211	HMDB38142	264.0134833	C10H16S4
m/z=274.0626	cis,trans-5'-Hydroxythalidomide	Met21705	HMDB13870	274.0589714	C13H10N2O5
m/z=274.0626	5-Hydroxythalidomide	Met15962	HMDB13871	274.0589714	C13H10N2O5
m/z=274.0626	Thalidomide arene oxide	Met15986	HMDB13872	274.0589714	C13H10N2O5
m/z=274.0626	4-Phenyl-1H,3H-naphtho[1,8-cd]pyran-1,3-dione	Met8903	HMDB41120	274.0629942	C18H10O3
m/z=274.1871	3-Hydroxytetradecanedioic acid	Met13609	HMDB00394	274.1780239	C14H26O5
m/z=274.1871	Nandrolone	Met25883	HMDB02725	274.1932801	C18H26O2
m/z=274.1871	1-Phenyl-1,3-dodecanedione	Met39714	HMDB35579	274.1932801	C18H26O2
m/z=274.1871	(10Z,14E,16E)-10,14,16-Octadecatrien-12-ynoic acid	Met41952	HMDB35963	274.1932801	C18H26O2
m/z=274.1871	Rhodinyl phenylacetate	Met11644	HMDB37191	274.1932801	C18H26O2
m/z=274.1871	Citronellyl alpha-toluate	Met19793	HMDB37230	274.1932801	C18H26O2
m/z=281.2698	Oleamide	Met39124	HMDB02117	281.2718648	C18H35NO
m/z=283.173	Histidinyl-Lysine	Met7275	HMDB28890	283.1644396	C12H21N5O3
m/z=283.173	Lysyl-Histidine	Met25601	HMDB28953	283.1644396	C12H21N5O3
m/z=286.1186	Histidinyl-Methionine	Met7274	HMDB28891	286.1099612	C11H18N4O3S
m/z=286.1186	Methionyl-Histidine	Met15558	HMDB28975	286.1099612	C11H18N4O3S
m/z=286.1186	4'-Hydroxy-5,7-dimethoxyflavan	Met20248	HMDB30152	286.1205091	C17H18O4
m/z=286.1186	Sativan	Met44089	HMDB30521	286.1205091	C17H18O4
m/z=286.1186	Isosativan	Met37353	HMDB34024	286.1205091	C17H18O4
m/z=286.1186	Myrigalone G	Met32615	HMDB41168	286.1205091	C17H18O4
m/z=286.1186	Myrigalone H	Met32616	HMDB41169	286.1205091	C17H18O4
m/z=286.1186	4'-Hydroxy-3,4,5-trimethoxystilbene	Met6317	HMDB41671	286.1205091	C17H18O4
m/z=286.1186	4-Hydroxy-3,5,4'-trimethoxystilbene	Met9446	HMDB41680	286.1205091	C17H18O4
m/z=297.2635	Palmitoleoyl Ethanolamide	Met31023	HMDB13648	297.2667794	C18H35NO2
m/z=316.0932	Homoferreirin	Met39413	HMDB30111	316.0946882	C17H16O6
m/z=316.0932	3-(3,4-Dihydroxybenzyl)-7-hydroxy-5-methoxy-4-chromanone	Met38763	HMDB33298	316.0946882	C17H16O6
m/z=316.0932	Melilotocarpan E	Met17808	HMDB33683	316.0946882	C17H16O6
m/z=316.0932	Melilotocarpan D	Met32260	HMDB33692	316.0946882	C17H16O6
m/z=316.0932	Olivin	Met30291	HMDB33797	316.0946882	C17H16O6
m/z=316.0932	Cajanol	Met17304	HMDB33924	316.0946882	C17H16O6
m/z=316.0932	5,8-Dihydroxy-3-(4-hydroxybenzyl)-7-methoxy-4-chromanone	Met11087	HMDB37251	316.0946882	C17H16O6

m/z=316.0932	5,7-Dihydroxy-3-(3-hydroxy-4-methoxybenzyl)-4-chromanone	Met30318	HMDB37477	316.0946882	C17H16O6
m/z=316.0932	3',5-Dihydroxy-4',7-dimethoxyflavanone	Met24610	HMDB37481	316.0946882	C17H16O6
m/z=316.0932	4',7-Dihydroxy-2',5-dimethoxyisoflavanone	Met8672	HMDB37749	316.0946882	C17H16O6
m/z=316.0932	Artocarpanone A	Met36797	HMDB41234	316.0946882	C17H16O6
m/z=316.0932	Violanone	Met34409	HMDB41790	316.0946882	C17H16O6
m/z=318.1042	4',7-Di-O-methylcatechin	Met26607	HMDB30663	318.1103383	C17H18O6
m/z=323.2731	Linoleoyl ethanolamide	Met40529	HMDB12252	323.2824294	C20H37NO2
m/z=333.2133	Mahanimbinol	Met21128	HMDB40992	333.2092645	C23H27NO
m/z=336.0738	S-Nitrosoglutathione	Met25835	HMDB04645	336.0739696	C10H16N4O7S
m/z=344.0792	Thiamine monophosphate	Met1902	HMDB02666	344.0708123	C12H17N4O4PS
m/z=344.0792	Thiamine monophosphate	Met2957	HMDB02666	344.0708123	C12H17N4O4PS
m/z=344.0792	Thiamine monophosphate	Met1365	HMDB02666	344.0708123	C12H17N4O4PS
m/z=344.0792	Theogallin	Met43712	HMDB39287	344.0743467	C14H16O10
m/z=371.174	N-[2-(3,4-Dimethoxyphenyl)ethyl]-3,4-dimethoxycinnamic acid amide	Met10634	HMDB32226	371.1732729	C21H25NO5
m/z=374.0725	Neodiospyrin	Met18499	HMDB29538	374.0790382	C22H14O6
m/z=382.0746	(+)-12a-Hydroxypachyrrhizone	Met32819	HMDB30774	382.0688674	C20H14O8
m/z=385.2813	3-Hydroxy-cis-5-tetradecenoylcarnitine	Met28143	HMDB13330	385.2828234	C21H39NO5
m/z=386.1856	Corchoionol C 9-glucoside	Met42740	HMDB29772	386.1940679	C19H30O8
m/z=386.1856	Citroside A	Met30704	HMDB30370	386.1940679	C19H30O8
m/z=386.1856	Sonchuionoside C	Met24981	HMDB35212	386.1940679	C19H30O8
m/z=386.1857	Corchoionol C 9-glucoside	Met42740	HMDB29772	386.1940679	C19H30O8
m/z=386.1857	Citroside A	Met30704	HMDB30370	386.1940679	C19H30O8
m/z=386.1857	Sonchuionoside C	Met24981	HMDB35212	386.1940679	C19H30O8
m/z=386.9697	5'-Hydroxylornoxicam	Met8177	HMDB13991	386.9750395	C13H10ClN3O5S2
m/z=387.356	25-Azacholesterol	Met23956	HMDB01028	387.3501151	C26H45NO
m/z=388.0988	Dopaxanthin quinone	Met6854	HMDB12220	388.0906655	C18H16N2O8
m/z=388.0988	Betanidin	Met25803	HMDB29407	388.0906655	C18H16N2O8
m/z=404.1957	Pisumionoside	Met20330	HMDB39947	404.2046326	C19H32O9
m/z=422.1628	3-(1,1-Dimethylallyl)scopoletin 7-glucoside	Met13486	HMDB32853	422.1576824	C21H26O9
m/z=422.2871	DHAP(18:0e)	Met19891	HMDB11142	422.2797256	C21H43O6P
m/z=424.3357	Alpha-Tocotrienol	Met1076	HMDB06327	424.3341307	C29H44O2
m/z=424.3357	Alpha-Tocotrienol	Met2558	HMDB06327	424.3341307	C29H44O2
m/z=424.3357	Alpha-Tocotrienol	Met2552	HMDB06327	424.3341307	C29H44O2
m/z=424.3357	(22E,24R)-Stigmasta-4,22-diene-3,6-dione	Met21656	HMDB38656	424.3341307	C29H44O2
m/z=426.1673	Mangostanol	Met18559	HMDB29868	426.1678532	C24H26O7
m/z=426.1673	Edulisin II	Met7596	HMDB30593	426.1678532	C24H26O7
m/z=426.1673	Archangelicin	Met41721	HMDB30845	426.1678532	C24H26O7
m/z=426.1673	Atrovirisidone	Met10067	HMDB36982	426.1678532	C24H26O7
m/z=426.1673	Mangostenol	Met26140	HMDB39912	426.1678532	C24H26O7
m/z=431.1047	Ochratoxin C	Met35768	HMDB29400	431.1135652	C22H22ClNO6

m/z=432.1976	S-Furanopetasitin	Met25564	HMDB36131	432.1970448	C24H32O5S
m/z=434.0375	Halosulfuron-methyl	Met18471	HMDB34859	434.0411453	C13H15ClN6O7S
m/z=434.1183	2-O-Caffeoylarbutin	Met36160	HMDB31347	434.1212969	C21H22O10
m/z=434.1183	Floribundoside	Met39355	HMDB33739	434.1212969	C21H22O10
m/z=434.1183	Eriodictin	Met24609	HMDB37480	434.1212969	C21H22O10
m/z=434.1183	5,7,8-Trihydroxyflavanone 7-glucoside	Met13397	HMDB38775	434.1212969	C21H22O10
m/z=434.1183	Dihydrogenistin	Met36318	HMDB39935	434.1212969	C21H22O10
m/z=434.1183	(2R,3R)-3,3',4',7-Tetrahydroxyflavanone 7-O-alpha-L-Rhamnopyranoside	Met30878	HMDB40536	434.1212969	C21H22O10
m/z=434.1183	5-Hydroxyaloin A	Met43889	HMDB40832	434.1212969	C21H22O10
m/z=434.1183	7-Hydroxyaloin B	Met33602	HMDB41150	434.1212969	C21H22O10
m/z=438.1474	7-Hydroxy-5-(4-hydroxy-2-oxopentyl)-2-methylchromone 7-glucoside	Met20842	HMDB34698	438.1525971	C21H26O10
m/z=438.1474	Cnidimol 7-glucoside	Met35258	HMDB40502	438.1525971	C21H26O10
m/z=448.1435	Isosakuranin	Met42797	HMDB29481	448.136947	C22H24O10
m/z=448.1435	Cycloartomunoxanthone	Met30971	HMDB29999	448.1522031	C26H24O7
m/z=448.1435	Artonol E	Met5688	HMDB30490	448.1522031	C26H24O7
m/z=448.1435	7-Hydroxy-8-O-methylaloin B	Met26013	HMDB31586	448.136947	C22H24O10
m/z=448.1435	Puddumin A	Met44275	HMDB33741	448.136947	C22H24O10
m/z=448.1435	Chalconosakuranetin	Met13950	HMDB37509	448.136947	C22H24O10
m/z=448.1435	Cycloartomunin	Met39344	HMDB38878	448.1522031	C26H24O7
m/z=448.1435	Aromadendrin 4'-methyl ether 7-rhamnoside	Met26471	HMDB40561	448.136947	C22H24O10
m/z=448.1435	Piperenol C	Met9896	HMDB41536	448.136947	C22H24O10
m/z=450.3381	Coprocholic acid	Met9074	HMDB00601	450.3345246	C27H46O5
m/z=450.3381	3a,7a,12a-Trihydroxy-5b-cholestanoic acid	Met4701	HMDB03873	450.3345246	C27H46O5
m/z=450.3381	3a,7a,12a-Trihydroxy-5b-cholestanoic acid	Met2786	HMDB03873	450.3345246	C27H46O5
m/z=450.3381	3a,7a,12a-Trihydroxy-5b-cholestanoic acid	Met2871	HMDB03873	450.3345246	C27H46O5
m/z=450.3381	3a,7a,12a-Trihydroxy-5b-cholestanoic acid	Met2840	HMDB03873	450.3345246	C27H46O5
m/z=463.0728	Adenylsuccinic acid	Met4101	HMDB00536	463.074043	C14H18N5O11P
m/z=463.0728	Chondroitin sulfate	Met10372	HMDB00580	463.0631897	C13H21NO15S
m/z=464.1005	Quercetin 3-galactoside	Met32818	HMDB30775	464.0954761	C21H20O12
m/z=464.1005	Myricetin 7-rhamnoside	Met29412	HMDB33132	464.0954761	C21H20O12
m/z=464.1005	Myricitrin	Met44352	HMDB34360	464.0954761	C21H20O12
m/z=464.1005	6-Hydroxykaempferol 7-glucoside	Met38941	HMDB34725	464.0954761	C21H20O12
m/z=464.1005	2'-Hydroxyisoorientin	Met22090	HMDB35883	464.0954761	C21H20O12
m/z=464.1005	Isoquercitrin	Met33749	HMDB37362	464.0954761	C21H20O12
m/z=464.1005	Quercetin 4'-glucoside	Met29446	HMDB37932	464.0954761	C21H20O12
m/z=464.1005	6-Hydroxykaempferol 3-glucoside	Met32727	HMDB40478	464.0954761	C21H20O12
m/z=465.1699	(E)-Squamosamide	Met21167	HMDB41088	465.1787522	C26H27NO7
m/z=467.1838	Bis-N-butyl phthalate	Met20289	HMDB31949	467.1791462	C22H29NO10
m/z=468.1693	Dukunolide D	Met41260	HMDB35732	468.1784179	C26H28O8

m/z=468.1693	Jangomolide	Met40272	HMDB38158	468.1784179	C26H28O8
m/z=472.28	Ixocarpanolide	Met13411	HMDB33899	472.282489	C28H40O6
m/z=472.28	Vamonolide	Met19290	HMDB37379	472.282489	C28H40O6
m/z=472.28	Macrocarpal B	Met33078	HMDB38704	472.282489	C28H40O6
m/z=472.28	Macrocarpal D	Met33653	HMDB38733	472.282489	C28H40O6
m/z=472.28	Macrocarpal E	Met33648	HMDB38734	472.282489	C28H40O6
m/z=472.28	Macrocarpal H	Met25733	HMDB41586	472.282489	C28H40O6
m/z=476.2152	Loperamide	Met11784	HMDB04999	476.223056	C29H33ClN2O2
m/z=478.0686	Quercetin 3-O-glucuronide	Met7973	HMDB29212	478.0747407	C21H18O13
m/z=478.0686	Quercetin-4'-glucuronide	Met7967	HMDB29214	478.0747407	C21H18O13
m/z=478.0686	Quercetin 4'-glucuronide	Met16338	HMDB33668	478.0747407	C21H18O13
m/z=478.0686	Neoglucobrassicin	Met21681	HMDB38384	478.0715863	C17H22N2O10S2
m/z=478.0686	Quercetin 3'-O-glucuronide	Met31693	HMDB41769	478.0747407	C21H18O13
m/z=478.0729	Quercetin 3-O-glucuronide	Met7973	HMDB29212	478.0747407	C21H18O13
m/z=478.0729	Quercetin-4'-glucuronide	Met7967	HMDB29214	478.0747407	C21H18O13
m/z=478.0729	Quercetin 4'-glucuronide	Met16338	HMDB33668	478.0747407	C21H18O13
m/z=478.0729	Neoglucobrassicin	Met21681	HMDB38384	478.0715863	C17H22N2O10S2
m/z=478.0729	Quercetin 3'-O-glucuronide	Met31693	HMDB41769	478.0747407	C21H18O13
m/z=482.1805	Melleolide D	Met37428	HMDB37042	482.1707457	C24H31ClO8
m/z=485.2783	Sarcodon scabrosus Depsipeptide	Met41665	HMDB41421	485.2737152	C23H39N3O8
m/z=490.2027	Cymorcin diglucoside	Met31409	HMDB39386	490.2050266	C22H34O12
m/z=492.1346	Tricin 7-glucoside	Met27923	HMDB30553	492.1267762	C23H24O12
m/z=492.1346	Tricin 7-glucoside	Met27923	HMDB30553	492.1267762	C23H24O12
m/z=492.1346	Licoagroside A	Met16811	HMDB35448	492.1267762	C23H24O12
m/z=492.1346	Licoagroside A	Met16811	HMDB35448	492.1267762	C23H24O12
m/z=492.1346	Americanin B	Met38443	HMDB37338	492.1420324	C27H24O9
m/z=492.1346	Americanin B	Met38443	HMDB37338	492.1420324	C27H24O9
m/z=492.1346	Limocitrin 3-rhamnoside	Met9534	HMDB37578	492.1267762	C23H24O12
m/z=492.1346	Limocitrin 3-rhamnoside	Met9534	HMDB37578	492.1267762	C23H24O12
m/z=492.1346	3',8-Dimethoxyapigenin 7-glucoside	Met26361	HMDB38825	492.1267762	C23H24O12
m/z=492.1346	3',8-Dimethoxyapigenin 7-glucoside	Met26361	HMDB38825	492.1267762	C23H24O12
m/z=492.1346	3',4',5-Trihydroxy-3,7-dimethoxyflavone 5-glucoside	Met5398	HMDB39336	492.1267762	C23H24O12
m/z=492.1346	3',4',5-Trihydroxy-3,7-dimethoxyflavone 5-glucoside	Met5398	HMDB39336	492.1267762	C23H24O12
m/z=492.1346	3',7-Dimethoxy-4',5,8-trihydroxyflavone 8-glucoside	Met17184	HMDB40479	492.1267762	C23H24O12
m/z=492.1346	3',7-Dimethoxy-4',5,8-trihydroxyflavone 8-glucoside	Met17184	HMDB40479	492.1267762	C23H24O12
m/z=500.174	Artonol C	Met20211	HMDB30489	500.1835033	C30H28O7
m/z=504.1671	Maltotriose	Met3968	HMDB01262	504.169035	C18H32O16
m/z=504.1671	Maltotriose	Met3970	HMDB01262	504.169035	C18H32O16
m/z=504.1671	Maltotriose	Met3976	HMDB01262	504.169035	C18H32O16

m/z=504.1671	Levan	Met38271	HMDB03539	504.169035	C18H32O16
m/z=504.1671	3-Galactosyllactose	Met41497	HMDB06599	504.169035	C18H32O16
m/z=504.1671	Dextrin	Met20460	HMDB06857	504.169035	C18H32O16
m/z=504.1671	1-Kestose	Met12650	HMDB11729	504.169035	C18H32O16
m/z=504.1671	Melezitose	Met37559	HMDB11730	504.169035	C18H32O16
m/z=504.1671	Gentiotriose	Met29594	HMDB29910	504.169035	C18H32O16
m/z=504.1671	Neokestose	Met44400	HMDB29921	504.169035	C18H32O16
m/z=504.1671	Galactotriose	Met44397	HMDB29922	504.169035	C18H32O16
m/z=504.1671	6-O-Glucosylmaltose	Met44396	HMDB29929	504.169035	C18H32O16
m/z=504.1671	beta-D-Fructofuranosyl alpha-D-glucopyranosyl-(1->4)-D-glucopyranoside	Met19430	HMDB29930	504.169035	C18H32O16
m/z=504.1671	Panose	Met19435	HMDB29937	504.169035	C18H32O16
m/z=504.1671	6-Kestose	Met41285	HMDB33673	504.169035	C18H32O16
m/z=504.1671	Umbelliferose	Met44287	HMDB33748	504.169035	C18H32O16
m/z=504.1671	Gentianose	Met18122	HMDB34072	504.169035	C18H32O16
m/z=504.1671	Fagopyritol B2	Met29877	HMDB35322	504.169035	C18H32O16
m/z=504.1671	beta-D-Galactopyranosyl-(1->2)-[beta-D-galactopyranosyl-(1->4)]-D-galactose	Met10057	HMDB38851	504.169035	C18H32O16
m/z=504.1671	beta-D-Galactopyranosyl-(1->4)-beta-D-galactopyranosyl-(1->4)-D-galactose	Met10058	HMDB38852	504.169035	C18H32O16
m/z=504.1671	beta-D-Galactopyranosyl-(1->3)-beta-D-galactopyranosyl-(1->6)-D-galactose	Met10059	HMDB38853	504.169035	C18H32O16
m/z=504.1671	3-beta-Gentiobiosylglucose	Met10422	HMDB39703	504.169035	C18H32O16
m/z=504.1671	alpha-D-Glucopyranosyl-(1->6)-alpha-D-glucopyranosyl-(1->2)-D-glucose	Met16646	HMDB39704	504.169035	C18H32O16
m/z=504.1671	4-beta-Laminaribiosylglucose	Met26591	HMDB39706	504.169035	C18H32O16
m/z=504.1671	alpha-D-Glucopyranosyl-(1->4)-alpha-D-glucopyranosyl-(1->6)-D-glucose	Met16643	HMDB39707	504.169035	C18H32O16
m/z=504.1671	3-beta-Cellobiosylglucose	Met26585	HMDB39708	504.169035	C18H32O16
m/z=504.1671	Fagopyritol A2	Met36236	HMDB40181	504.169035	C18H32O16
m/z=504.1671	Sophorotriose	Met35677	HMDB40984	504.169035	C18H32O16
m/z=504.1671	Nephritogenoside	Met9029	HMDB41948	504.169035	C18H32O16
m/z=508.2302	Acetyl-T2 Toxin	Met24960	HMDB33164	508.2308474	C26H36O10
m/z=508.2302	Mozambioside	Met37643	HMDB37002	508.2308474	C26H36O10
m/z=508.2302	Cafamarine	Met17008	HMDB37003	508.2308474	C26H36O10
m/z=508.2302	Gibberellin A37 glucosyl ester	Met42053	HMDB38611	508.2308474	C26H36O10
m/z=508.493	4-Hydroxy-16,18-tritriacontanedione	Met37390	HMDB39536	508.4855459	C33H64O3
m/z=510.2325	Deuteroporphyrin IX	Met26234	HMDB00579	510.2267055	C30H30N4O4
m/z=515.3007	Taurocholic acid	Met3797	HMDB00036	515.2916735	C26H45NO7S
m/z=515.3007	Taurocholic acid	Met3788	HMDB00036	515.2916735	C26H45NO7S
m/z=515.3007	Taurocholic acid	Met3791	HMDB00036	515.2916735	C26H45NO7S
m/z=515.3007	Tauroursocholic acid	Met8768	HMDB00889	515.2916735	C26H45NO7S
m/z=515.3007	Taurallocholic acid	Met8253	HMDB00922	515.2916735	C26H45NO7S
m/z=515.3007	Tauro-b-muricholic acid	Met32974	HMDB00932	515.2916735	C26H45NO7S

m/z=515.3007	LysoPC(18:4(6Z,9Z,12Z,15Z))	Met37045	HMDB10389	515.3011893	C26H46NO7P
m/z=515.3007	Taurohyocholate	Met19012	HMDB11637	515.2916735	C26H45NO7S
m/z=530.1977	Artonin Q	Met8907	HMDB41124	530.1940679	C31H30O8
m/z=534.11	6''-Malonylastragalin	Met43846	HMDB37434	534.1009554	C24H22O14
m/z=534.11	4',5-Dihydroxy-3,3'-dimethoxy-6,7-methylenedioxyflavone 4'-glucuronide	Met18558	HMDB37758	534.1009554	C24H22O14
m/z=534.11	3,5-Dihydroxy-3',4'-dimethoxy-6,7-methylenedioxyflavone 3-glucuronide	Met38921	HMDB38266	534.1009554	C24H22O14
m/z=534.11	2'-Hydroxygenistein 7-(6''-malonylglucoside)	Met21854	HMDB39247	534.1009554	C24H22O14
m/z=534.5089	Reticulatamol	Met30437	HMDB41023	534.501196	C35H66O3
m/z=556.1058	Ephedrannin A	Met35363	HMDB37654	556.1005615	C30H20O11
m/z=574.2096	Tetrahydrofolyl-[Glu](2)	Met36632	HMDB06825	574.2135746	C24H30N8O9
m/z=574.3184	Ganoderic acid alpha	Met37182	HMDB33024	574.3141831	C32H46O9
m/z=574.3184	Ganoderic acid K	Met10027	HMDB35986	574.3141831	C32H46O9
m/z=578.2066	8-Acetoxypinoresinol 4-glucoside	Met24024	HMDB33283	578.1999412	C28H34O13
m/z=58.0419	Acetone	Met4346	HMDB01659	58.04186481	C3H6O
m/z=58.0419	Acetone	Met4338	HMDB01659	58.04186481	C3H6O
m/z=58.0419	Acetone	Met4348	HMDB01659	58.04186481	C3H6O
m/z=58.0419	Propanal	Met40247	HMDB03366	58.04186481	C3H6O
m/z=58.0419	Methyloxirane	Met33100	HMDB31558	58.04186481	C3H6O
m/z=58.0419	Allyl alcohol	Met14489	HMDB31652	58.04186481	C3H6O
m/z=580.2166	(+)-7-epi-Syringaresinol 4'-glucoside	Met38918	HMDB38261	580.2155912	C28H36O13
m/z=586.2005	Physalin E acetate	Met40824	HMDB31878	586.2050266	C30H34O12
m/z=596.179	Eriocitrin	Met33985	HMDB05811	596.1741204	C27H32O15
m/z=596.179	Isorubrofusarin 10-gentiobioside	Met36914	HMDB34609	596.1741204	C27H32O15
m/z=596.179	(2R)-6,8-Diglucopyranosyl-4',5,7-trihydroxyflavanone	Met25947	HMDB37407	596.1741204	C27H32O15
m/z=596.179	Pinobanksin 5-[galactosyl-(1->4)-glucoside]	Met19293	HMDB37506	596.1741204	C27H32O15
m/z=596.179	Rubrofusarin 6-gentiobioside	Met31459	HMDB38478	596.1741204	C27H32O15
m/z=596.179	Cassiaside C	Met42272	HMDB38550	596.1741204	C27H32O15
m/z=610.1973	Hesperetin 7-neohesperidoside	Met28509	HMDB30748	610.1897704	C28H34O15
m/z=610.1973	Protochlorophyllide	Met10688	HMDB31148	610.206662	C35H30MgN4O5
m/z=610.1973	4'-Hydroxyacetophenone 4'-[4-hydroxy-3,5-dimethoxybenzoyl-(->5)-apiosyl-(1->2)-glucoside]	Met24253	HMDB36333	610.1897704	C28H34O15
m/z=612.1747	Safflomin A	Met27930	HMDB30558	612.169035	C27H32O16
m/z=612.1747	Carthamidin 6,7-diglucoside	Met15240	HMDB40125	612.169035	C27H32O16
m/z=612.1747	Aromadendrin 3,7-diglucoside	Met24797	HMDB40559	612.169035	C27H32O16
m/z=612.1747	Hydroxysafflor yellow A	Met38149	HMDB40677	612.169035	C27H32O16
m/z=612.4774	DG(14:0/22:6(4Z,7Z,10Z,13Z,16Z,19Z)/0:0)	Met40929	HMDB07034	612.4753752	C39H64O5
m/z=612.4774	DG(14:1(9Z)/22:5(4Z,7Z,10Z,13Z,16Z)/0:0)	Met34936	HMDB07061	612.4753752	C39H64O5
m/z=612.4774	DG(14:1(9Z)/22:5(7Z,10Z,13Z,16Z,19Z)/0:0)	Met34935	HMDB07062	612.4753752	C39H64O5

m/z=612.4774	DG(16:1(9Z)/20:5(5Z,8Z,11Z,14Z,17Z)/0:0)	Met37010	HMDB07143	612.4753752	C39H64O5
m/z=612.4774	DG(18:2(9Z,12Z)/18:4(6Z,9Z,12Z,15Z)/0:0)	Met13130	HMDB07251	612.4753752	C39H64O5
m/z=612.4774	DG(18:3(6Z,9Z,12Z)/18:3(6Z,9Z,12Z)/0:0)	Met42408	HMDB07278	612.4753752	C39H64O5
m/z=612.4774	DG(18:3(6Z,9Z,12Z)/18:3(9Z,12Z,15Z)/0:0)	Met42409	HMDB07279	612.4753752	C39H64O5
m/z=612.4774	DG(18:3(9Z,12Z,15Z)/18:3(6Z,9Z,12Z)/0:0)	Met19464	HMDB07307	612.4753752	C39H64O5
m/z=612.4774	DG(18:3(9Z,12Z,15Z)/18:3(9Z,12Z,15Z)/0:0)	Met13530	HMDB07308	612.4753752	C39H64O5
m/z=612.4774	DG(18:4(6Z,9Z,12Z,15Z)/18:2(9Z,12Z)/0:0)	Met44444	HMDB07335	612.4753752	C39H64O5
m/z=612.4774	DG(20:5(5Z,8Z,11Z,14Z,17Z)/16:1(9Z)/0:0)	Met10973	HMDB07563	612.4753752	C39H64O5
m/z=612.4774	DG(22:5(4Z,7Z,10Z,13Z,16Z)/14:1(9Z)/0:0)	Met9665	HMDB07705	612.4753752	C39H64O5
m/z=612.4774	DG(22:5(7Z,10Z,13Z,16Z,19Z)/14:1(9Z)/0:0)	Met18581	HMDB07734	612.4753752	C39H64O5
m/z=612.4774	DG(22:6(4Z,7Z,10Z,13Z,16Z,19Z)/14:0/0:0)	Met24239	HMDB07762	612.4753752	C39H64O5
m/z=612.4774	DG(14:0/0:0/22:6n3)	Met16232	HMDB55980	612.4753752	C39H64O5
m/z=612.4774	DG(14:1n5/0:0/22:5n6)	Met33686	HMDB56149	612.4753752	C39H64O5
m/z=612.4774	DG(14:1n5/0:0/22:5n3)	Met8999	HMDB56154	612.4753752	C39H64O5
m/z=612.4774	DG(16:1n7/0:0/20:5n3)	Met19218	HMDB56174	612.4753752	C39H64O5
m/z=612.4774	DG(18:3n6/0:0/18:3n6)	Met7353	HMDB56296	612.4753752	C39H64O5
m/z=612.4774	DG(18:3n6/0:0/18:3n3)	Met30539	HMDB56303	612.4753752	C39H64O5
m/z=612.4774	DG(18:3n3/0:0/18:3n3)	Met44458	HMDB56366	612.4753752	C39H64O5
m/z=614.1806	Catechin 3',4'-diglucoside	Met19315	HMDB37950	614.184685	C27H34O16
m/z=614.1806	Catechin 3',5-diglucoside	Met19316	HMDB37951	614.184685	C27H34O16
m/z=614.1806	Catechin 3',7-diglucoside	Met19317	HMDB37952	614.184685	C27H34O16
m/z=614.1815	Catechin 3',4'-diglucoside	Met19315	HMDB37950	614.184685	C27H34O16
m/z=614.1815	Catechin 3',5-diglucoside	Met19316	HMDB37951	614.184685	C27H34O16
m/z=614.1815	Catechin 3',7-diglucoside	Met19317	HMDB37952	614.184685	C27H34O16
m/z=629.3715	Janthitrem G	Met19185	HMDB30531	629.3716384	C39H51NO6
m/z=633.1855	Pyranocyanin A	Met26852	HMDB35420	633.1819454	C30H33O15
m/z=636.1647	Quercetin 3-(4''-acetylrhamnoside) 7-rhamnoside	Met5395	HMDB39333	636.169035	C29H32O16
m/z=636.1647	Kaempferol 3-(6''-acetylgalactoside) 7-rhamnoside	Met30881	HMDB40539	636.169035	C29H32O16
m/z=640.1353	Nelumboside	Met6734	HMDB38464	640.1275641	C27H28O18
m/z=665.6623	Cer(d18:0/25:0)	Met17087	HMDB11770	665.6685957	C43H87NO3
m/z=666.2185	Glycogen	Met19005	HMDB00757	666.2218584	C24H42O21
m/z=666.2185	Maltotetraose	Met621	HMDB01296	666.2218584	C24H42O21
m/z=666.2185	Maltotetraose	Met1772	HMDB01296	666.2218584	C24H42O21
m/z=666.2185	Stachyose	Met24619	HMDB03553	666.2218584	C24H42O21
m/z=666.2185	Mannan	Met19429	HMDB29931	666.2218584	C24H42O21
m/z=666.2185	Fagopyritol B3	Met29876	HMDB35323	666.2218584	C24H42O21
m/z=666.2185	Bifurcose	Met22746	HMDB38490	666.2218584	C24H42O21
m/z=666.2185	Neobifurcose	Met39338	HMDB38870	666.2218584	C24H42O21
m/z=666.2185	Sesamose	Met39339	HMDB38871	666.2218584	C24H42O21
m/z=666.2185	3-beta-Glucosylcellotriose	Met13095	HMDB39173	666.2218584	C24H42O21

m/z=666.2185	3-beta-Cellobiosylcellobiose	Met25930	HMDB39174	666.2218584	C24H42O21
m/z=666.2185	Nystose	Met25932	HMDB39176	666.2218584	C24H42O21
m/z=666.2185	Tetramethylquercetin 3-rutinoside	Met5399	HMDB39337	666.2159852	C31H38O16
m/z=666.2185	Fagopyritol A3	Met36240	HMDB40182	666.2218584	C24H42O21
m/z=681.4365	PE(14:1(9Z)/18:4(6Z,9Z,12Z,15Z))	Met37225	HMDB08865	681.4369545	C37H64NO8P
m/z=681.4365	PE(18:4(6Z,9Z,12Z,15Z)/14:1(9Z))	Met22585	HMDB09185	681.4369545	C37H64NO8P
m/z=681.4365	7-Epizucchini factor A	Met11227	HMDB36405	681.439324	C44H59NO5
m/z=683.4492	PE(14:0/18:4(6Z,9Z,12Z,15Z))	Met31322	HMDB08832	683.4526046	C37H66NO8P
m/z=683.4492	PE(14:1(9Z)/18:3(6Z,9Z,12Z))	Met37227	HMDB08863	683.4526046	C37H66NO8P
m/z=683.4492	PE(14:1(9Z)/18:3(9Z,12Z,15Z))	Met37224	HMDB08864	683.4526046	C37H66NO8P
m/z=683.4492	PE(18:3(6Z,9Z,12Z)/14:1(9Z))	Met35726	HMDB09119	683.4526046	C37H66NO8P
m/z=683.4492	PE(18:3(9Z,12Z,15Z)/14:1(9Z))	Met15454	HMDB09152	683.4526046	C37H66NO8P
m/z=683.4492	PE(18:4(6Z,9Z,12Z,15Z)/14:0)	Met22584	HMDB09184	683.4526046	C37H66NO8P
m/z=684.2369	Citbismine C	Met10175	HMDB41435	684.23191	C37H36N2O11
m/z=700.1371	Theaflavate B	Met12352	HMDB33038	700.1428202	C36H28O15
m/z=700.1371	(S)-Skyrin 2-glucoside	Met32886	HMDB36320	700.1428202	C36H28O15
m/z=717.5649	PC(14:0/P-18:0)	Met21935	HMDB07896	717.5672404	C40H80NO7P
m/z=717.5649	PC(16:0/P-16:0)	Met23883	HMDB07994	717.5672404	C40H80NO7P
m/z=717.5649	PC(P-16:0/16:0)	Met28199	HMDB11206	717.5672404	C40H80NO7P
m/z=717.5649	PC(P-18:0/14:0)	Met32547	HMDB11236	717.5672404	C40H80NO7P
m/z=717.5649	PC(o-16:0/16:1(9Z))	Met10609	HMDB13404	717.5672404	C40H80NO7P
m/z=727.4437	PS(14:1(9Z)/18:3(9Z,12Z,15Z))	Met27683	HMDB12348	727.4424339	C38H66NO10P
m/z=727.4437	PS(18:3(9Z,12Z,15Z)/14:1(9Z))	Met34377	HMDB12408	727.4424339	C38H66NO10P
m/z=742.2466	Hexacarboxylporphyrin I	Met33468	HMDB00743	742.2486227	C38H38N4O12
m/z=742.2466	Porphinehexacarboxylic acid	Met14667	HMDB00780	742.2486227	C38H38N4O12
m/z=742.2466	Hexacarboxylporphyrin III	Met5707	HMDB01952	742.2486227	C38H38N4O12
m/z=742.2469	Hexacarboxylporphyrin I	Met33468	HMDB00743	742.2486227	C38H38N4O12
m/z=742.2469	Porphinehexacarboxylic acid	Met14667	HMDB00780	742.2486227	C38H38N4O12
m/z=742.2469	Hexacarboxylporphyrin III	Met5707	HMDB01952	742.2486227	C38H38N4O12
m/z=742.4758	PG(16:1(9Z)/18:3(6Z,9Z,12Z))	Met36410	HMDB10591	742.478485	C40H71O10P
m/z=742.4758	PG(16:1(9Z)/18:3(9Z,12Z,15Z))	Met36409	HMDB10592	742.478485	C40H71O10P
m/z=742.4758	PG(18:3(6Z,9Z,12Z)/16:1(9Z))	Met42825	HMDB10661	742.478485	C40H71O10P
m/z=742.4758	PG(18:3(9Z,12Z,15Z)/16:1(9Z))	Met28150	HMDB10676	742.478485	C40H71O10P
m/z=773.2238	Cyanidin 3,3',5-triglucoside	Met9106	HMDB37973	773.2140334	C33H41O21
m/z=773.2238	Cyanidin 3-sophorotrioside	Met41208	HMDB37995	773.2140334	C33H41O21
m/z=773.2238	Cyanidin 3-sophoroside 5-glucoside	Met37398	HMDB38487	773.2140334	C33H41O21
m/z=773.2238	Cyanidin 3-diglucoside 5-glucoside	Met37622	HMDB41716	773.2140334	C33H41O21
m/z=789.6309	PC(14:0/22:0)	Met36513	HMDB07886	789.6247553	C44H88NO8P
m/z=789.6309	PC(16:0/20:0)	Met5403	HMDB07977	789.6247553	C44H88NO8P
m/z=789.6309	PC(18:0/18:0)	Met44165	HMDB08036	789.6247553	C44H88NO8P
m/z=789.6309	PC(20:0/16:0)	Met10185	HMDB08265	789.6247553	C44H88NO8P

m/z=789.6309	PC(22:0/14:0)	Met41375	HMDB08525	789.6247553	C44H88NO8P
m/z=789.6309	PE(15:0/24:0)	Met39815	HMDB08914	789.6247553	C44H88NO8P
m/z=789.6309	PE(24:0/15:0)	Met8004	HMDB09714	789.6247553	C44H88NO8P